Post Drill Report

Barramundi #1, T27P

Bass Basin, Australia

Prepared for:

MINERAL RESOURCES TASMANIA

By:

GLOBEX Far East
Memorial City Plaza II
820 Gessner, Suite #1680
Houston, Texas 77024

and

Robinson & Associates
Suite #150, 1700 Redbud
McKinney, Texas 75069

January 3, 2000

TABLE OF CONTENTS

FIGURES

PRE-DRILL CONCEPTS

The details of earlier work in support of drilling this well are available in two previous reports and the presentation guide attached in Appendices A through D. These reports are summarized below for convenience.

Regional geologic work done by GLOBEX prior to being granted the exploration license, concluded that the Gippsland and Bass Basins shared the same tectonic history. In addition, cores taken from the productive Latrobe section in the Gippsland are almost indistinguishable from the Eastern View Coal Measures (EVCM) of the Bass Basin. Oils from wells in both basins have the same signature, indicating similar source rock development. When taken together, it seemed the Bass should contain large fields in a "sweet spot" similar to the Kingfisher area in the Gippsland, where the thickest source rocks are in juxtaposition with the excellent reservoirs. We thought the most likely area for such a juxtaposition to occur in the Bass was along the southern margin of block T27P.

Previous Work

The initial attraction to the Bass was heightened by the availability of large tracts of acreage in an area where earlier exploration activity had prepared the way for new concepts and modern technologies to yield major discoveries. Of the twenty-nine wells drilled in the Basin only one (Yolla) had encountered potentially commercial quantities of hydrocarbons. The encouraging tests in the Yolla well demonstrated the effectiveness of the hydrocarbon generating system in the Bass Basin and its potential to deliver world class reserves. The remainder of the wells presented a challenge to explain why they were unsuccessful, since all of them were located on structures defined by seismic data.

A depositional model was developed which explained the distribution of thick, high quality reservoir to the north and poorly sorted, bioturbated sands containing high percentages of lithic fragments to the south. This model and the accompanying maps in Appendix C show that the preferred area of reservoir quality lay across the northeastern margin of the basin where thick barrier sandstones were stacked in thick sequences. This area also coincides with the lower EVCM basin thalwig where the thickest

hydrocarbon generating shale and coal sequences accumulated in anoxic conditions. It was in this area that the possibility of major new fields might be found.

Within this preferred area which crosses, or is on trend with T27P, were eight wells, which were drilled on various types of structures. All of these wells encountered excellent reservoir sands and contained significant hydrocarbon shows. None of these structures, however, proved to be effective traps. In fact, along the northern margin of the basin, only the Yolla well encountered significant trapped hydrocarbons, and it is located significantly further from the basin margin in the basin thalwig. From the initial stages of our work it was evident that the main exploration risk in the Bass Basin would be related to trapping seals and documenting trap integrity.

Trap / Seal Integrity

Simple structural reconstructions of seismic lines tying Cormorant and Tilana wells reveal these structures to have very late movement, well into the Miocene or later. Similar reconstructions across Yolla, however show little or no movement. Shallow seismic isopachs above 0.5 seconds, indicate a series of thicks and thins parallel to the Bassian Rise. Our interpretation of this trend was that late lateral movement along the major basin forming fault had created adjustment zones and pop up structures, such as Cormorant. Over Barramundi, there was no obvious young structural movement.

When seismic data tying the Cormorant and Tilana wells was examined at high magnification on our workstation, hundreds of diffraction vertices could be seen throughout the Demons' Bluff seal interval. When the same interval was compared to Yolla or Barramundi, there seemed to be a marked decrease in diffraction vertices and cross hatching. We interpreted this to mean that Barramundi and Yolla were free of fractures and seal integrity had been maintained.

A third line of investigation into seal integrity lay in the direction of direct hydrocarbon detection. Boral has published its efforts to document its reserves at Yolla utilizing direct hydrocarbon detection technology. Esso has also been utilizing these methods at Bream Field. If hydrocarbon indicators are a reliable indication of hydrocarbon accumulation, then they constitute defacto proof of seal integrity.

During the early phase of the structural interpretation, an obvious amplitude anomaly across the Barramundi structure presented itself. This anomaly was analyzed and qualified as a valid hydrocarbon indicator, as discussed in the attached AVO Report. Since shear wave velocity information was not available, great emphasis was placed on measured seismic amplitude response at wells with similar reservoir properties.

Direct seismic ties were available at Yolla, Tilana, and Cormorant. From measured normal incidence and offset responses at Tilana and Cormorant, it was clear that the wet sand response was a negative intercept and neutral offset gradient. Yolla, however displayed a more negative intercept and a positive offset gradient. These were the responses predicted in our modeling efforts using default values for Poisson's ratio. We

were also able to replicate the hydrocarbon response at Cormorant by performing a Gassman substitution in the wet target sand.

Using default values for Poisson's Ratio and published values for coals, we were able to generate forward models that matched the observed seismic response of both wet and productive wells. The Barramundi anomaly mimicked the productive seismic response seen at Yolla and generally conformed to the structural trap as mapped. Accordingly we concluded that the Barramundi anomaly represented a hydrocarbon filled reservoir, which would imply effective trap seals.

These three approaches were thought to be sufficient to deal with the risk of ineffective trap seals, which we believed constituted the greatest exploration risk in this play.

SUMMARY OF RESULTS

The Barramundi well reached total depth of 2100 meters on October 2, 1999, after penetrating the anticipated reservoir section in the EVCM according to depth prognosis without encountering a commercial hydrocarbon accumulation.

Evaluating the results of the Barramundi test naturally began with the open hole logs. It was evident from the first examination that the some of the logs contained unusual and anomalous readings. The more important observations are listed below:

Observations From Field Logs

Dipole Sonic Imager (DSI):

- The amplitude of the fast shear wave event is dramatically attenuated from 1250 to 1450 meters and is erratic in amplitude below.
- The V_p / V_s ratio displays large variations over a relatively short interval

Caliper (HCAL):

- While most of the hole was relatively smooth, large borehole breakouts occur below 1400 meters.
- These breakouts occur in high sand count zones.

Formation Evaluation Log (FEL):

- After carrying encouraging shows of up to eighty units of background gas, there was a steady decline from 1250 meters and continuing through the lower Demon's Bluff shale seal interval into the prospective EVCM interval.
- Within this zone, background gas actually decreases in permeable, sandy intervals.

Direct Observations

Log Curves Display

Figure 1

Velocity (V_p, V_s, V_p/ V_s):

- Compressional velocities, (V_p) , increases with depth, with variations due to lithology. There is however, a slope change in this increase between 1100 and 1300 meters.
- Shear wave velocities, (V_s), are also increasing with depth, but along a steeper, more inconsistent slope. These behaviors result in a anomalous V_p / V_s curve
- V_p/ V_s curve displays two large anomalies with the first at 1000 meters – 1180 meters, and the second at 1180 meters - 1400 meters. The magnitude of these anomalies represents a base line shift of over 25%.

Density (RHOB):

- Density is seen to increase slightly with depth (2.0 to 2.1 g/cc) over the 1300 meter interval logged, but does not represent the amount of compaction one would expect.
- There are three major base line shifts in the compaction slope as shown in the density increase with depth curve at 1000, 1180 and 1500 meters.
- These shifts are not associated with major lithologic changes.

Impedence Amplitude (AI):

- A large change in AI is seen at the depth where the amplitude anomaly was mapped, where the V_p/ V_s and Poisson's Ratio curves also show base line shifts.

Poisson's Ratio (PR):

- Poisson's Ratio displays a range of values from 0.4 to 0.25 which falls within a "normal" range.
- Rather than appearing as a smooth decreasing with depth curve, as is typical, there are large bulges, and slope changes in the curve that are not "normal" and produce large distortion in offset seismic amplitudes such as were mapped prior to drilling the Barramundi well.

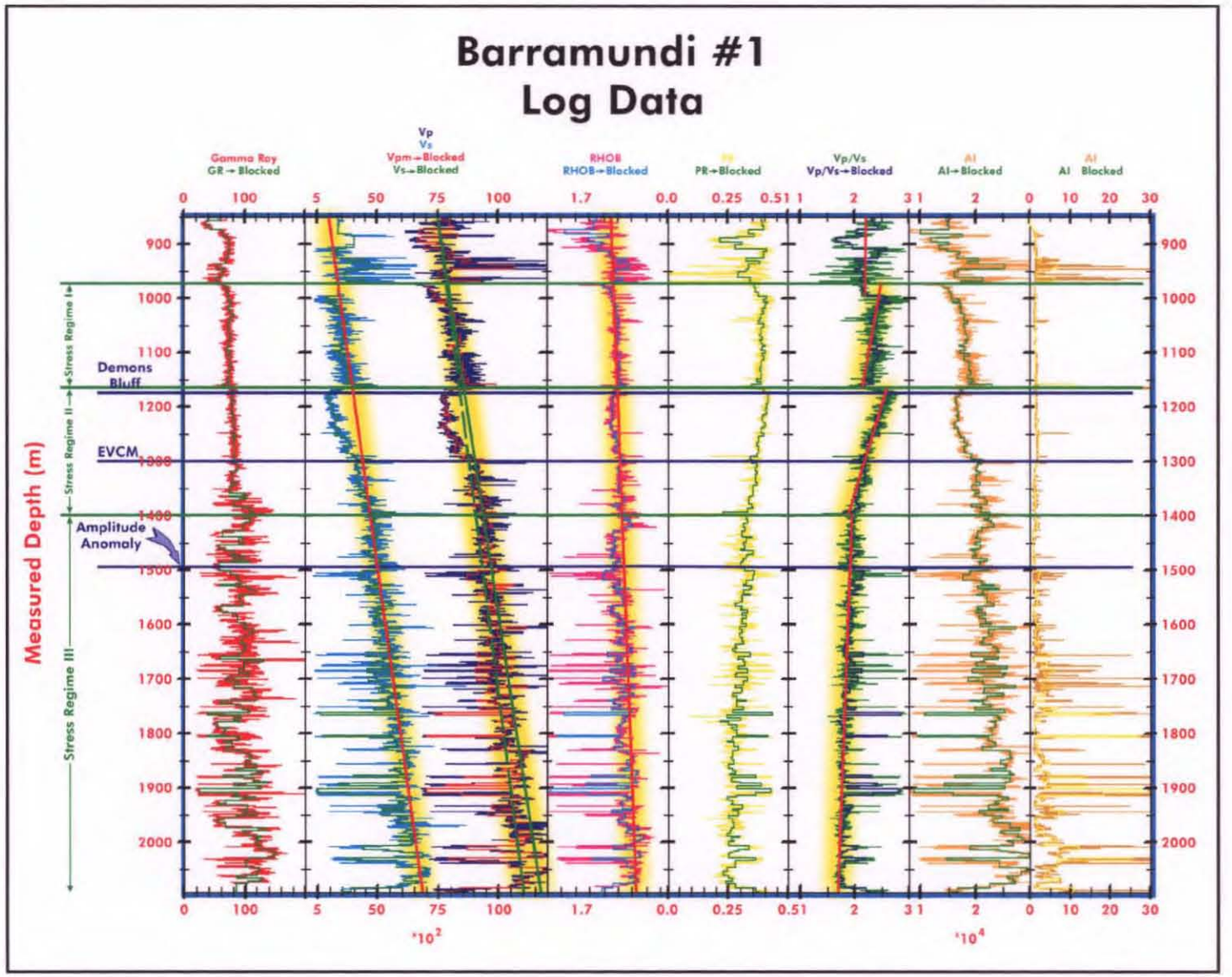
Barramundi #1
Log Data
Gamma Ray
GR→Blocked
Vp
Vs
Vpm→Blocked
Vs→Blocked
RHOB
RHOB→Blocked
PR→Blocked
Vp/Vs
Vp/Vs→Blocked
AI
AI→Blocked
AI
AI Blocked
Measured Depth (m)
Stress Regime I
Stress Regime II
Stress Regime III
Demons Bluff
EVCM
Amplitude Anomaly
5 cm

Figure 1

ANALYSIS AND DISCUSSION

To better understand these observations, analytical displays were created to better diagnose their underlying causes and their significance. Our first concern was to understand what generated the normal incidence and offset amplitude anomaly on which our reservoir predictions were based.

Reflection Amplitude and AVO Anomaly:

Measured values for shear and compressional velocities, along with computed values for Poisson's Ratio were used to develop an offset response model, (Figures 2 and 3). From this model, a strong trough at 1.3 seconds (two way travel time) can be seen. The behavior of this reflector corresponds exactly to the amplitude anomaly which was mapped, and on which our hydrocarbon predictions were based. This work was completed prior to drilling the Barramundi well.

This trough diminishes in amplitude with offset distance, mimicking the observed hydrocarbon response seen at Yolla. The identical response was also obtained when Gassman substitution was performed during forward AVO modeling at Cormorant (more fully described in AVO Report, Appendix B). In brief, forward modeling of the Barramundi data set yields an anomaly with the same response as that of a hydrocarbon filled reservoir, yet no hydrocarbon accumulation was present.

Further examination of offset amplitude behaviors shows strong amplitude increases with offset between 0.9 and 1.040 seconds. These offset anomalies both occur at major baseline shifts in the V_p / V_s curve, and are not related to lithology breaks or formation tops. Additionally, the magnitude of these shifts, (as much as 25%), are greater than could be produced by changes in pore fluids or lithology within a clastic sequence. If these two possibilities are eliminated, then the relationship between V_p and V_s must be responding to changes in stresses within the rock matrix. To further explore this hypothesis we produced several additional analytical products.

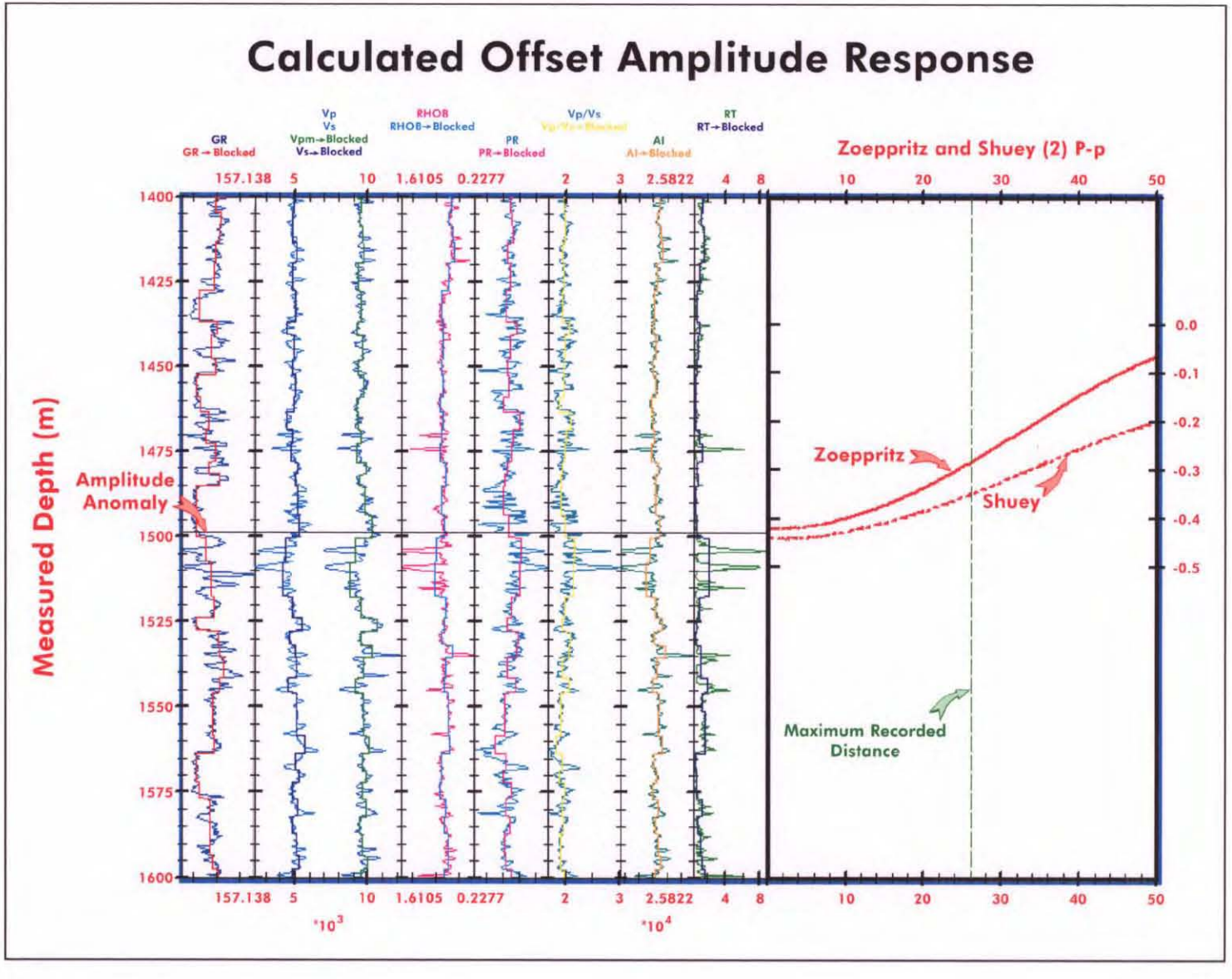
Calculated Offset Amplitude Response
GR
GR→Blocked
Vp
Vs
Vpm→Blocked
Vs→Blocked
RHOB
RHOB→Blocked
PR
PR→Blocked
Vp/Vs
AI
AI→Blocked
RT
RT→Blocked
Zoeppritz and Shuey (2) P-p
157.138
5
10
1.6105
0.2277
2
3
2.5822
4
8
10
20
30
40
50
1400
1425
1450
1475
1500
1525
1550
1575
1600
Measured Depth (m)
Amplitude Anomaly
0.0
-0.1
-0.2
-0.3
-0.4
-0.5
Zoeppritz
Shuey
Maximum Recorded Distance
*10^3
*10^4
5 cm

Figure 2

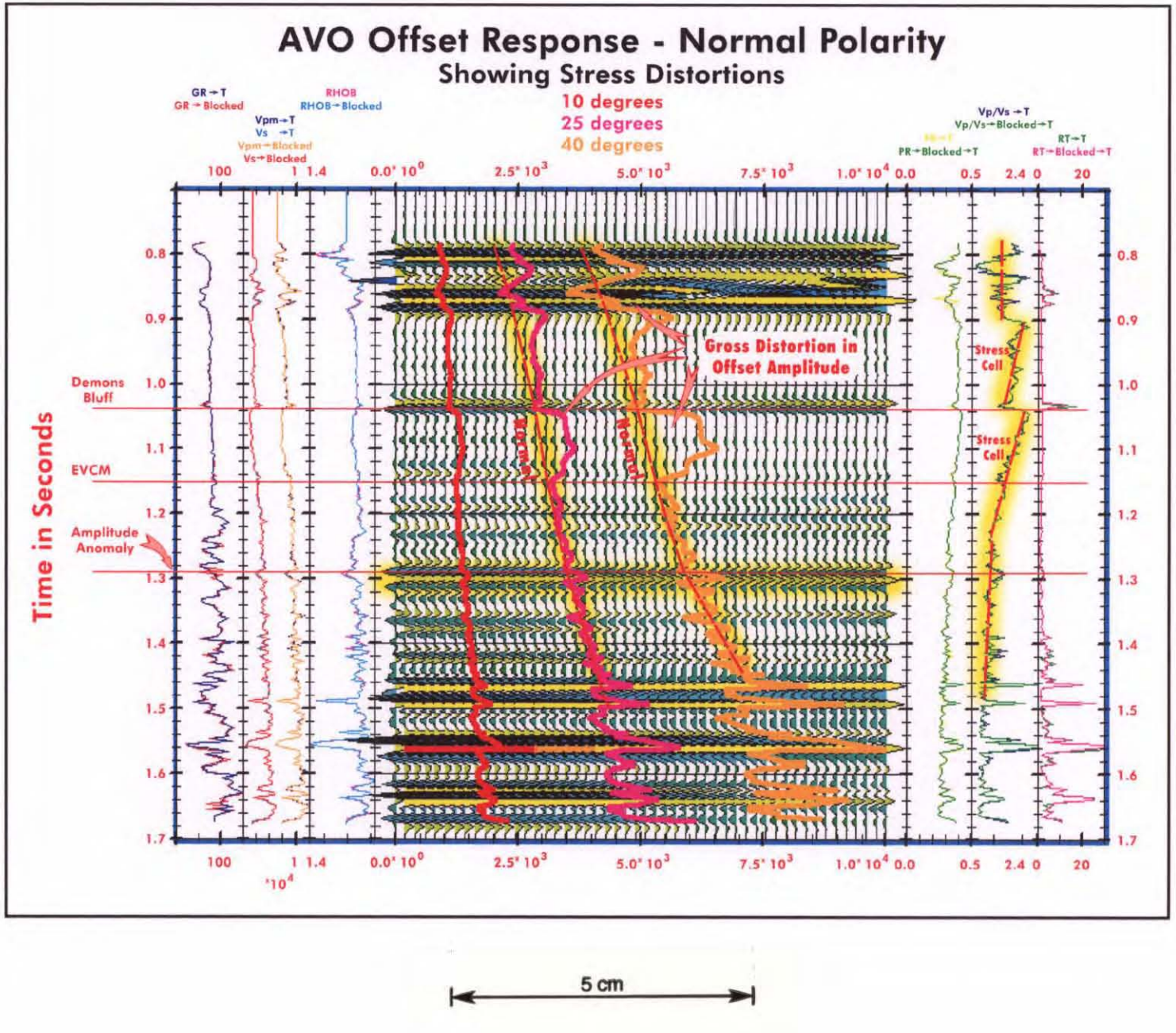
AVO Offset Response - Normal Polarity
Showing Stress Distortions
10 degrees
25 degrees
40 degrees
GR → T
GR → Blocked
RHOB
RHOB → Blocked
Vpm → T
Vs → T
Vpm → Blocked
Vs → Blocked
Vp/Vs → T
Vp/Vs → Blocked → T
PR → Blocked → T
RT → T
RT → Blocked → T
Gross Distortion in Offset Amplitude
Stress Cell
Stress Cell
Demons Bluff
EVCM
Amplitude Anomaly
Time in Seconds
5 cm

Figure 3

V_p / V_s vs. DT Cross Plotting:

Barramundi data were cross-plotted on a standard V_p / V_s vs. DT lithology template, and are shown below (Figure 4). This display, which includes data points from all lithologies, generally conforms to the lithology template to an approximate depth of 1200 meters. At this point, a major displacement of the trend or "normal" curve occurs. The magnitude of this displacement represents a 15% shift on V_p / V_s axis. Comparing this range shift along the V_p / V_s axis, to that due to the difference in porosity or lithologies associated sand or shale in the template (approximately 10%), reveals that the observed shift is 50% greater.

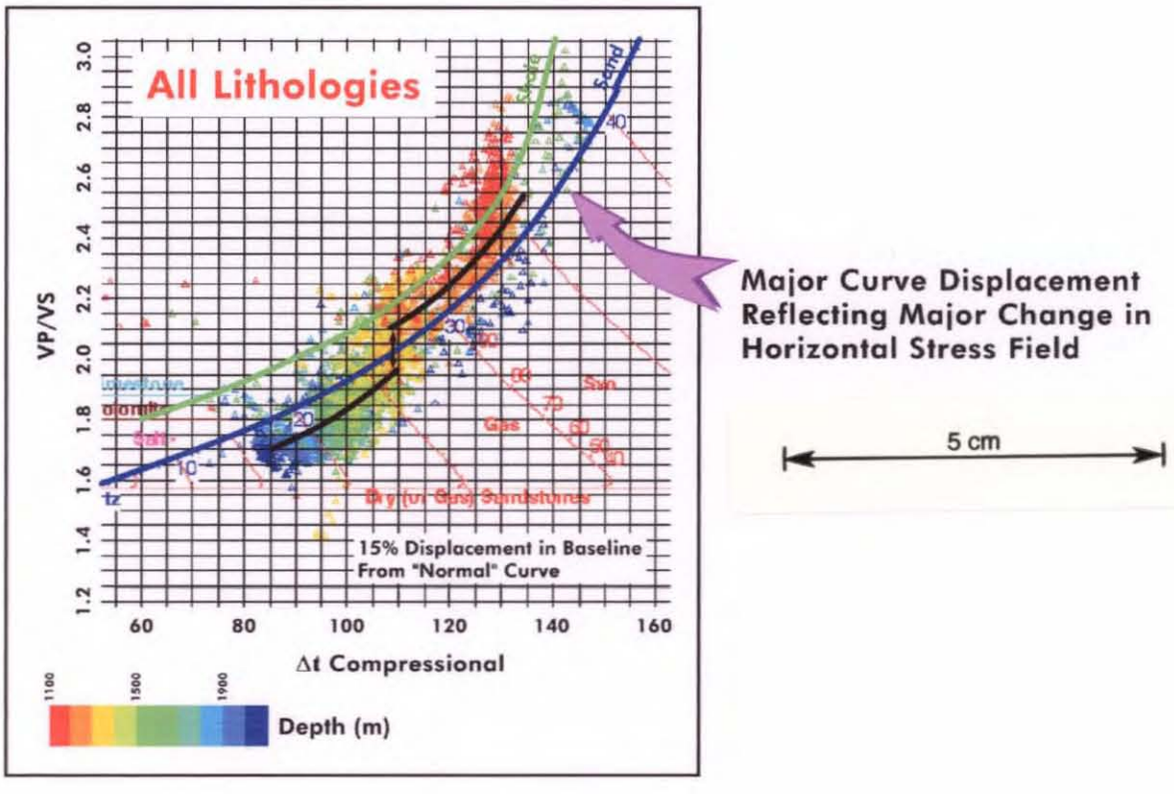

Figure 4

To further explore this point, the data were sorted by lithology as determined by multimineral volumetric analysis from well logs using Geoquest's Elan process. Since coal represents a major velocity and density anomaly, we began by repoltting the data excepting data points associated with coals resulting in the plot shown below in Figure 5.

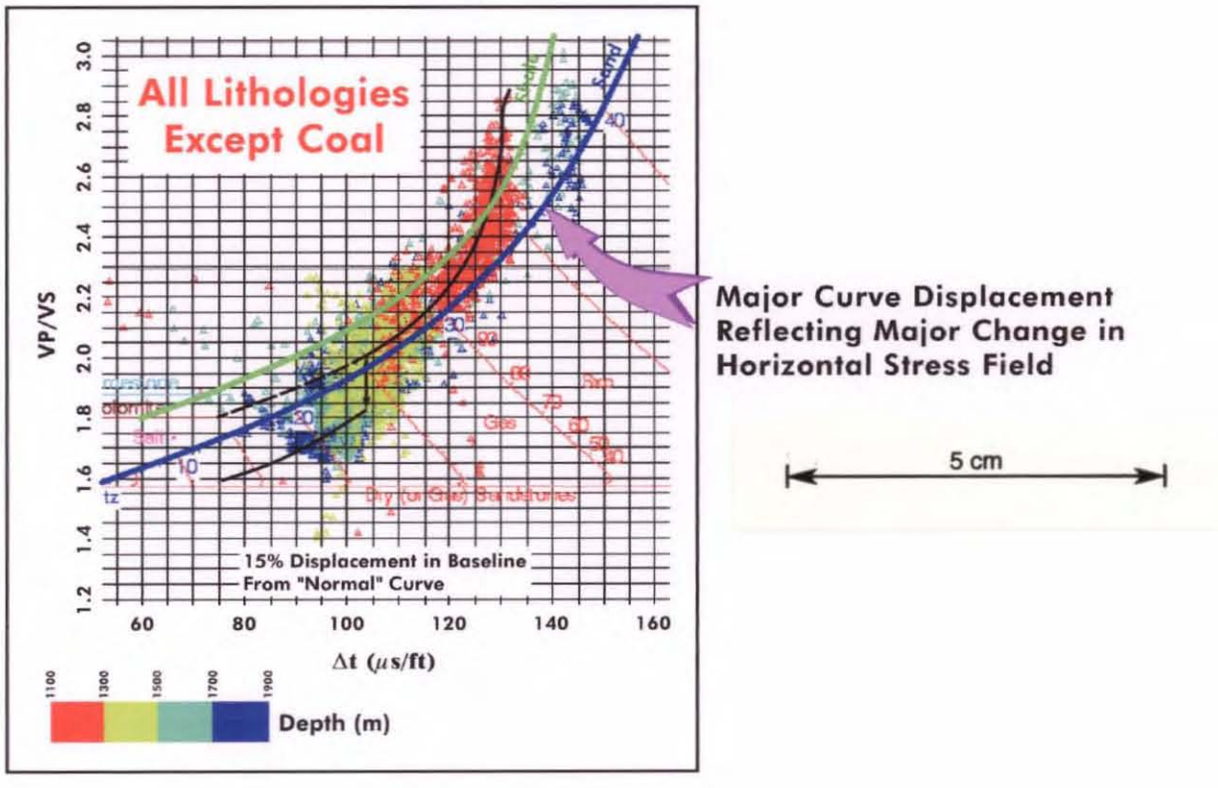

Figure 5

Comparing this plot to the plot including coals, it is apparent that the presence of coals has little to do with the trend line shift observed in both plots. To test the hypothesis that lithology is irrelevant to lithologic effects, we resorted the data and plotted the points related to sandstones only. The results of this plot are show below in Figure 6.

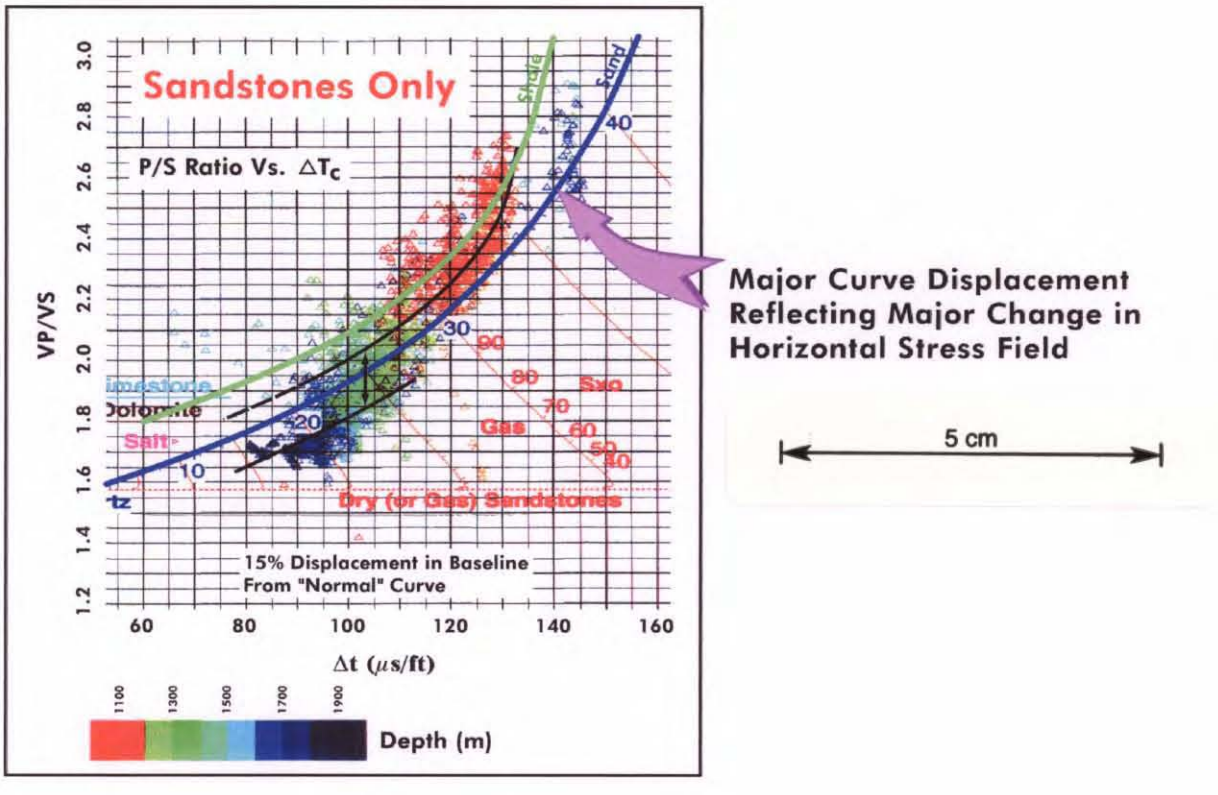

Figure 6

From the these plots, it is evident that the apparent baseline shift is not associated with any lithology or lithologic changes and the amount of the shift is greater than range of values between lithologic classes. An interesting point is shown when the points

between 1100 and 1300 meters are plotted with an expanded color scale as is shown below in Figure 7.

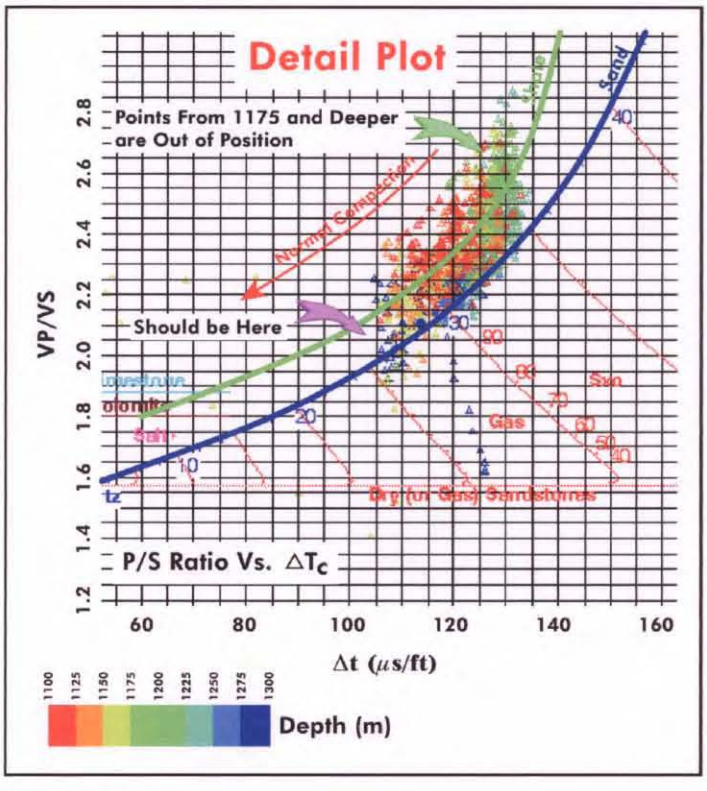

Figure 7

5 cm

Here we see a reversal of the normal trend of shallow points plotting towards the upper right and deeper points plotting progressively towards the lower left. This occurs as points from 1180 to 1300 meters plotting higher (shallower) on the trend curve than points from 1100 to 1180 meters.

Taken together, this behavior indicates the presence of large, variable horizontal stresses and strains in and around the borehole. We began to investigate this further to determine the direction and magnitude of these stresses.

BARRAMUNDI #1 ANALYTICAL LOG DISLPAY

Caliban Calculations of Borehole Breakout and Ovalization:

Below 1400 meters, there are major borehole breakouts accompanied by a significant ovalization of the borehole. The magnitude of these breakouts are at least 6 inches over gauge (12 inches), which would represent an increase in hole size of 50%. The size of these breakouts and the ovalization of the borehole indicate strong, unbalanced horizontal stresses surrounding the borehole.

The orientation of these breakouts can be determined by the ovalization of the hole and this was also calculated. The major axis of the ellipse is oriented northwest with the minor axis oriented towards the northeast, suggesting a principal stress axis lying along a northeast – southwest axis. This degree of ovalization of the borehole also suggests strong unbalanced forces in the horizontal stress field.

Pseudo Images from SHDT:

To detect formation fracturing, pseudo images were created by converting azimuth positioned resistivity readings from high-resolution dipmeter recorded data to create a 360° image of the borehole.

From the shallowest interval logged at 1272 meters, there are apparent fractures in this image as seen on the Barramundi #1 Analytical Log Display. These fractures vary in density, but are present throughout the lower portion of the hole. The question immediately arises whether these fractures are open, thereby presenting potential seal problems.

Fracture Interpretation Based on HALS Data:

Azimuth controlled induction resistivity readings played out in an orthogonal set show an anisotropy of readings usually associated with open fractures. Some of these are highlighted with arrows on the Barramundi #1 Analytical Log Display. The more

prominent of these, are supported by fracture picks on the Pseudo Borehole Images also seen on the Barramundi #1 Analytical Log Display.

Mechanical Properties Borehole Stability Log:

The calculated horizontal stress from 1160 to 1280 meters is equal or greater than the total vertical stress. This zone also corresponds to the onset of fractures in the borehole and borehole breakouts as shown on the Barramundi #1 Analytical Log Display. Within this zone the calculated minimum safe mud weights to prevent formation fluids from entering the borehole exceeds the "normal" or "hydrostatic" gradient, even though no abnormal pore pressures were encountered in this well. This upward shift in the calculated safe mud weight is due to the abnormal stress regime on the matrix being interpreted by the software as stress due to pore fluid pressure. This zone is also associated with a major increase in Poisson's Ratio which is related to horizontal and vertical stresses.

Below 1280 meters and into the major break out zone at 1400 meters, calculated horizontal stresses stay below the total calculated overburden stress and the calculated safe or minimum mud weight returns to a "normal" or "hydrostatic "gradient. This point is coincident with the base of the second anomaly in the Poisson's Ratio curve, and indicates that at least some of the excess stress is relieved by fracturing. To examine the extent and density of fracturing, several additional displays were created:

Stonely Fracture Log:

From the Dipole Sonic Imager log a Stonely Fracture Log was produced, which uses the Stonely Wave traveling along the borehole wall to detect open fractures in the formation. A brief description of how the Stonely Wave propagates, and its interpretative uses, is appended to this report (Appendix F). Examination of this product clearly shows the entire Demon's Bluff increasingly fractured from 1170 meters, extending down into the top of EVCM. The density and magnitude of open fractures increase up to the point where the major borehole breakouts begin at 1425 meters. When placed beside the other borehole tools and products discussed above, as is seen on the Barramundi #1 Analytical Log Display, this key piece helps throw light on the unusual measurements and calculations described above.

INTERPRETATIVE CONCLUSIONS

A study of the data presented here and in the original data set recorded in the borehole has let us to the following interpretative conclusions.

Geologic Conclusions:

- The formations penetrated in this borehole are under large, unbalanced present day stresses.
- These stresses have resulted in strains that have been manifested both as fractures and faults.
- Barramundi failed to contain commercial hydrocarbons by the lack of effective seals related to these fractures, which was recognized as the major risk prior to drilling.
- The principal stress axis is northeast – southwest.
- There appear to be three major stress regimens between;
    1) 1000 to 1180 meters
    2) 1180 to 1480 meters
    3) 1500 to Total Depth
- Each of these stress zones are characterized by;
    1) Increasing fracture density and magnitude
    2) Total loss of vertical seal
    3) Major borehole breakouts
- The stress field is likely related to the creation of the Barramundi structure, and lateral movement along faulting parallel to the basin margin.

Geophysical Conclusion:

- The stress changes at 1500 meters are responsible for the Normal Incidence and AVO anomaly mapped across the Barramundi structure.
- Since the anomaly generally fits the Barramundi structure, we conclude the stress field causing the anomaly, also extends across and is related to the structure.
- Stresses operating on the rock matrix are controlling seismic response in V_p, V_s and Poisson's Ratio to an extent greater than sand/shale lithology or pore fluids.
- The stress environment precludes the use of Direct Hydrocarbon Detection methods such as AVO.

Possible Follow On Work

Although it is clear from a qualitative standpoint, that Barramundi was unsuccessful because of seal failure, several things could be done to determine how general this problem is across the Bass Basin and the T27P permit.

1) Calculate the fracture gradient at Cormorant, Tilana, Dondu and Yolla wells and compare to Barramundi.

2) Determine critical hydraulic pressures for the Demons' Bluff seal.

3) Map Basin Stress regime utilizing AVO methods

4) Geologic study to determine which tectonic movements are responsible for the generating the stress and strain fields associated with this problem.

BIBLIOGRAPHY

Lowry, D.C., Fighting Fractured Flamingo – Lessons From Rambler–1, Timor Sea, 1996, APPEA Journal

Keep, M., Powell, McA., and Baillie, P.W., Neogene Deformation of the North West Shelf, Australia

O'Brien, G.W., Higgins, R., Symonds, P., Quaife, P., Colwell, J., and Blevin, J., Basement Control on the Development of Extensional Systems in Australia's Timor Sea: An Example of Hybrid Hard Linked/Soft Linked Faulting?, 1996, APPEA Journal

Kaldi, J.G., O'Brien, G.W., and Kivior, T., Seal Capacity and Hydrocarbon Accumulation History in Dynamic Petroleum Systems: The East Java Basin, Indonesia and the Timor Sea Region, Australia, 1999, APPEA Journal

Upton, P., Baxter, K., and O'Brien, G.W., Coupled Mechanical/Fluid Flow Models of Trap Integrity and Fault Reactivation: Application to the North West Shelf of Australia, 1998, AAPEA Journal

Hillis, R.R., Crosby, D.G., and Khurana, A.K., A Modified Fracture Gradient Relation and Its Application to East Texas and the Timor Sea, 1997 APPEA Journal

Castillo, David A., Hillis, Richard R., Asquith, Keven, and Fischer, Mike, State of Stress in the Timor Sea area, based on Deep Wellbore Observations and Frictional Failure Criteria: Application to Fault-trap integrity

Hillis, Richard R., Mechanisms of Dynamic Seal Failure in the Timor Sea and Central North Sea Basins

Geological Overview

Globex Far East is operator of Block T 27/P, a 1.8 million acre exploration permit located in 70 meter water depths in the Bass Basin of Australia. The Bass Basin is a Late Mesozoic-Cenozoic intracratonic basin trending northwest to southeast between Victoria and Northern Tasmania with an area of approximately 65,000 sq. kilometers. It is separated from the Otway Basin to the west and northwest by the King Island-Mornington Peninsula Rise and from the Gippsland Basin to the east by the Paleozoic rocks of the Bassian Rise.

The overall structural evolution of the Bass Basin is generally extensional, following a thermal sag phase associated with the successful separation of Australia and Antarctica beginning in the earliest Cretaceous and persisting through the Eocene. Mild wrenching as a result of Tertiary transpression has helped to form many of the prospects mapped in the T 27/P permit and is clearly evident on the seismic data.

The main stratigraphic units of interest for petroleum exploration in the Bass Basin are the Otway Group (Upper Jurassic-Lower Cretaceous), the siliclastic Furneaux Group (Upper Cretaceous-Paleocene), the siliclastic coal bearing Bass Group (Eocene), and the Torquay Group (Oligocene).

The primary exploration target within the Bass Basin is the Eastern View - Coal Measures petroleum system which is comprised of reservoir and source sequences within the Bass and Furneaux Groups. This proven petroleum system is well documented at the Yolla Field (30 MMBO and 500 BCF estimated), discovered by Amoco in 1985 and located 9.5 kilometers southwest of the T 27/P permit boundary, Yolla Field produces from deltaic and shoreline sandstones of the Eastern View. These sands are on average 15 meters thick, but have been observed as thick as 100 meters, with porosity ranging between 15 and 20 percent. Production tests with yields as high as 11.8 mmcf of gas per day and 892 barrels of condensate have been reported from the Yolla #1 well. Subsequent drilling and testing of oil reservoirs in the Yolla-1, Tilana-1 and the Pelican-5 wells, illustrates that these Middle and Late Eocene sandstones maintain good reservoir characteristics (porosity and permeability) at depths exceeding 3,000 meters.

Source rocks within these sections are equivalent to the Latrobe Group in the Gippsland Basin which are proven to contain commercial accumulations of crude oil. Geochemical analysis of hydrocarbons produced at the Yolla #1 indicate Type II kerogens in the lower Eocene (which is generating the majority of the oil in the field), and a mixture of Type II and Type III kerogens in the Upper Paleocene section. A secondary petroleum system within the Upper Cretaceous Otway Group is also recognized to contain source rocks, possible reservoirs and suitable sealing units, although very limited data are available to detail this system.

Structural timing of trap formation is a key element in the Bass Basin. A late Miocene to early Pliocene lateral movement can be seen to overprint some structures in the basin. Many of the early dry holes appear to have been drilled on these structures. In the deeper portions of the basin, where the best source rocks are thought to exist, migration of hydrocarbons probably began in the Miocene just prior to this lateral movement, and continues to this day in the shallow portions of the basin. The growth history exhibited by several of the features, which were dry when drilled, seems to indicate these late forming structures were not in place during the main pulse of hydrocarbon migration and therefore never had the chance to capture hydrocarbons. In other cases, the recent structural movement has reactivated pre-existing fault systems, thereby rupturing hydrocarbon traps and allowing hydrocarbons to escape.

Structures that have not been affected by this recent structural overprint are the subject of the Globex exploration effort.

Geophysical Overview

In June of 1996, Exploration Consultants began a seismic interpretation on newly acquired seismic data located in Permit T /27P of the Bass Basin in southern Australia. Utilizing existing seismic control, Globex had previously identified several prospects within the block and had undertaken a large 2-D seismic program to verify the structural closure on these prospects prior to drilling wildcat wells. The largest of these prospects, Barramundi, was assigned top priority for mapping and the decision was made at Globex to begin an interpretation of the seismic data on paper prints in order to meet the short term deadline of completing time structure maps on the main horizons of interest in the shortest time possible.

The newly acquired BB96 seismic survey was acquired in February of 1996 utilizing a seismic vessel owned and operated by the Australian Geological Survey Organization (AGSO). This data exhibited excellent internal reflection strength which tied lines within the survey in a consistent fashion. However when tying the older data sets acquired in the area by Amoco (TNK4 and TQH5 series) misties varying between twenty six and thirty eight milliseconds were observed. Additionally, the older data did not consistently tie lines of similar vintage within each survey. These problems are related possibly to navigation and positioning errors and/or the fact that not all data was processed consistently as a single grid. Globex was advised that any interpretation on the workstation should include recomputing the navigation information of all lines.

Exploration Consultants was also asked to provide quality control during the final processing phase of the new seismic program which was being completed as the interpretation project was begun. On examination of field data, it was apparent that the data set contained large amounts of recorded noise. These data were recorded in rough seas and cable jerk was very evident on many records. In view of the time constraints, it was decided to scale the noise to a more acceptable signal to noise ration by using a pre - stack AGC. This approach lead to a more balanced stack section that did not produce migrated noise in the migration process.

A traditional paper interpretation was completed and time maps on the Demon's Bluff and Eastern View horizons were delivered on August 20, 1996. It was determined that the Barramundi area contained at least one drillable prospect, and a tentative drilling location was selected. In addition, two overlays were presented that illustrated potential Normal Incidence amplitude anomalies which had been recognized during the interpretation process. These anomalies, which possibly indicate the presence of hydrocarbons on the Barramundi Prospect, were not subjected to a rigorous qualification process but were presented for consideration by any future work program.

After delivery of the initial seismic mapping over the Barramundi Prospect, a second, larger interpretation project covering the entire permit was defined and implemented for Globex by Exploration Consultants. This project integrated the recently completed prospect mapping on Barramundi with seismic data covering the entire T 27/P permit area. All available SEGY traces were loaded on a geophysical work station along with recomputed shot point locations. Five horizons were mapped over the entire 3700 kilometer seismic grid.

Volcanics Layer

Both the top and base of the volcanic layer were mapped, since elsewhere in the Bass Basin, the thickness of this layer changes dramatically and is known to contain large interval velocity variations, which have been documented to distort the time structures mapped below. The accompanying isochron shows that over the southern end of the Barramundi Prospect several thicks in this interval can be seen. Interval transit times in surrounding wells indicate a range of interval velocities in the volcaniclastics between 7,500 and 11,000 feet per second. These volcaniclastics are replacing lithologies whose interval velocities range between 6,500 and 7,500 feet per second.

As a result of these observations, it is evident that to properly convert time surfaces to depth a tightly sampled velocity database will need to be constructed. Interval velocities computed from seismic stacking velocities can be used to build an average velocity data volume for this purpose. Stacking velocities used in processing the BB96 data have been reserved and additionally, Exploration Consultants has digitized the stacking velocities displayed on paper sections of the TNK 4and TQH 5 surveys in the Barramundi area. These velocities can be readily processed into a suitable velocity volume which is suitable for depth conversion.

Top Demon's Bluff

The Top of Demon's Bluff is an excellent log marker and is consistent over the entire area. It is also a distinct seismic marker and was a key horizon in establishing well ties to synthetic seismograms. This layer also acts as a regional seal for the petroleum system and is useful as a reconstruction horizon for isopachs to study structural timing relative to seal systems.

Top Eastern View

Log character at this horizon indicates a transitional boundary with considerable variation. Consequently, seismic response at this horizon is somewhat inconsistent. The Top Eastern View map accompanying this report was made on a relatively consistent seismic event corresponding to the top of excellent reservoir sands in the Esso Cormorant #1 well. This seismic map is approximately 50 meters (165 feet)deeper than the Top Eastern View log pick.

Middle Eastern View

This horizon was mapped on a relatively strong positive amplitude within the Eastern View which is roughly equivalent to Upper M. diversus. While this horizon shows considerably more structural relief than the Top Eastern View, the seismic interpretation at this level is plagued with interfering multiples, making event identification somewhat questionable.

Additional Interpretational Work

In addition to structural mapping, other aspects of interpretation were investigated and recommendations have been made regarding;

- Depth conversion of seismic times taking into consideration the velocity effects of thick volcaniclastic layers on the final depth maps
- Amplitude versus Offset (AVO) analysis as a tool to evaluate the amplitude anomalies mapped on the Barramundi Prospect
- Regional seismic interpretation to evaluate the potential of the deeper Paleocene and Cretaceous section as a secondary objective.

Prospect Overview

Critical Trapping Elements

With the discovery of the Yolla Field by Amoco, all critical elements of the petroleum system were established. This same petroleum system should be present on the T27/P block. Common elements shared with the Yolla Field include the Demon's Bluff shale which provides an effective seal across the region, and both areas are adjacent to the major basinal source kitchen. The reservoir sands at Yolla are present and somewhat thicker in wells on the T27P permit. The critical factor in exploration success seems to be in timing of trap formation relative to hydrocarbon migration.

One of the major challenges of this interpretative review was to explain why wells drilled in this basin on prominent structures prior to the discovery by Amoco at Yolla Field, were unsuccessful. Of particular concern were the Bass #2, Cormorant #1, and Tilana #1 structures. These wells were drilled on the crest of significant structures, on trend or nearby to Block T 27/P.

Cormorant and Tilana Structures

Across both of these structures, there appears to have been Upper Miocene movement which may have breached reservoir seals. This hypothesis is supported in the Cormorant #1 well when considering the large volumes of residual oil in cores taken within the Eastern View reservoir sands.

At Tilana, there is reason to doubt that a structure even existed at time of hydrocarbon migration. Deeper seismic reflections across the Tilana structure show no evidence of thinning. In fact, Tilana seems to have been produced by trans-tensional movement in mid to upper Miocene times, well after the main pulse of hydrocarbon migration.

Bass Ridge

The Bass Ridge is a large structurally positive element approximately thirty kilometers across, exhibiting early emergence during the Cretaceous. The Bass #2 well was drilled on the crest of this feature without finding a commercial hydrocarbon accumulation. Around the perimeter, and defining the flanks of this structure are large normal faults which can be dated as active during the deposition of the Eastern View. It is possible that these faults isolated the crest of the Bass Ridge from migrating hydrocarbons, moving out of the source kitchen immediately adjacent to the west. This hypothesis therefore highlights the Humpback and Red Emperor Prospects as the first major traps on the main migration pathway from the rich source kitchen in the basin deep.

Yolla Field

Yolla Field is an upthrown fault closure, which formed during the early Eocene and remained undisturbed after deposition of the Demon's Bluff seal. Seismic line BB96-54 was shot over both the Yolla and Tilana structures. The differences in structural timing between productive and dry structures (early vs. late) is evident from this profile.

Drillable Prospects

Four main prospective areas have been identified, each containing significant structural closures (ranging between 5,000 and 10,000 acres each) that exhibit growth histories favorable to the trapping of hydrocarbons. These areas which have been assigned prospect names, are discussed individually.

5 cm

BARRAMUNDI PROSPECT

Prospect Type:	Faulted Nose	
Nearest Well Control:	Cormorant #1, Bass #1 and Yolla #1	
Prospective Area:	13,500 acres	
Unrisked Reserves:	13,500 x 250 bbl/ac ft x 100 ft = 337.5 MMBO	
Drilling Depths:	Eastern View	2,300 meters (7,550 ft.)
	Middle Eastern View	2,500 meters (9,000 ft.)
Major Risk:	Fault seals	

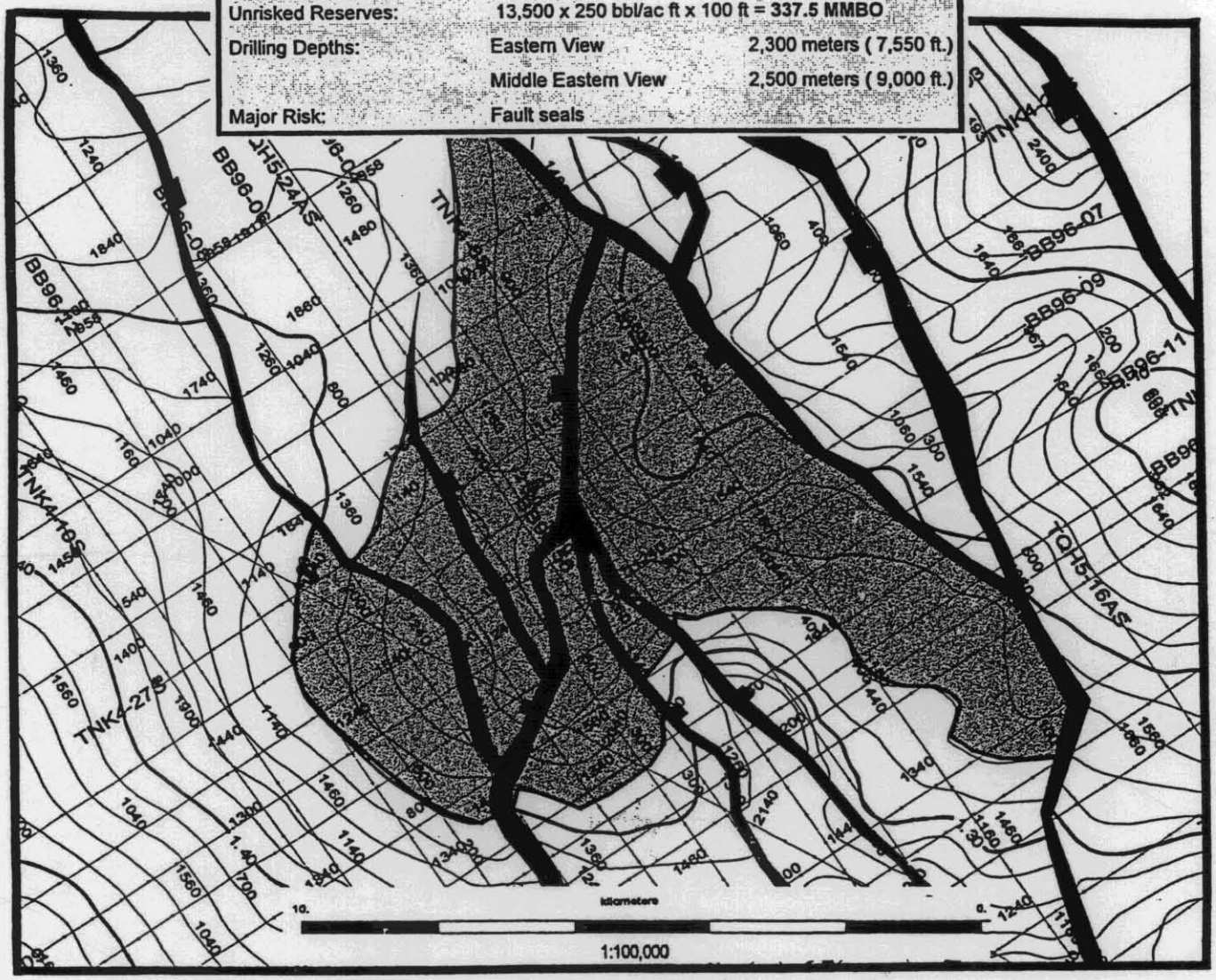

Above the Demon's Bluff horizon, there is little, if any expression to the Barramundi feature. At the Demon's Bluff, Barramundi is expressed as a strong nose projecting out into the Bass Deep Basin. During Eastern View time, active faults cut across this nose showing dip changes and interval growth for prospective Eastern View traps, which were charged after the Demon's Bluff seal was in place. Below the Middle Eastern View, seismic dips indicate that Barrimundi develops into a faulted anticlinal closure with dip into a master fault trending northwest and downthrown to the sowthwest

Excellent Reservoir sands seen in the Cormorant #1, are likely to be present over Barramundi, and the amount of residual hydrocarbons seen in cores indicates an active migration pathway system from the adjacent Bass Deep Basin. Unlike the Cormorant structure, Barramundi does not display seal rupturing upper Miocene movement.

5 cm

BLUE FIN PROSPECT

Prospect Type:	Faulted Anticline	
Nearest Well Control:	Dondu #1	
Prospect Area:	5372 acres	
Unrisked Reserves:	5372 acres x 250 bbl / ac ft x 50 ft = 67 MMBO	
Drilling Depths:	Eastern View	2,500 meters (8,200 ft.)
	Middle Eastern View	2,950 meters (9,700 ft.)
Major Risk:	Structural closure to north	

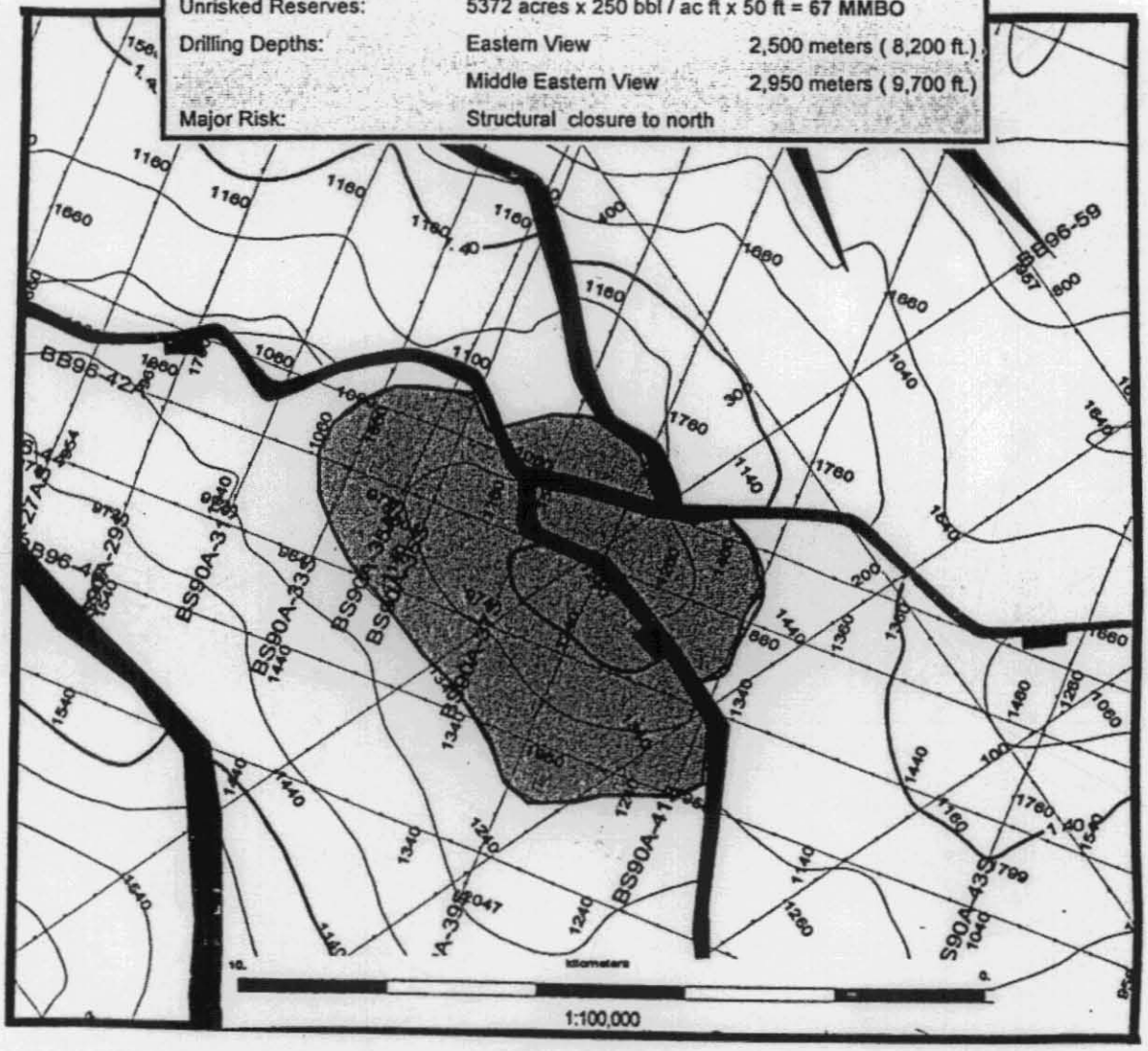

Blue Fin appears to be a pop-up structure associated with a change in direction of an adjacent transtensional fault, similar to, but smaller than the Yolla Field structure. Both of these features are located in the Eastern View source kitchen, and show no evidence of movement post Demon's Bluff.

5 cm

HUMPBACK PROSPECT

Prospect Type:	Faulted Anticline
Nearest Well Control:	Bass #2, Yurongi #1
Prospective Area:	13,956 acres
Unrisked Reserves:	13,956 ac x 250 bb / ac ft x 100 ft = 349 MMBO
Drilling Depths:	Eastern View 2,150 meters (7,000 ft.)
	Middle Eastern View 2,600 meters (8,500 ft.)
Major Risk:	Access to migrating hydrocarbons

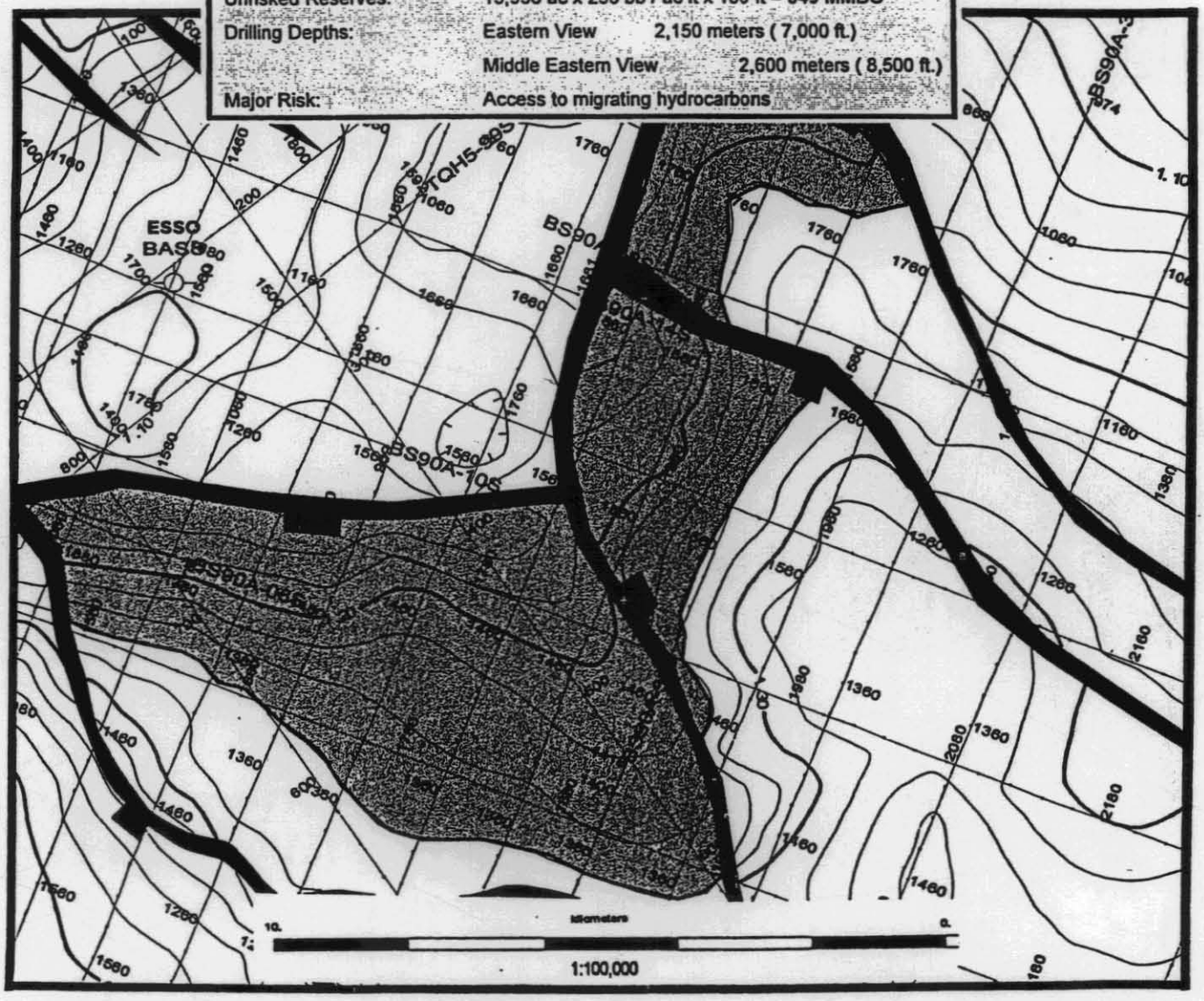

Humpback Prospect is located on the flanks of the Bass Ridge, which appears to be a pre Eocene structure with roots well into the Cretaceous. On the periphery, and defining the flanks of the ridge, are large normal faults associated with downwarp during the formation of Bass Basin Deep. These faults would have been in place when hydrocarbon migration began in the early Miocene, cutting off the crest of the ridge and forming prospective traps around the periphery of the ridge. Esso drilled their Yurongi #1 on the flank of the ridge in an apparent attempt to test this concept. However their location is over 100 milliseconds downdip from either Humpback or Red Emperor. The excellent Eastern View sands seen the Yurongi well should be present at both Humpback and Red Emperor.

5 cm

RED EMPEROR PROSPECT

Prospect Type:	Faulted Anticline	
Nearest Well Control:	Yurongi #1, Bass #2	
Prospective Area:	9124 acres	
Unrisked Reserves:	9124 ac x 250 bbl / ac ft x 100 ft = 228 MMBO	
Drilling Depths:	Eastern View	2,150 meters (7,050 ft.)
	Middle Eastern View	2,600 meters (8,500 ft.)
Major Risk:	Fault seals	

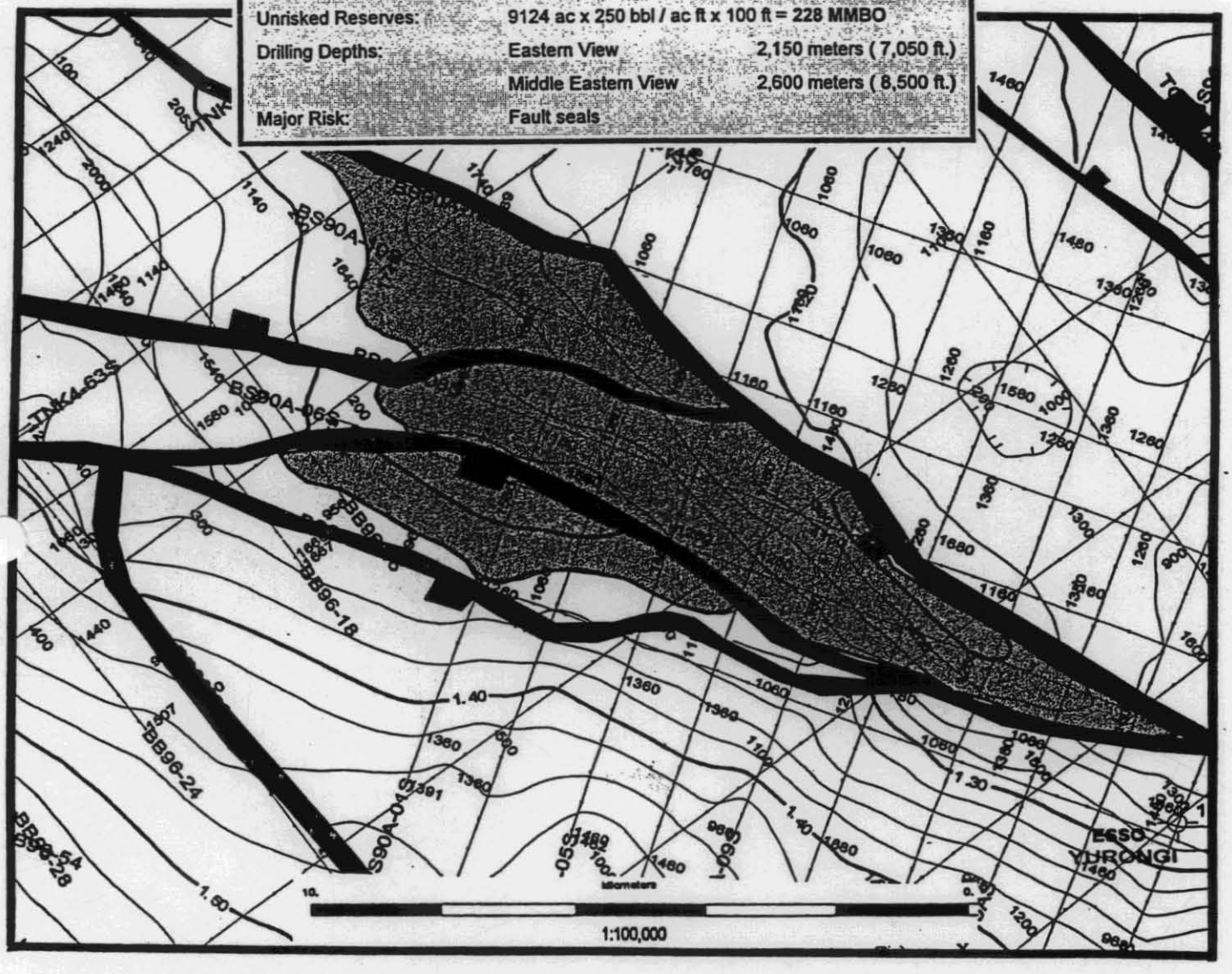

Red Emperor Prospect is located on the flanks of the Bass Ridge, which appears to be a pre Eocene structure with roots well into the Cretaceous. On the periphery, and defining the flanks of the ridge, are large normal faults associated with downwarp during the formation of Bass Basin Deep. These faults would have been in place when hydrocarbon migration began in the early Miocene, cutting off the crest of the ridge and forming prospective traps around the periphery of the ridge. Esso drilled their Yurongi #1 on the flank of the ridge in an apparent attempt to test this concept. However their location is over 100 milliseconds downdip from either Humpback or Red Emperor. The excellent Eastern View sands seen the Yurongi well should be present at both Humpback and Red Emperor.

Seismic Control

In block T 27/P, approximately 1,200 kilometers of vintage seismic data acquired variously by Shell, and Amoco and Bridge have been reprocessed and in addition to the new seismic which was acquired by Globex in February of 1996. All 3,700 kilometers of seismic has been mapped on five horizons which include:

- Top Volcanics
- Base Volcanics
- Demon's Bluff
- Eastern View Coal Measures (EVCM)
- Middle Eastern View

Seismic horizon identification was achieved by computing synthetic seismograms in the key wells which directly tie the seismic grid under evaluation. These wells include:

- Cormorant -1
- Dondu -1
- Nangkero -1
- Tilana -1
- Yolla -1
- Yurongi -1

At each well, the reflection series tops were correlated based on seismic character, log character as well as tops based paleo control. Plots of each synthetic seismogram and the resulting seismic ties are included with the final maps and seismic sections in the maps volume of this report.

Due to time constraints, match filters to phase tie each of the various survey vintages were not produced, but each survey was time shifted to tie the Globex BB96 survey which provided a baseline for corrections. Average bulk time shifts applied ranged between 15 and 28 milliseconds. Seismic data is considered to be of good quality for all horizons mapped except for the Middle Eastern View. The Middle Eastern View horizon is highly effected by multiple reflections from the relatively hard sea floor which were not sufficiently suppressed by the initial data processing.

BARRAMUNDI PROSPECT

AVO REPORT

BLOCK T27P
BASS BASIN AUSTRALIA

Presented to:

GLOBAL EXPLORATION INC.

Dallas, Texas, USA

By:

EXPLORATION CONSULTANTS
Suite #106, 8499 Greenville
Dallas, Texas, USA 85231
(214) 503 – 7066

April, 97

CONTENTS

CONCLUSIONS

- There are normal incidence and AVO anomalies over the Barramundi Prospect which represent fault bounded reservoirs

- Estimates of reservoir thickness range upwards from one hundred eighteen feet, to as much as 300 feet.

- These Reservoirs cover an area of some fourteen thousand acres.

- They are likely filled with oil and dissolved gas whose GOR ranges from 1700 to greater than 4500 : 1.

- Potential Reserves are estimated to be 420 Million barrels of oil.

- There are additional anomalies among the coaly portion of the EVCM, which are not included in this analysis.

Overview and Results

Normal Incidence Investigation

During the early stages of Barrimundi structural interpretation, an obvious amplitude anomaly was observed covering the Barramundi structure. It was realized that this anomaly was very likely a Direct Hydrocarbon Indicator (DHI). This investigation was initiated to determine if this anomaly could be supported by an in depth examination.

A Normal Incidence interpretation of this DHI anomaly in the Barramundi prospect indicated that it was similar to the anomaly observed in seismic over Yolla field. These anomalies are characterized by:

- Seismic trough representing the top Eastern View pay sand
- Trough increased in amplitude on structure;
- Time thickness (side peak to side peak) of trough increases up dip;
- Trough dims in amplitude downdip at a common record section time.

The depth of the trough is interpreted as relating to the relative increase in hydrocarbon saturation of the reservoir. Likewise, the increasing isochron thickness of the anomaly is related to the relative reduction in the interval transit time due to hydrocarbons replacing formation water. The simultaneous termination of these characteristics at a common downdip seismic record section time, is interpreted to signify a common downdip water level in the reservoir.

By overlaying the anomaly isochron map on the AVO anomaly outline map, it appears that twenty-six milliseconds is the downdip limit of the normal incidence anomaly. If this represents the water leg of the reservoir, then using values for porosity and matrix velocity seen in the Cormorant, then the calculated thickness of the sand is 118 feet. Utilizing the same parameters, and holding sand thickness constant, then isochron thickness greater than thirty feet are hydrocarbon productive with increasing GOR with larger isochron values. This translates into an oil productive area of about 10,000 acres and a high condensate yield a productive area of about 2500 acres. These thickness do not include the main body of the sand seen the cormorant well, but are simply for the uppermost EVCM sand, which is also the cleanest sand. The reservoirs below exhibit anomalous characteristics, but are more difficult to analyze because of their variable porosity and the presence of coals.

Amplitude vs. Offset Investigation

In the seismic offset domain, synthetic models generated from well logs, and actual seismic well ties, indicate that pay sands in the Yolla Field display a negative normal incidence intercept (trough) and a positive amplitude gradient. A similar pattern is observed over the Barramundi prospect which transitions into a flat gradient and shallow intercept time at a common downdip seismic record section time. This latter pattern is characteristic of water bearing sands, as seen in the Cormorant well tie. These responses are illustrated below:

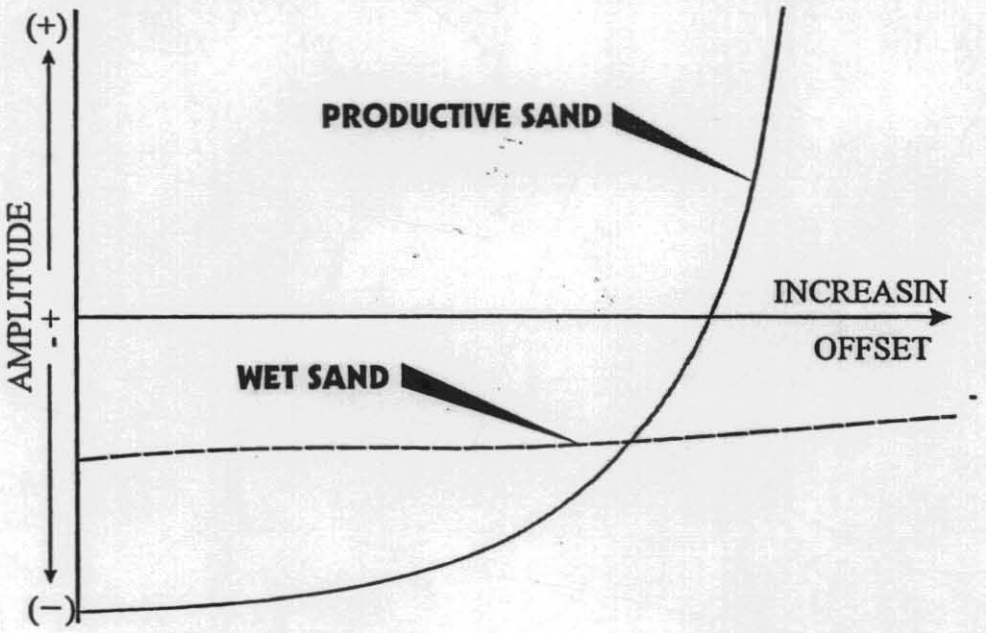

The Barramundi Prospect AVO anomaly:

- Is coincident with the area of the Normal Incidence anomaly
- Fits the structural interpretation
- Is similar to the anomaly seen over Yolla Field
- Third term curvature increases along the pattern of the NI isochron

Oil is distinguished from gas by greater AVO curvature and deeper negative intercept value. It must be said however that increasing reservoir porosity can produce this same effect. However given the same porosity, the effect produced by the difference in pore fluids is illustrated below:

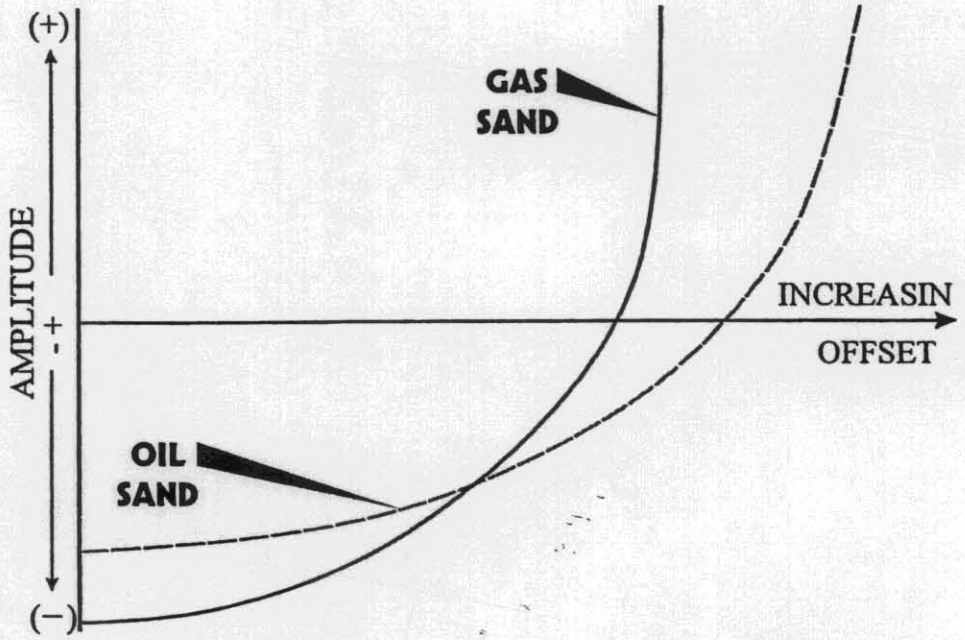

Interpretation of AVO responses in the Bass Basin is complicated by the presence of coals and igneous materials in the prospective section as well as interfering multiples in the middle and lower EVCM. These responses are shown in the following figures:

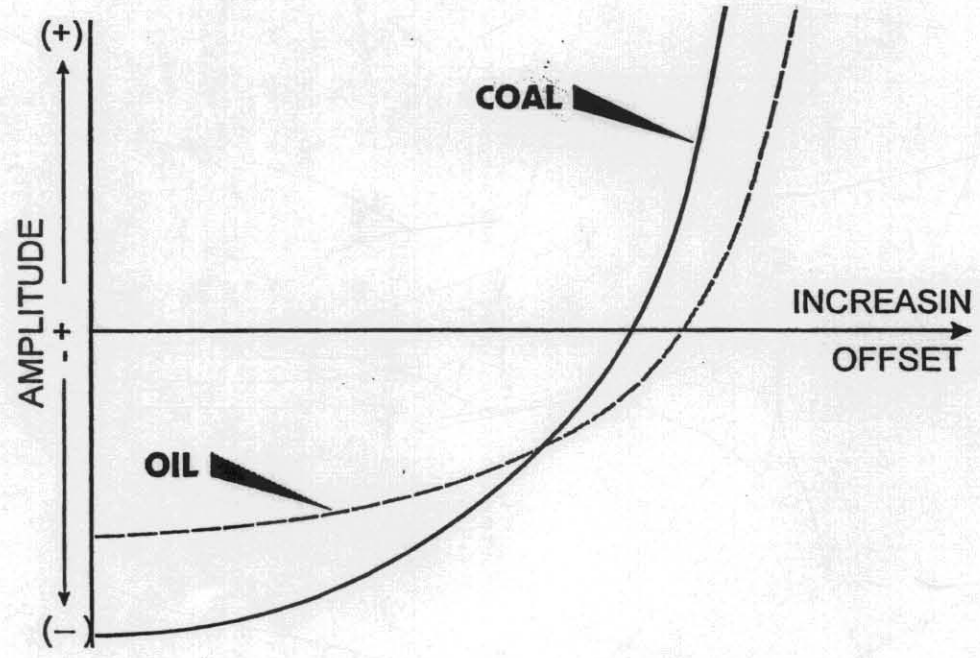

The response of igneous bodies is distinctly different from that of prospective reservoirs, as illustrated below:

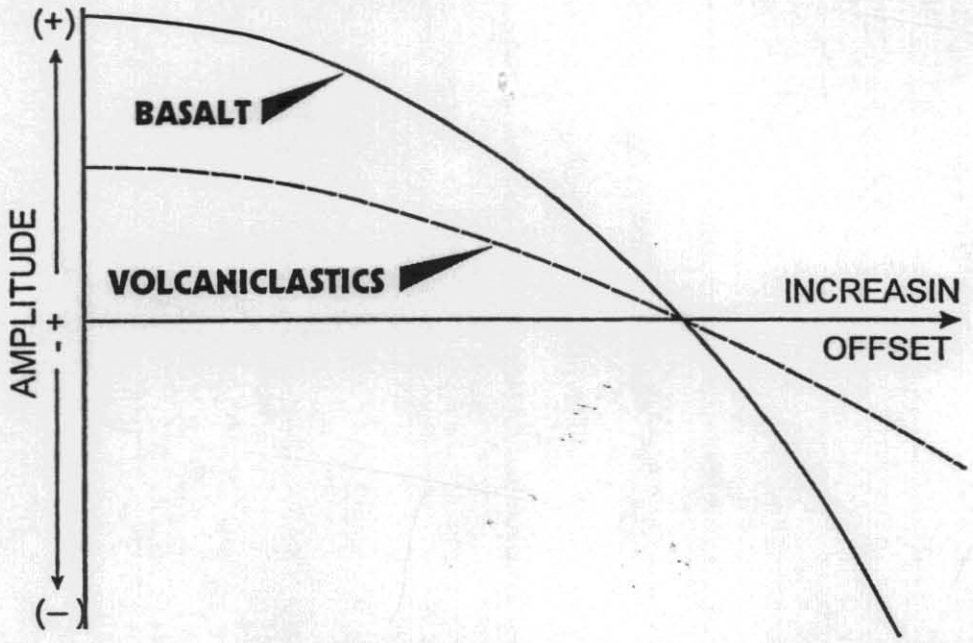

Clearly, basalts and volcaniclastics are easily distinguishable from other lithologies. However, separating coals from productive sands is more difficult, in that the normal incidence intercept is negative and the amplitude gradient is positive for both.

Spatial Mapping

Since the target of this project , hydrocarbon filled reservoirs, and coals have the same general offset response, they must be identified by other means. By mapping the spatial distribution of the anomaly in question, and comparing its behavior with structural position, we were able to distinguish coal from hydrocarbon filled reservoirs. Because its environment of deposition controls the distribution of coal, there is no reason for coal to conform to the present day structure trap, as does the Barramundi anomaly.

Spatial mapping of the following Normal Incidence and AVO hydrocarbon indicators was done, and these maps are attached to this report in the AVO Interpretation Map Atlas:

- RMS Amplitude
- Anomaly Isochron
- Product Gradient
- AVO Anomaly Extents
- Instantaneous Amplitude

From the **RMS amplitude map**, it is evident that line to line amplitudes ties need to be adjusted through Line Tie and Grid Balance processes. Future work on this project needs to incorporate this step. In general, a qualitative relationship between depth of trough amplitude and structural position is apparent, supporting the hydrocarbon filled reservoir interpretation.

The **Anomaly Isochron map** is contoured on the anomaly's side lobe to side lobe time thickness. This map shows an apparent time thickness increase from the flanks of the structure to the crest of almost 40%. It is very suggestive that the isochron fits the time structure map. By comparing the isochron to structure, it appears that an isochron time thickness of 0.027 seconds represents the spill point of the structure, and probably the downdip limit of producable hydrocarbons. This conclusion is supported by the limits of hydrocarbon response shown on the AVO Anomaly Extents map. The magnitude of isochron thickness increase is interpreted as a strong hydrocarbon indicator, which we believe is related to increasing amounts of dissolved gas in the reservoir as one moves up dip.

Because of the amplitude grid not being balanced, the product gradients do not tie from line to line on the **Product Gradient map**. There is however, a strong relationship between higher structural position and increasing negative product gradient, which is another indication of hydrocarbons.

The **AVO Anomaly Extents map** portrays the downdip limit of AVO Hydrocarbon Response, connected from line to line to indicate the overall shape of the anomaly. This Outline, when compared to anomaly time structure, follows the general shape of the time structure.

Mapping Conclusions

It was admitted from the outset, that on an individual normal incidence or AVO profile, we would be unable to distinguish between coal and hydrocarbon saturated reservoirs. By analyzing the spatial patterns of these responses, we are able to eliminate coal as an interpretative choice, since we find no reason to explain why coal should:

- Thicken over the present day structure.
- Truncate downdip at a common structural point.
- Appear in a stratigraphic section relatively free of coal in the Cormorant

However, all of these characteristics are typical of hydrocarbon filled reservoirs.

Individually, each of these observations is suggestive of a hydrocarbon filled reservoir. However, it is the combined weight of each of these mapped indicators overlain and compared to one another, and to the Barramundi

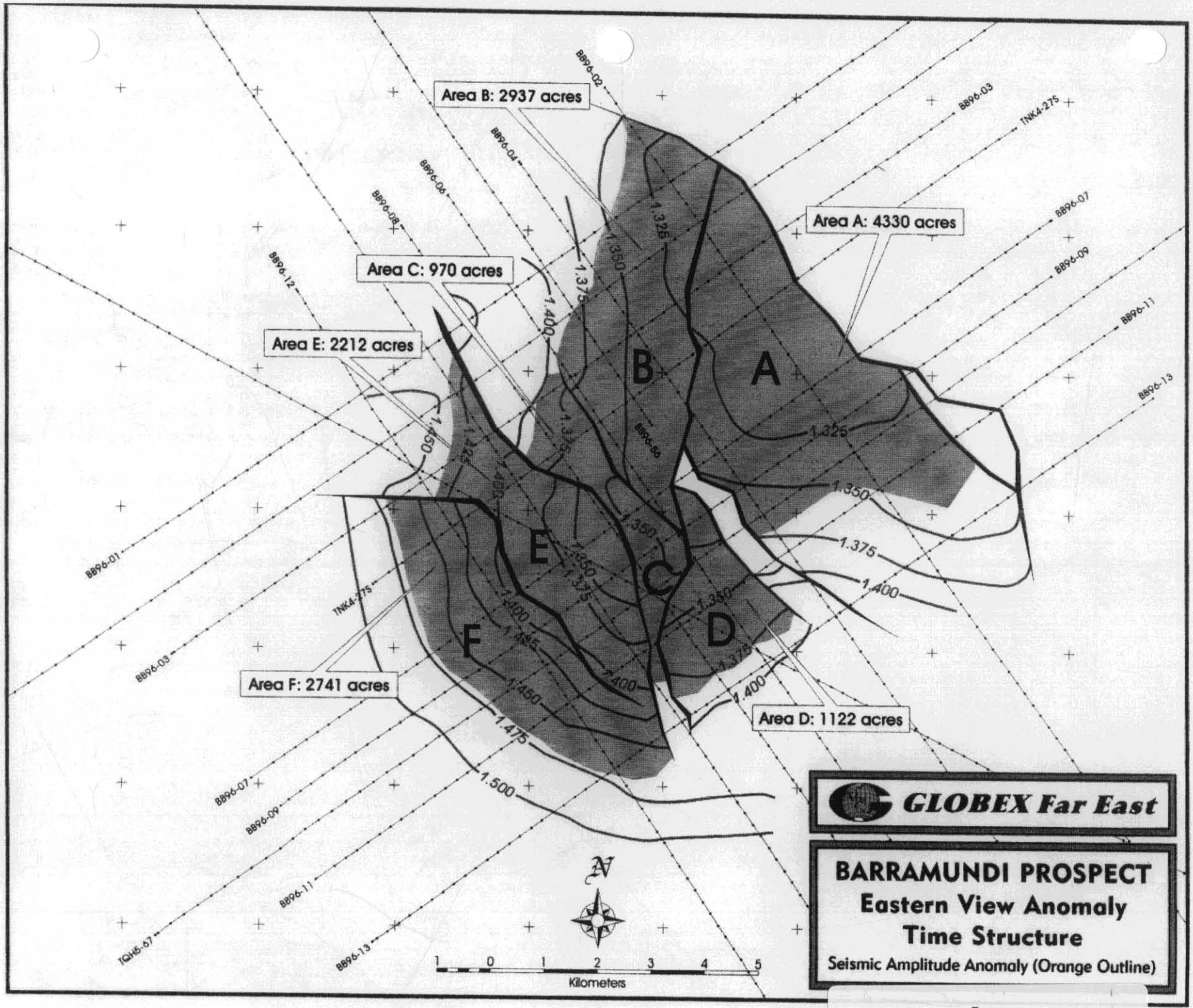

Barramundi Prospect

structure, leads to the conclusion that the observed Barramundi anomaly is a valid hydrocarbon indicator, similar to that producing in the Yolla Field. Further indications are that reservoir porosity, areal extent and thickness are greater at Barramundi than at Yolla, an indication supported by the quality of Upper EVCM sands seen at Cormorant.

Reservoir Thickness Calculation

Since the absolute thickness of reservoir sandstone was unknown, we assumed the trough to peak time interval represented the time thickness of the reservoir. Utilizing matrix velocities from the Cormorant this resulted in a thickness of 118 feet. We also assumed that this thickness remained constant over the Barramundi structure, which necessitated varying the reservoir GOR to explain the isochron thickening up dip. These assumptions also result in a water level at approximately the 0.027 sec isochron.

While we believe this assumptions to be reasonable, and consistent with the data, there are other assumptions that could be made. For example, the change in isochron thickness can be explained by varying the porosity and pay thickness. The strong relationship of isochron thickness to structural position compelled us to explain this behavior by varying the GOR between 1700 and 4500:1

Given the amount of seismic waveform tuning in response to this stratigraphic section, and the sand thickness in the Cormorant well, it is entirely possible that the base of the sand is masked and is actually much thicker. Possible thicknesses range up to a half wavelength or more, in the order of 250 to 300 feet.

Estimated Reserves

The AVO anomaly covers more than 14,000 acres, in six fault bounded compartments. Using a recovery factor of 250 barrels oil per acre-foot and an average pay thickness of 120 feet:

14,000 ac ft x 250 bbs / ac ft x 120 ft = **420 million barrels oil**

DHI Investigation

Seismic Processing

During the acquisition of the current data set, five-foot seas and more were typical, which is characteristic for Bass Strait. Some fifteen lines had to be re-shot because of noise problems, mostly in the form of cable jerk. This noise is widely separated from reflected arrivals and a simple K-F filter was found to be extremely effective in dealing with this problem. Another problem, associated with the sea conditions was the variation in air gun depth. This caused a variable source pulse and source strength. Shot consistent amplitude recovery was found to be necessary to balance amplitude from one shot to the next.

Among the EVCM sands and shales, are interbedded basalts, coals and other volcanic products, which are strong seismic markers, particularly in the middle and lower EVCM. Also in the Miocene volcanic interval above the Demons Bluff, there are some strong seismic contrasts. These markers set up a system of interbed multiples, which is too complex for deconvolution to handle effectively. By picking closely spaced panels and inputting them into a tightly constrained Tau-P process, followed by deconvolution, we were able to dramatically improve the reflection to multiple amplitudes as is shown in the following examples.

5 cm

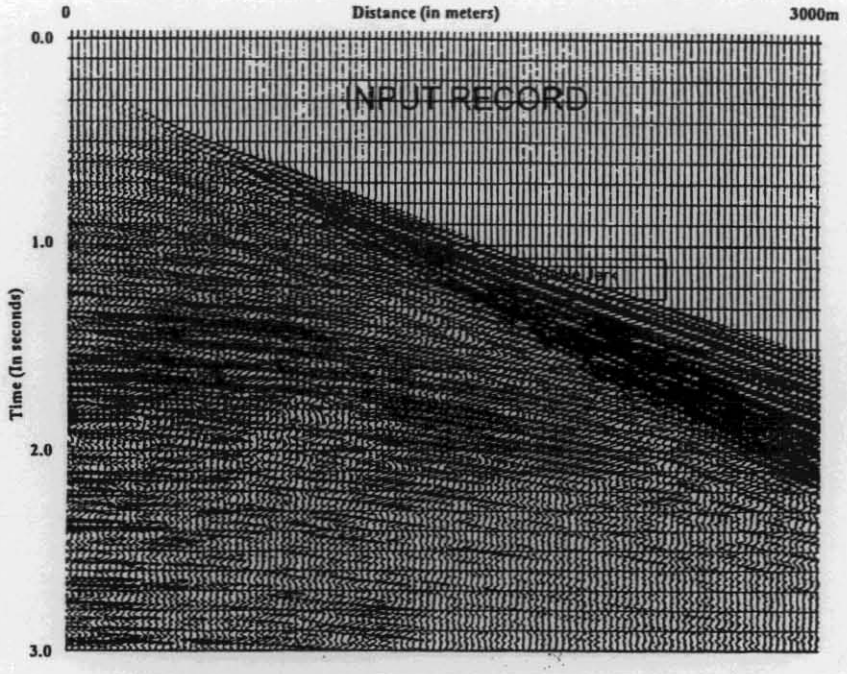
0
Distance (in meters)
3000m
0.0
INPUT RECORD
1.0
Time (In seconds)
2.0
3.0

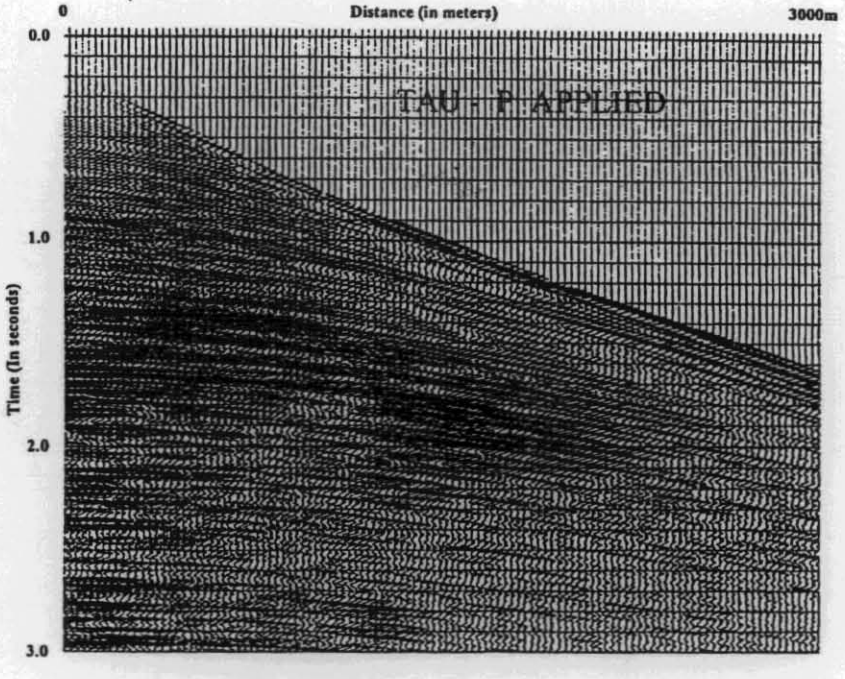
0
Distance (in meters)
3000m
0.0
TAU - P APPLIED
1.0
Time (In seconds)
2.0
3.0

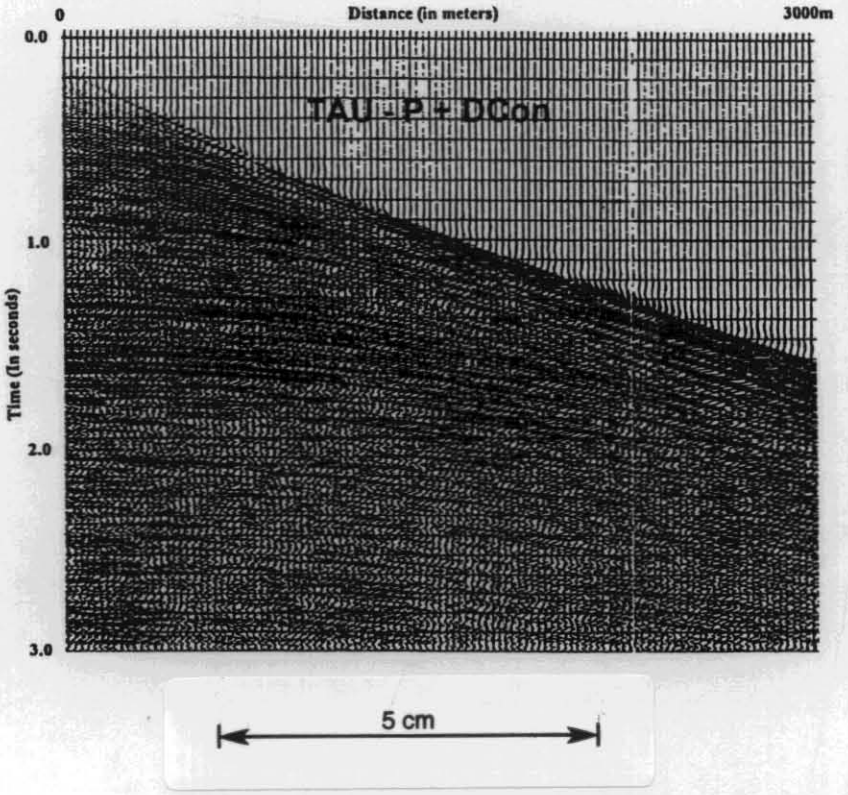

Supergather Signal enhancement

Through comparison of noise reduction achieved from three on one to five on one, it was found that the three on one supergather was sufficient to suppress random noise without enhancing the multiple content. This also acted to moderate some of the shot to shot amplitude variations, in addition to the one second window in which shot wise amplitude balancing was run.

After preprocessing, the data were processed for AVO interpretation and analysis. AVO Attributes Calculated for each line and are found in the Seismic Atlas appended to this report. A brief discussion of the interpretative significance of these attributes is given in the interpretation section. The attributes generated were:

- Normal Incidence Stack
- Instantaneous Amp
- Instantaneous Phase
- Instantaneous Frequency
- Product Gradient

Well Log Models

The lithology of the EVCM contains some prominent seismic markers. The extremes range from high seismic impedance lithologies such as basalts to low impedance lithologies such as coals. Three wells were modeled to determine the Normal Incidence and AVO Response, these were:

- AMOCO #1 Tilana
- AMOCO #1 Yolla
- ESSO #1 Cormorant

These models were generated using GMA software. In each model, Normal Incidence traces were derived using a wavelet whose frequency content matched that of the data. Offset traces were then calculated to determine the AVO response for the zone of interest. Values for formation density and compresional velocity were taken from density and sonic curves furnished in the digital well log suite. Default values were used for Poisson's ratio, except for coals, which were taken from published values for Permian coals in southeast Australia. In the study wells, the opportunity was present to model the following lithologies:

- coal
- basalt
- volcaniclastics
- wet reservoir sands
- oil bearing reservoir sands

These lithologies are identified in the lithology column of the models attached in APPENDIX III. By varying the thickness of one of these lithologies, it was possible not only to model the seismic response to the actual thickness found in the well, but determine the response of the end members as has been done for pay and coal thickness presented in APENDIX III

From these models, it was determined that:

- Eastern View pay sands will be displayed on the BB96 data as a trough

- Wet sands are shown as a weak normal incidence trough and flat offset gradient as is shown in the figure below:

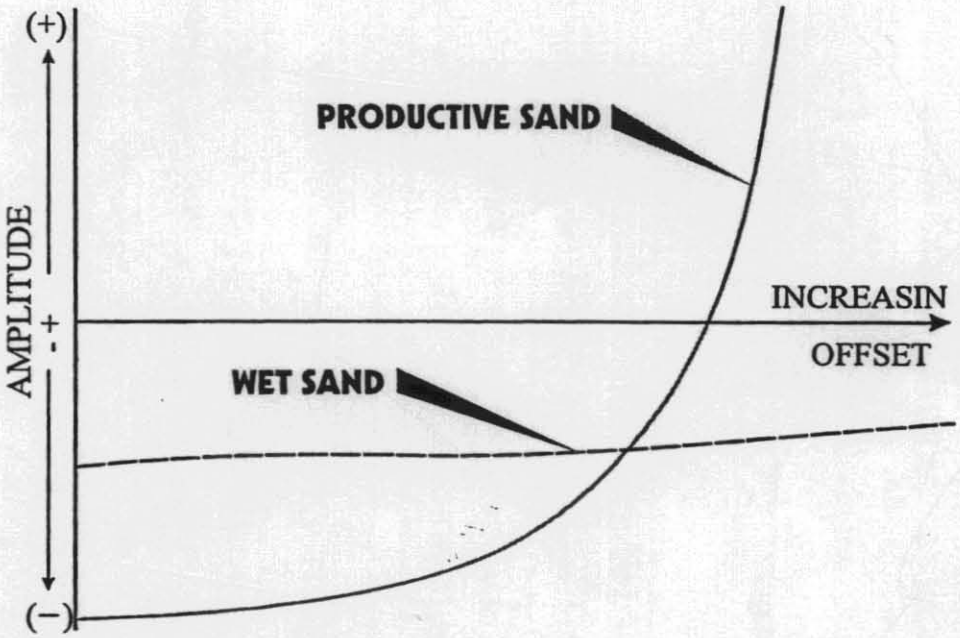

- Hydrocarbon bearing sands are displayed as a larger negative trough at normal incidence. The AVO response of hydrocarbon sands is a positive gradient with strong curvature beyond reflection angles of 27° as shown in the figure above.

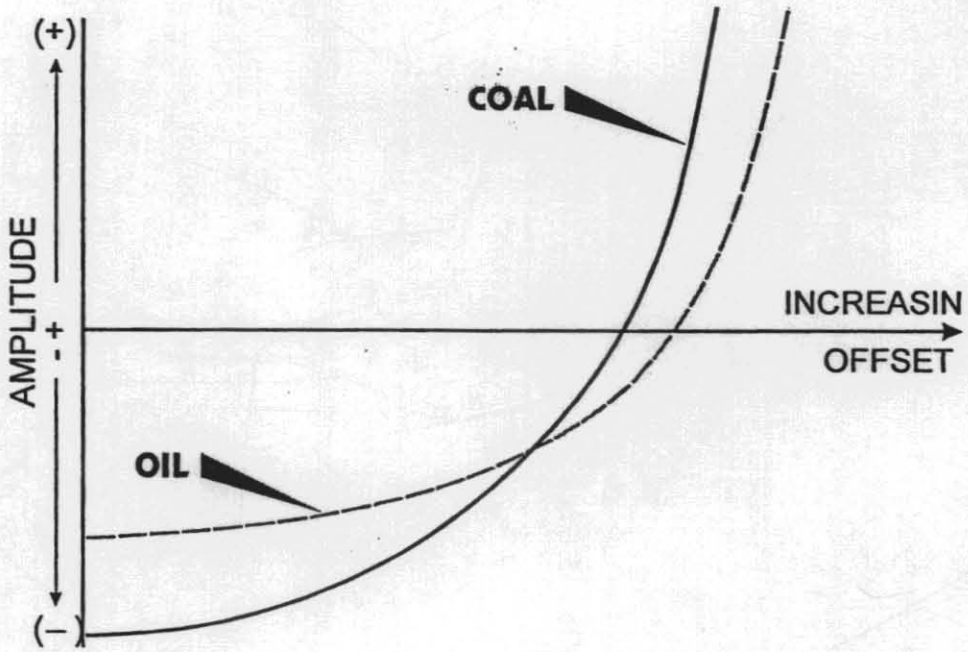

- The AVO response of coal in the Eastern View is similar to that of an oil pay sand. This is not surprising since coal has high porosity and high hydrocarbon saturation as is shown in the figure above.

- There is little or no distinction between oil pay sands and coals, in the normal incidence domain. We will have to rely on the fact that oil filled reservoir sands will conform to the structural trap and coals will not.

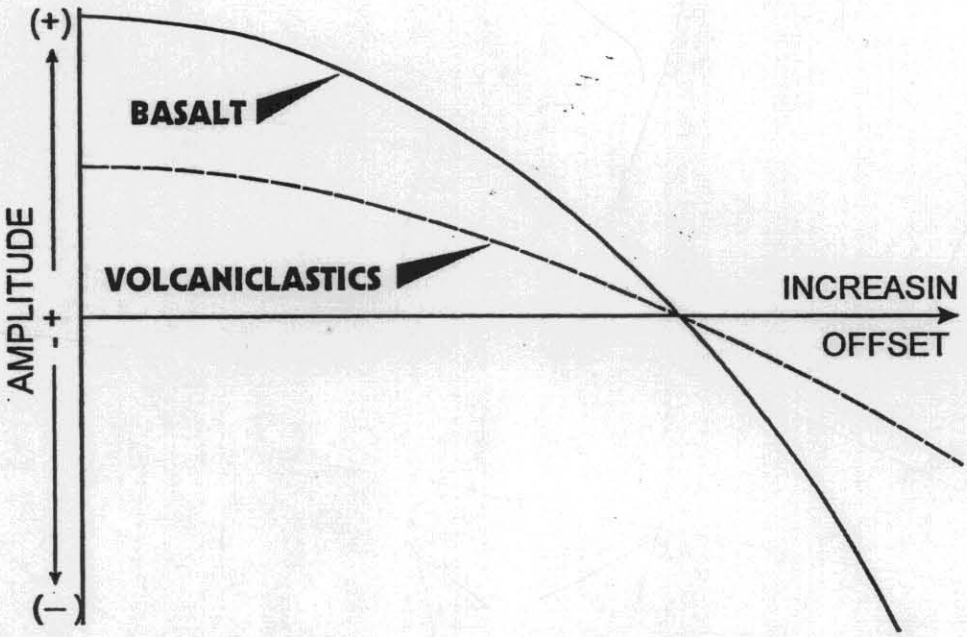

- Basalts have a distinctive Normal Incidence and AVO signature. Starting with a strong positive reflection coefficient at zero offset, the amplitudes response is flat out to a reflection angle of about 26°, where the reflectivity rapidly diminishes to zero at about 35°, as seen in the illustration below:

- Volcaniclastics show a wide variation of both normal incidence and AVO behaviors. Typically these are seen as positive reflections with flat to slightly negative offset amplitude gradients as is depicted in the illustration below.

Cormorant Well Model

The normal incidence model indicates weak negative reflections for the wet sands in the upper most EVCM between depth1 and depth2. Similarly, the AVO response for these sands is flat to slightly negative. Below these sands are a series of strong negative reflectors with positive AVO gradients associated with the coal series.

For the thickest of these sands, marked as S_2 on the model, a Gassmann substitution of the pore fluids was made from water bearing to high GOR oil. Note the significantly deeper trough and strongly positive (less negative) amplitude with offset gradient. It is this sand interval which correlates with the Normal Incidence and AVO anomaly seen at Barrimundi. The modeled anomaly is very similar to the anomaly over the Barramundi Prospect, an example of which is shown in the AVO Interpretation section of this report.

About a thousand feet below the Top of EVCM there are a series of thin coals (three to six feet), which due to their spacing set up a tuning effect that results in a bright banded set of reflectors. These reflectors can be traced from the line BB96-50 tie to the Cormorant well, across to the Barrimundi Prospect. This band of reflectors largely prevented us from being able to evaluate potential deeper anomalies.

Yolla Well Model

Of primary interest in this well is the productive zones. The forty-foot thick oil pay zone at about 6000 feet, immediately below the Top of EVCM, is expressed as a seismic trough. Several tests were taken in this zone resulting in flow rates from 1198 BO and 2.2 MMCF to 892 BO and 11.8 MMCF. This results in calculated GOR's from 1836:1 to 3377:1, depending on the zone tested. This variable GOR, from what has to be the same reservoir, is in our view due to permeability variations within the zone tested. Since gas is about 100 times more permeable than oil, we believe the lower figure more accurately represents reservoir gas saturation. Seismically, this sand is characterized by a larger negative trough at normal incidence, than wet sands, and in the offset domain shows a positive gradient with strong curvature beyond reflection angles of 27° .

A significant amount of dry gas, up to 15 MMCF was tested in a lower zone below 9000 feet, but this sand appears to be relatively tight from well logs, and it is problematical that this zone could sustain these rates. Since the vertical separation between these two zones is insufficient to explain this dramatic difference in GOR, and the fact that most of the source rocks in this portion of the basin are still within the oil generation phase, we also assume this is related to reservoir permeability. This zone models with much the same response as

the oil zone above, which may be further evidence that ratio of dissolved gas is much lower than indicated by the production test. The fact that the Normal Incidence and AVO response is much weaker than that of the shallower zone, when in fact gas should give a stronger response, is also taken to mean this interval is lower in porosity.

Also of interest is the response of the three hundred-foot thick Igneous layer around 8500 feet. The seismic response of this layer is totally unlike any of the other lithologies modeled in this well. Starting with a strong positive reflection coefficient at zero offset, the amplitudes response is flat out to a reflection angle of about 26°, where the reflectivity rapidly diminishes to zero at about 35°.

Tilana Well Model

This well was chosen to model because of the relatively thick volcaniclastic and igneous layers within the EVCM. The nearly homogenous igneous body at approximately 6700 feet exhibits minor internal reflectivity, while the volcaniclastics layer from 10,000 feet to TD is seismically active with strong internal reflectors, related to variety of textures, densities and matrix velocities typical of these types of rocks.

Predictive Analysis

Limiting Factors

As in every DHI investigation, there are limiting factors affecting NI and AVO Interpretation. Below are factors, which were weighed during the investigation, along with our assessment of the impact each factor has in contributing to the overall accuracy of our predictions:

- *Lack of shear wave information from any wells in this basin* required us to use default values for shear velocities. The greatest cause of concern was the values to be used for coal. There is an extremely wide range of possible values for coal depending on the type of coal, depth of burial, hydrocarbon saturation etc. For this study, values used were taken from published values given for Permian coals in Southeast Australia. These values, if in error probably de-emphasize the effect of coal.

- *Less than optimum cable lengths* were used in all of the seismic data acquired in this area. Since the AVO effect of pay sands is most prominent beyond reflection angles of 27°, a streamer length of 15,000 feet would have been desirable. This longer cable would also magnify the cable jerk noise problems discussed earlier.

- *Inadequate source input.* On the weaker shot records it was apparent that there was a loss of reflection amplitude simply due to spherical spreading on all events, not just the event under discussion. It is our view that these records represent a small sample of the overall database. In addition, the effect of the three on one supergather was to minimize this effect.

- *Inconsistent source input.* Due to wave action, the air guns were firing at varying water depths affecting source strength and signal. Again the effects of the supergather helped mitigate this problem.

- *Noisy input records.* In an effort to reduce noise, seismic processing was necessary which had the potential of disturbing the amplitude relationships we were trying to measure. Every possible precaution was taken to ensure that this didn't happen.

- *Lack of amplitude tie.* Due to the problems discussed above, and software limitations, it was not possible to deal with this problem effectively. Consequently were reluctant to make quantitative judgments, regarding bed thickness involving tuning.

- *Amount of faulting in reservoir.* The segmented reservoir in this case meant that in any segment, there were a limited number of common downdip terminations with which pinpoint water levels.

Conclusions

- There are normal incidence and AVO anomalies over the Barramundi Prospect which represent fault bounded reservoirs

- Estimates of reservoir thickness range upwards from one hundred eighteen feet, to as much as 300 feet.

- These Reservoirs cover an area of some fourteen thousand acres.

- They are likely filled with oil and dissolved gas whose GOR ranges from 1700 to greater than 4500: 1.

- Potential Reserves are estimated to be 420 Million barrels of oil.

- There are additional anomalies among the coaly portion of the EVCM, which are not included in this analysis.

Future Work

A great deal more analytical interpretative work could be done on this data set to enhance its predictive results. There are several important preconditions to initiating an extended study. These are:

- Gaining a better well tie within the anomaly area
- Obtaining pertinent shear wave data
- Grid balance and amplitude tie data set

Meeting these requirements would enable us to perform an AVO inversion which, would greatly enhance our ability to predict:

- Sand thickness
- Reservoir porosity
- Reservoir fluids and GOR
- Enable to look for pays in the lithologically more complex Middle EVCM

Guide to Presentation Exhibits

In the late Mesozoic, during the separation of Tasmania from continental Australia, three major sedimentary basins were formed. From west to east, these basins are known as the Otway Basin, the Bass Basin, and the Gippsland Basin. As a result of intense exploration and drilling over three decades, the Gippsland Basin, which is the most prolific producer of hydrocarbons in Australia has produced over six billion barrels oil and gas from more than a dozen world class fields.

The major oil and gas reserves in the Gippsland Basin are produced from the *Latrobe Petroleum System* comprised of Eocene aged sandstone reservoirs that are sourced by Eocene and Paleocene coals and shales of the Latrobe Group. **This same geology is present in the Bass Basin.** When cores from these sister basins are compared, they are indistinguishable. **Thus, the Bass Basin should be as prolific as its more heavily explored neighbor.**

It was this observation that led *Globex*, among other companies, to take a new look at the geographically larger Bass Basin to determine if high impact exploration opportunities might still exist. The T27/P Block operated by *Globex* incorporates an area that can encompass all of the production within the Gippsland Basin (see: *Generalized Top Latrobe Structure*, GIPPSLAND / BASS BASIN ANALOGY display)

Gippsland Geology

Regional tectonic elements affecting the basins of the Bass Strait are shown on the FACIES DEVELOPMENT display, which shows these basins being formed by trans-tensional forces acting across the Pangean Continental Plate as it broke up during the late Mesozoic. The Gippsland Basin was filled with clastics from source grounds located in the present day State of Victoria transported from northwest to southeast during the Cretaceous through the Eocene. The best production from these upper Latrobe (Paleocene to Eocene) clastic reservoirs is located in the deepest part of the basin. These reservoirs were charged by migrating hydrocarbons which were generated in deeper Latrobe Group coals and shales.

This preferred area, associated with this production is shown on the seismic cross section (GIPPSLAND/BASS BASIN ANALOGY) as the fault bounded central deep where the richest source rock accumulated in the greatest thickness. From the *Generalized Latrobe Structure,* it can be seen that there are no significant fields on either bounding terrace, away from the source kitchen, indicating a lack of effective long distance hydrocarbon migration. To portray a sense of scale, the outline of the Globex license is portrayed on the *Generalized Top Latrobe Structure map*.

Bass Basin Stratigraphy

The Bass Basin results from the same set of regional tectonic elements that effect the entire Bass Strait shown on the FACIES DEVELOPMENT display. The basin was formed by trans-tensional forces acting on the thinned and extended crust underlying the

Bass Strait. The basin of the Bass Strait opened as an irregular series of sharply divided sub-basins created and separated by transform faults. The deepest of these sub-basins, quickly formed permanent, anoxic lacustrine environments, where coaly and agal source material accumulated. Within the Bass Basin, the greatest volume of these source rocks is depicted as the Paleocene thick shown on the PALEOCENE GEOGRAPHY display. Based on analogy with the distribution of prolific production observed directly adjacent to the source kitchen mapped in the Gippsland Basin, it is our conviction that any major exploration opportunity will be found in close proximity to the *source kitchen*, which crosses the southwest portion of the Globex permit. As rifting and regional subsidence continued, these basins were connected into larger lacustrine bodies supporting large-scale currents and tides, which tended to oxygenate and suppress source rock production.

The source grounds which provided sediments to fill the Bass Basin are located in present day Tasmania to the south, and are comprised of a complex of metamorphic and igneous rocks of Paleozoic age. This source area provided sediments containing a strong lithic component. The effects of this lithic component are evident when observing the extremely low permeabilities and porosities (depicted on the *Core Plug Analysis* - FACIES DEVELOPMENT montage), plotted from core plugs located on the southern margin of the basin. This area of the basin is closer to the point of sediment input and less prone to clean up due to winnowing and resorting. It is this poor quality reservoir that has precluded commercial success in the southern half of the basin. Five wells drilled on the Pelican structure, near the southern margin, all encountered hydrocarbons, but their sustained flow rates are not commercial.

The high values of porosity and permeability shown on the *Core Plug Analysis* display are from samples taken from wells located on the margin of the on-trend with the Globex permit. Calculated mineral volumes for individual wells in this trend are displayed on the *Reservoirs of the Barrier Bar Trend,* FACIES DEVELOPMENT montage, along with calculated values of porosity and permeability. This trend of highly porous and permeable sands were deposited along the northern flank of the basin as migrating lacustrine bars, which are composed of reworked sands from the deltas fringing the southern margin of the basin. These sands have been extensively winnowed and sorted. Bars were formed by strong circulation patterns, which developed in the increasingly large and open body of water covering the basin at the close of the Eastern View regressive cycle and the beginning of the Demon's Bluff transgressive cycle.

Stacked sequences of these sands have been penetrated in close proximity to the Globex block that measure up to one hundred and fifty (150) meters thick. **It is only in this area of the Bass Basin that the combination of excellent reservoirs and thick proven, hydrocarbon source rocks are found on well structured Eastern View fault closures. In this immense area (nearly two million acres), only nine wells have been drilled in this highly prospective trend, one of which encountered commercial hydrocarbons.**

Bass Basin Structure

As is depicted on the *Present Day Structure* portion of the PALEOCENE GEOPGRAPHY display, the Bass Basin is an asymmetric extensional basin, whose thalwig runs northwest – southeast along the north east flank of the basin through the

Globex permit. The section below the Top Eastern View (Eocene Reservoir), shown in green is dominated by tilted fault blocks. Faults are largely buried and do not cut high into the shallow section. Above the Demon's Bluff (Eocene Top Seal), shown in yellow, basin sag and fill characterize the section.

The PROSPECTS AND LEADS display illustrates the trap styles that dominate the prospective barrier bar sand trend mapped at top of Eastern View. Interpretation of over 5,000 km of 2D seismic reveals tilted fault blocks and anticlines, some of which have been tested by earlier operators. Four currently identified prospective areas within the block are highlighted in orange. Three of these prospects are shown on this display and Barramundi Prospect is shown separately on the Barramundi Prospect display. Prior to discussing these areas, it is useful to analyze what has been done in the Bass Basin by previous exploration operators.

Results of Previous Activity

Of the nine wells drilled in the trend, all encountered thick barrier sands, and two found commercial accumulations of hydrocarbons which is designated as Yolla Field. The Yolla #1 discovery well was tested at nearly 900 barrels of oil and 12 MMCF gas per day. This wildcat discovery was successfully appraised this year by the drilling of the Yolla #2 well located two and a half (2.5) kilometers to the south of the Yolla #1 discovery. Reserves for the Yolla structure are somewhat uncertain at this time, with the operator releasing very little information. Our estimate of Yolla Field reserves is approximately 100 million barrels of light gravity crude and 400 BCF of gas.

Four other wells, Cormorant, King, Tilana and Dondu were drilled on impressive structures, but all exhibit very late structural movement that could have breached any existing trap. This explanation is supported by the fact that both Cormorant and Tilana contained significant amounts of residual hydrocarbons in the upper Eastern View.

Bass #2 was drilled on the crest of a huge anticline, and penetrated a small section of the Eastern View before suspending operations after encountering igneous rocks of unknown age at 1,891 meters. Modern seismic data over this feature reveals a large basement pop-up structure, which was probably formed by lateral movement associated with basin opening. None of the Paleocene or upper Cretaceous, which should be prospective, has been tested on this enormous structure.

The Nangkero #1 and Yurongi #1 wells both seem to be poorly positioned with respect to structural trapping. In fact, a review of recently acquired seismic data over Nangkero fails to show a valid reason to drill a test at that location.

Barramundi Prospect

Globex plans to drill the first exploration well on the Barramundi Prospect. Almost 14,000 prospective acres are mapped under fault closure at the Eastern View level. Referring to the BARRAMUNDI PROSPECT display, structural control is supplied by thirty (30) 2D seismic lines, including nineteen (19) lines recently acquired by Globex. Excellent reservoir quality sands are demonstrated at the nearby Cormorant #1 well, where the logs illustrate over a hundred meters of sand in the upper Eastern View, with

porosities averaging nearly thirty percent (30%) and average permeabilities of nearly one Darcy. Within this sand, a prominent seismic amplitude anomaly, shown on the *Seismic Anomaly Depth Map,* has been mapped and correlated to the depth structure map.

Direct Hydrocarbon Detection: Normal Incidence

Operators in the Bass Strait have recently begun using direct hydrocarbon detection (DHI) methods to delineate hydrocarbon filled reservoirs. In the Gippsland Basin, Esso has published papers describing the use of normal incidence seismic amplitudes to map the extent of the gas / oil contact and the oil / water contact with considerable success. Their published data, shown on the ANALOGS display, shows hydrocarbon filled reservoirs are indicated by a prominent bright trough (in red) across the productive area of Bream Field. These interpretative conclusions have been confirmed by the drilling of several wells, and are an integral part of their field development program.

In the Bass Basin, Boral has based their reserve estimates of the Yolla Field on extensive DHI work in both the normal incidence and offset domain. A high amplitude trough (red reflection) is associated with the productive sand at the top of the Eastern View in the Yolla discovery well. This prominent red trough, which increases in amplitude and widens updip to the bounding fault, is seen on the *Yolla Field* ANALOGS display.

Referring to the BARRAMUNDI ANOMALY display, mapped over the Barramundi Prospect is a Direct Hydrocarbon Indicator. Shown both in dip and strike views on seismic sections between 1.3 and 1.4 seconds twt, the bright red trough, which gains strength and broadens updip mimics the anomaly observed over Yolla Field. As shown by the green outline on the *Amplitude Anomaly Depth Map,* the bright spot anomaly fits the present day Barramundi Structure, consistent with the behavior of a hydrocarbon filled reservoir. The *Amplitude Anomaly Isochron Map* shows an isochron thick associated with the crest of the structure, suggesting higher hydrocarbon saturations and / or higher gas to oil ratios higher on the structure.

Direct Hydrocarbon: Offset Domain

Given the pronounced amplitude effect associated with hydrocarbon filled reservoirs in the normal incidence domain, a substantial hydrocarbon effect would be anticipated, and is observed in the offset domain. As is shown by the actual and modeled offset responses on the BARRAMUNDI ANOMALY display, hydrocarbons are expressed by a negative intercept and positive offset gradient. Utilizing Gassman's fluid substitution, the same reservoir sand saturated with water results in a smaller negative intercept and flat offset gradient. This is consistent with the anomaly observed at Yolla, where the low amplitude trough below the water contact exhibits a flat gradient that becomes a deeper trough and a positive gradient above the water level in the productive portion of the reservoir.

Referring to the EASTERN VIEW AMPLITUDE ANOMALY display, offset amplitudes are displayed for selected gathered records over the Barramundi anomaly. It is evident that offset amplitudes outside the green outline, depicting the normal

incidence DHI, exhibit a flat response, while those inside the green outline, exhibit a positive AVO gradient. This behavior mimics that of the Yolla anomaly, leading to the conclusion that this anomaly is a valid hydrocarbon indicator.

5 cm

Fig. 1

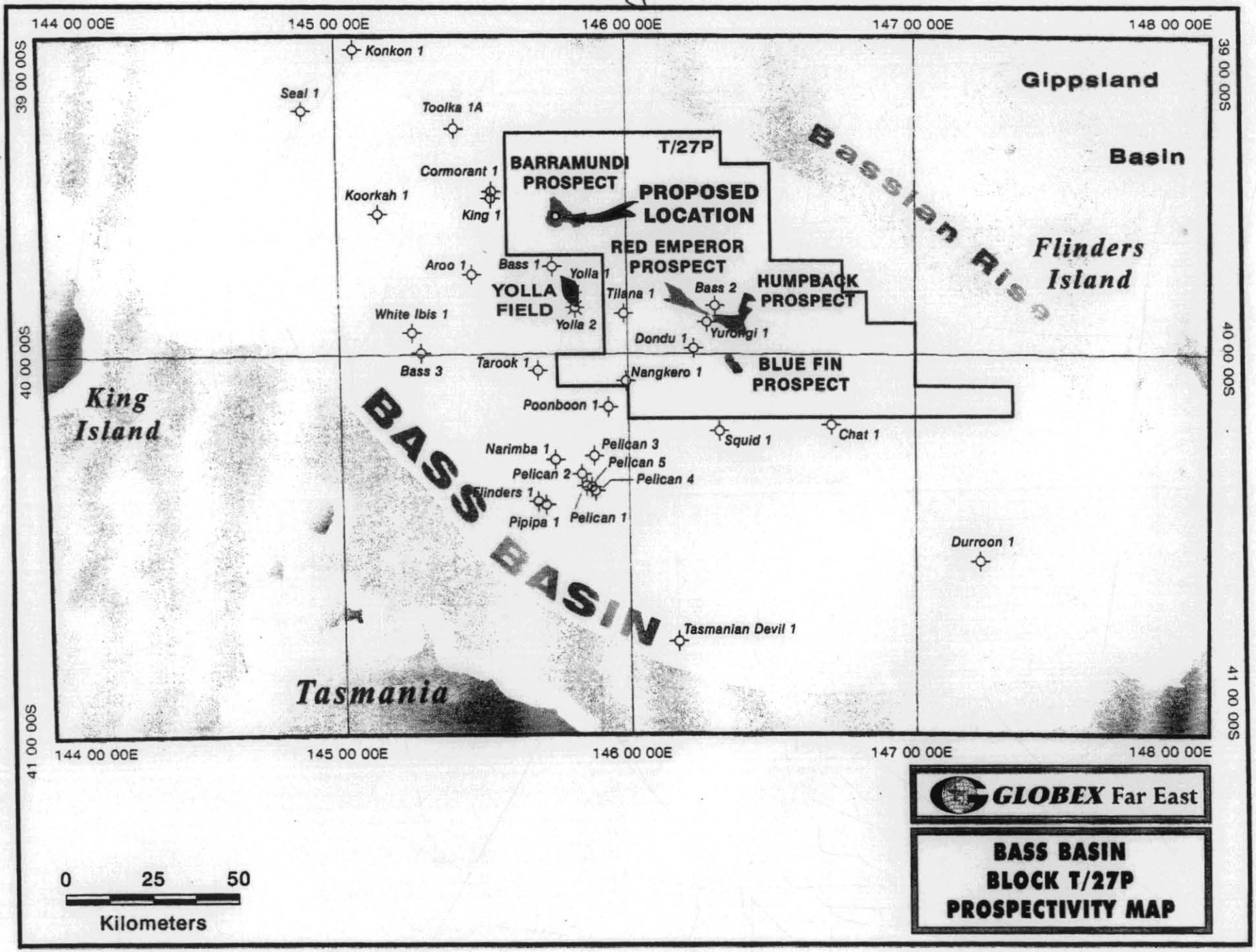

5710558

Fig 2

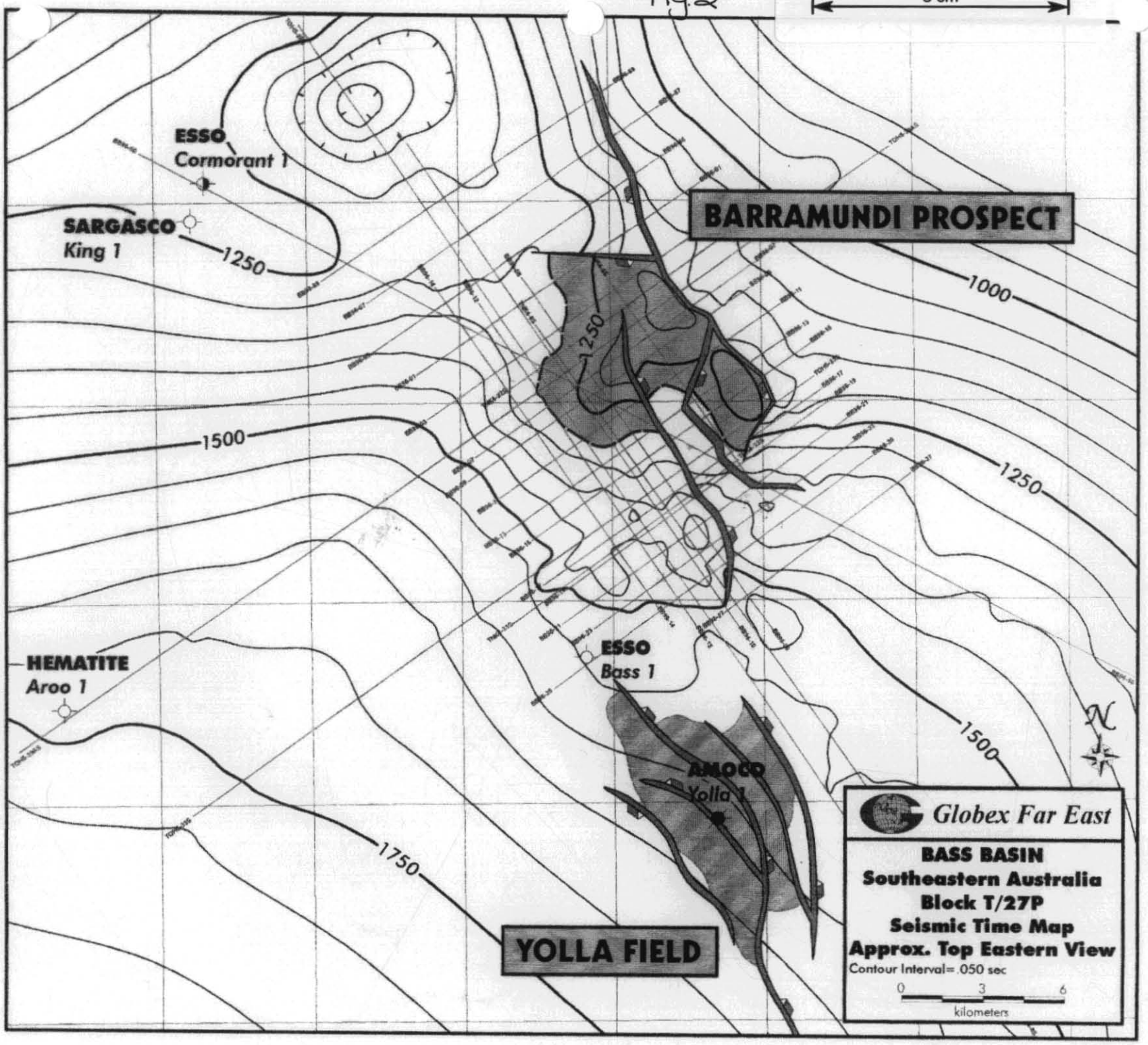

5710559

Fig. 3

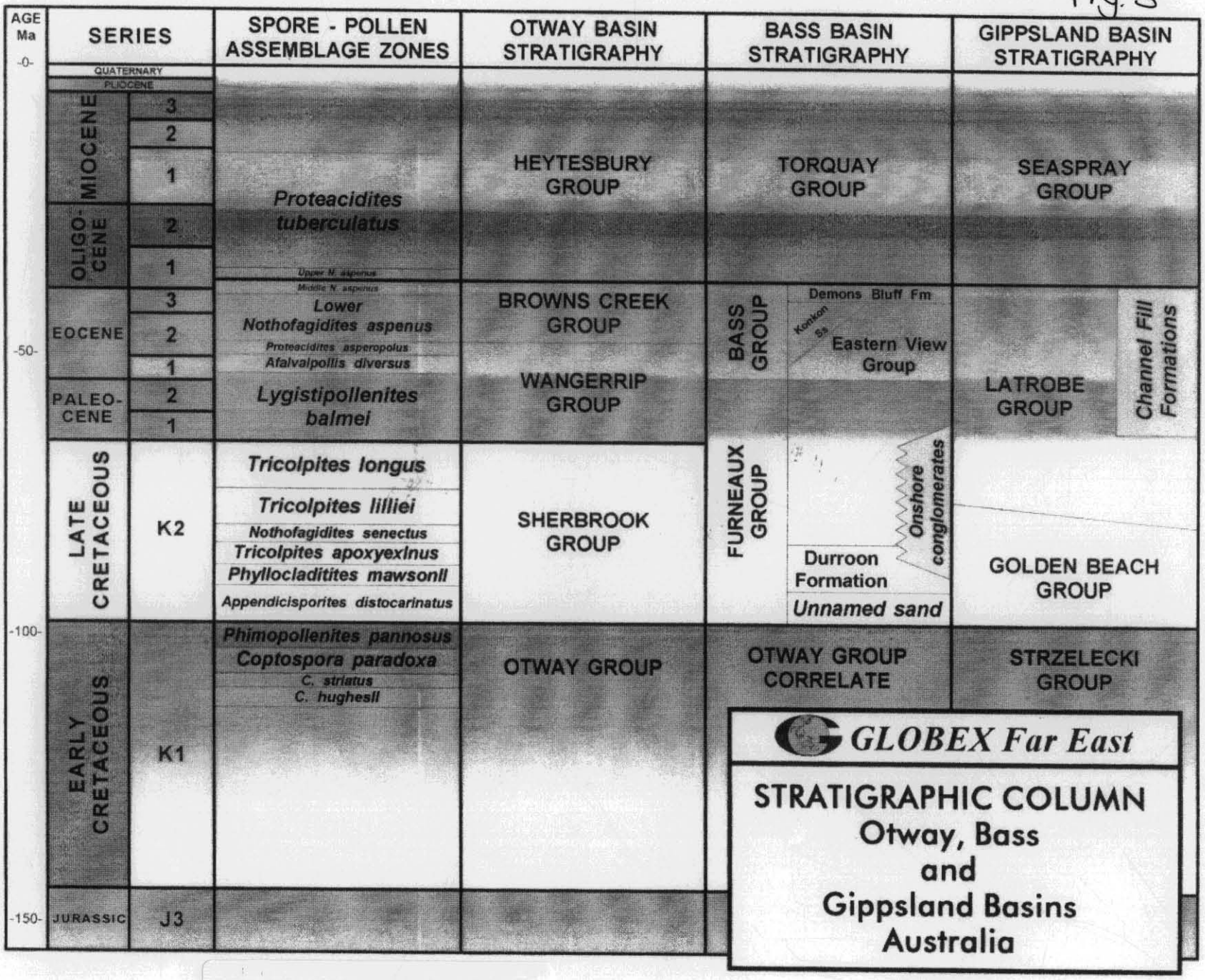

GLOBEX Far East

STRATIGRAPHIC COLUMN
Otway, Bass and Gippsland Basins Australia

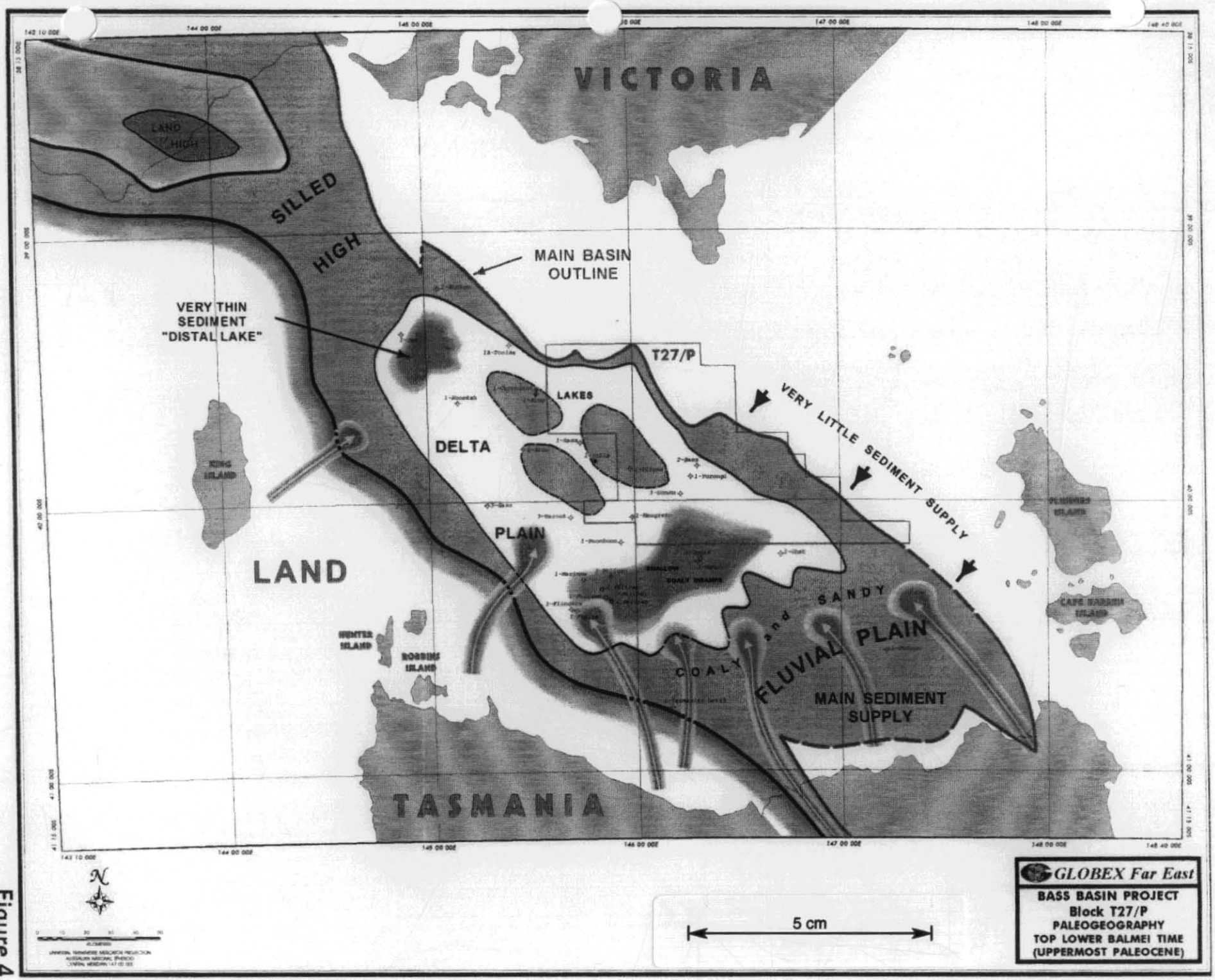

Figure 4

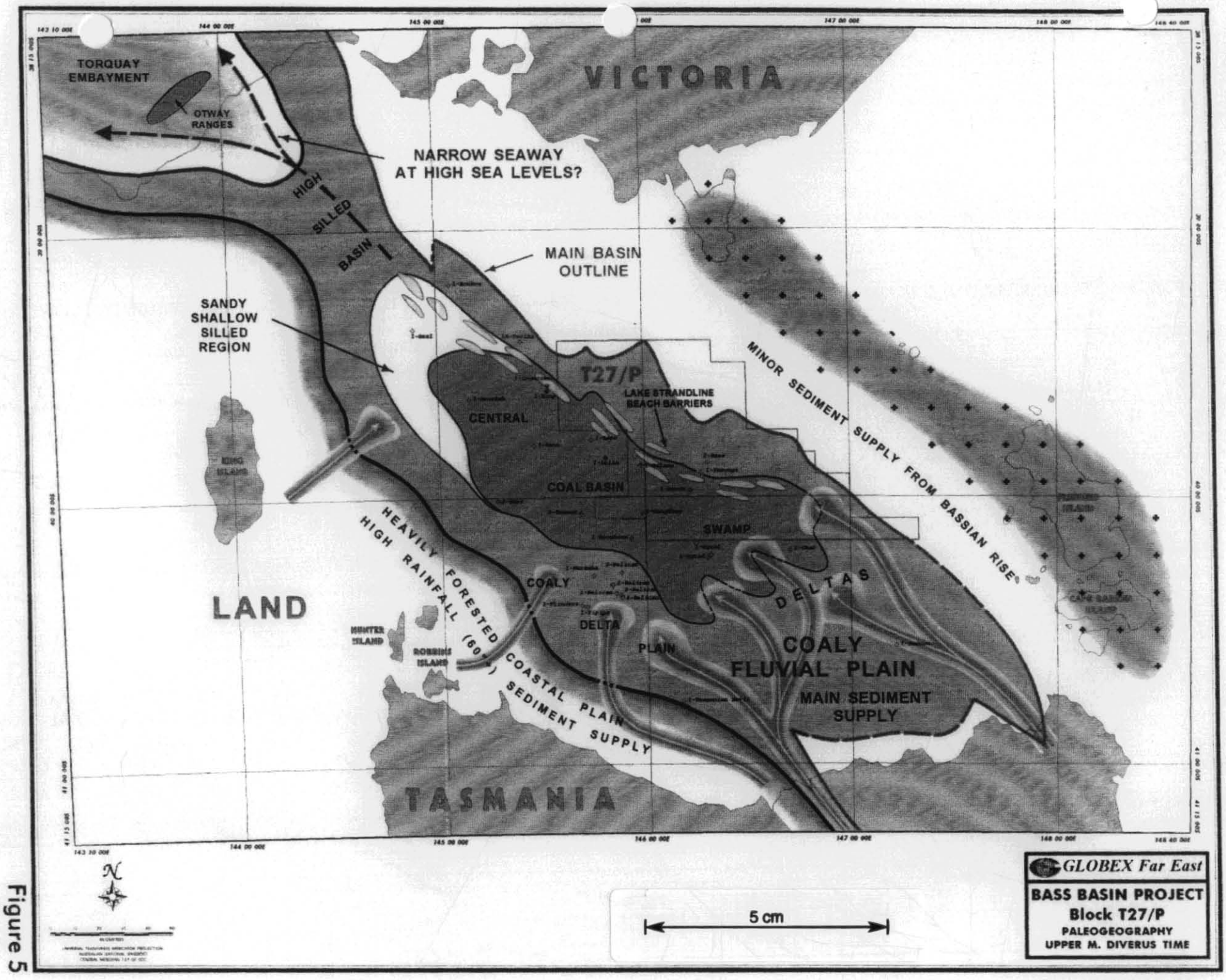

Figure 5

5710062

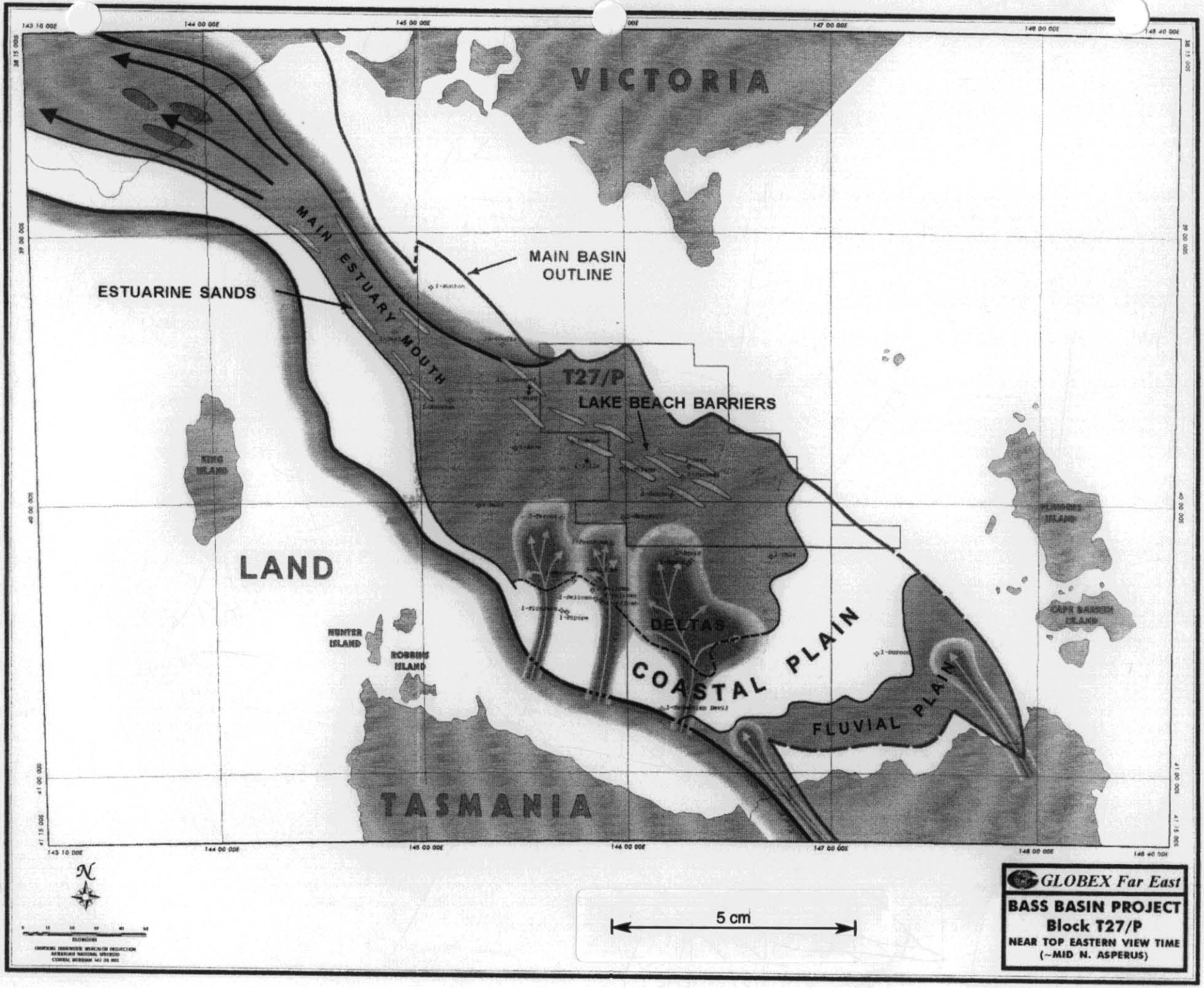

Figure 6

5710 63

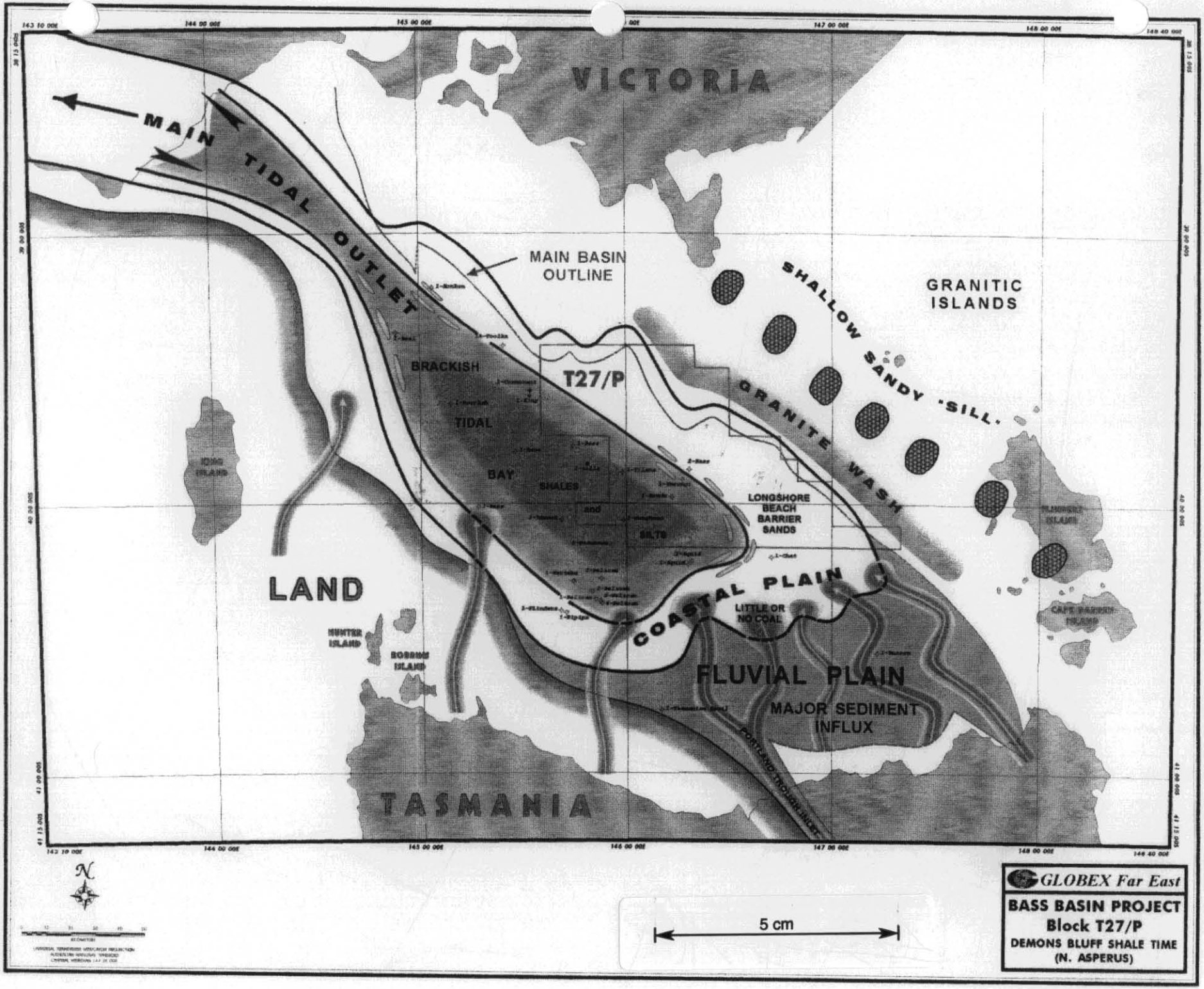

Figure 7

GLOBEX Far East BARRAMUNDI #1 PRE-DRILL CONCEPTS

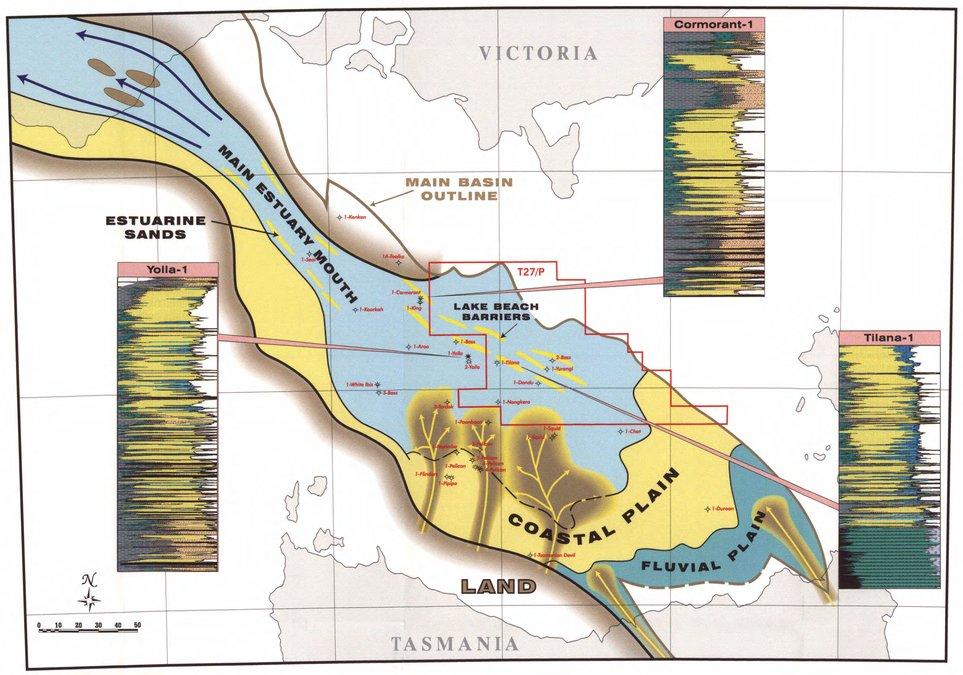

RESERVOIRS OF THE BARRIER BAR TREND

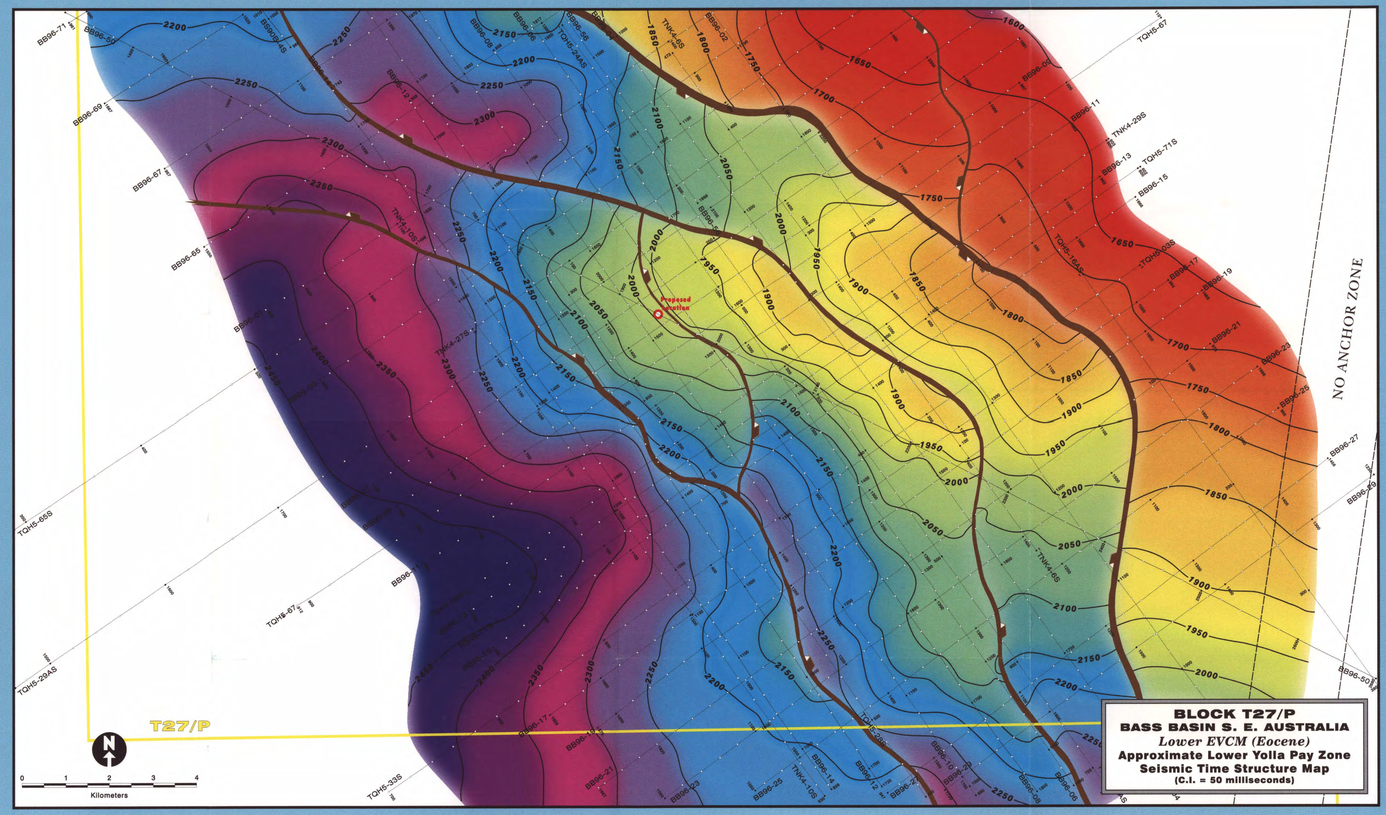

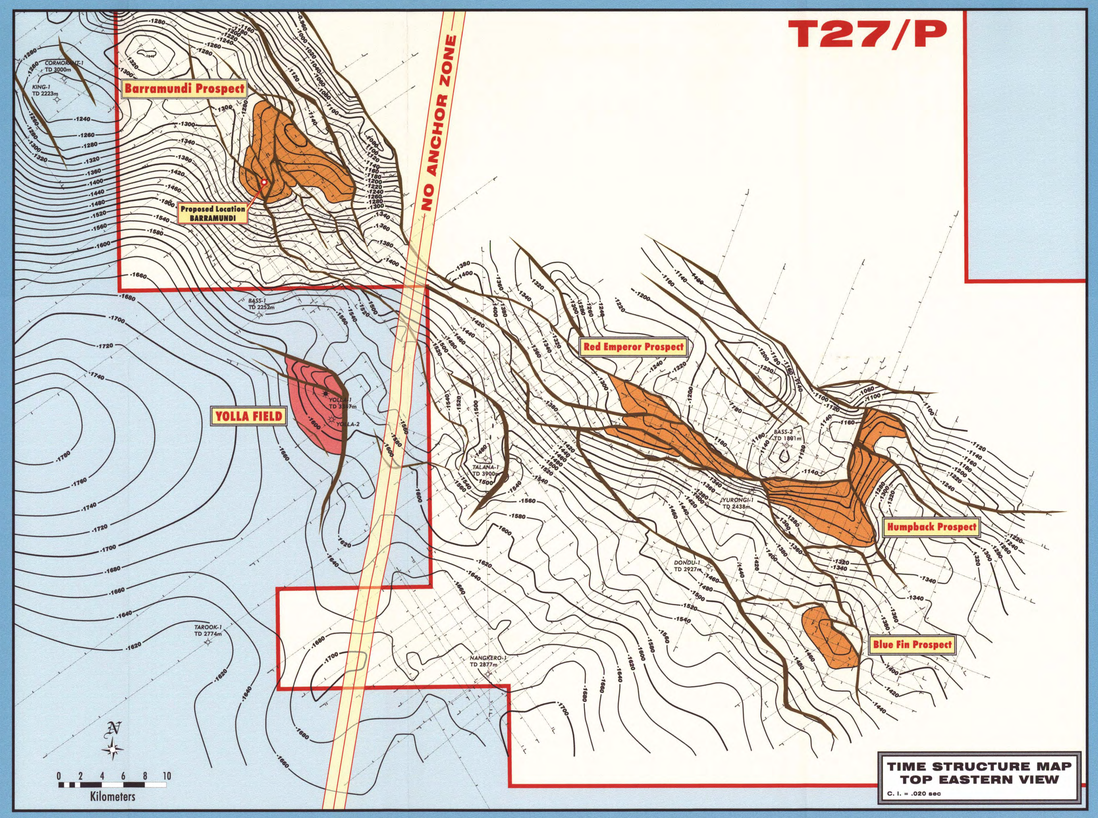

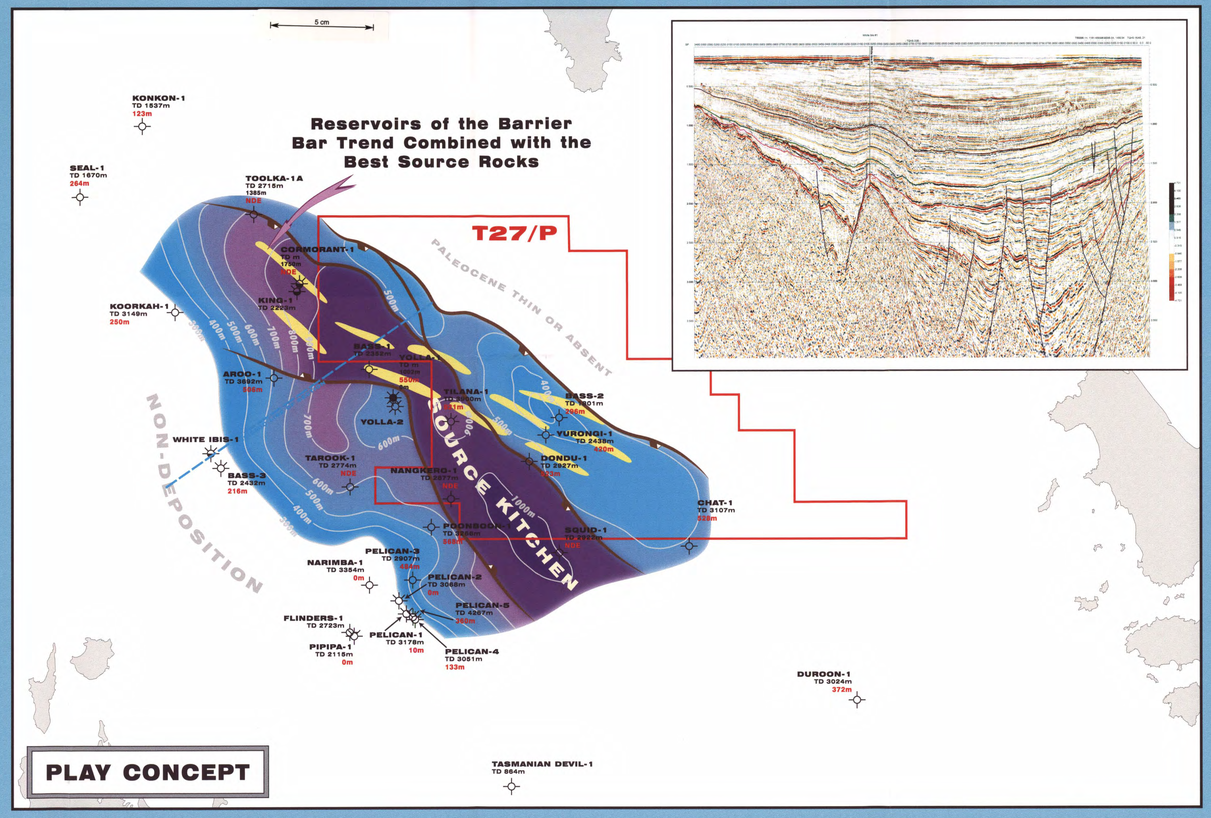

GLOBEX Far East BARRAMUNDI #1

ANALYTICAL LOG DISPLAY

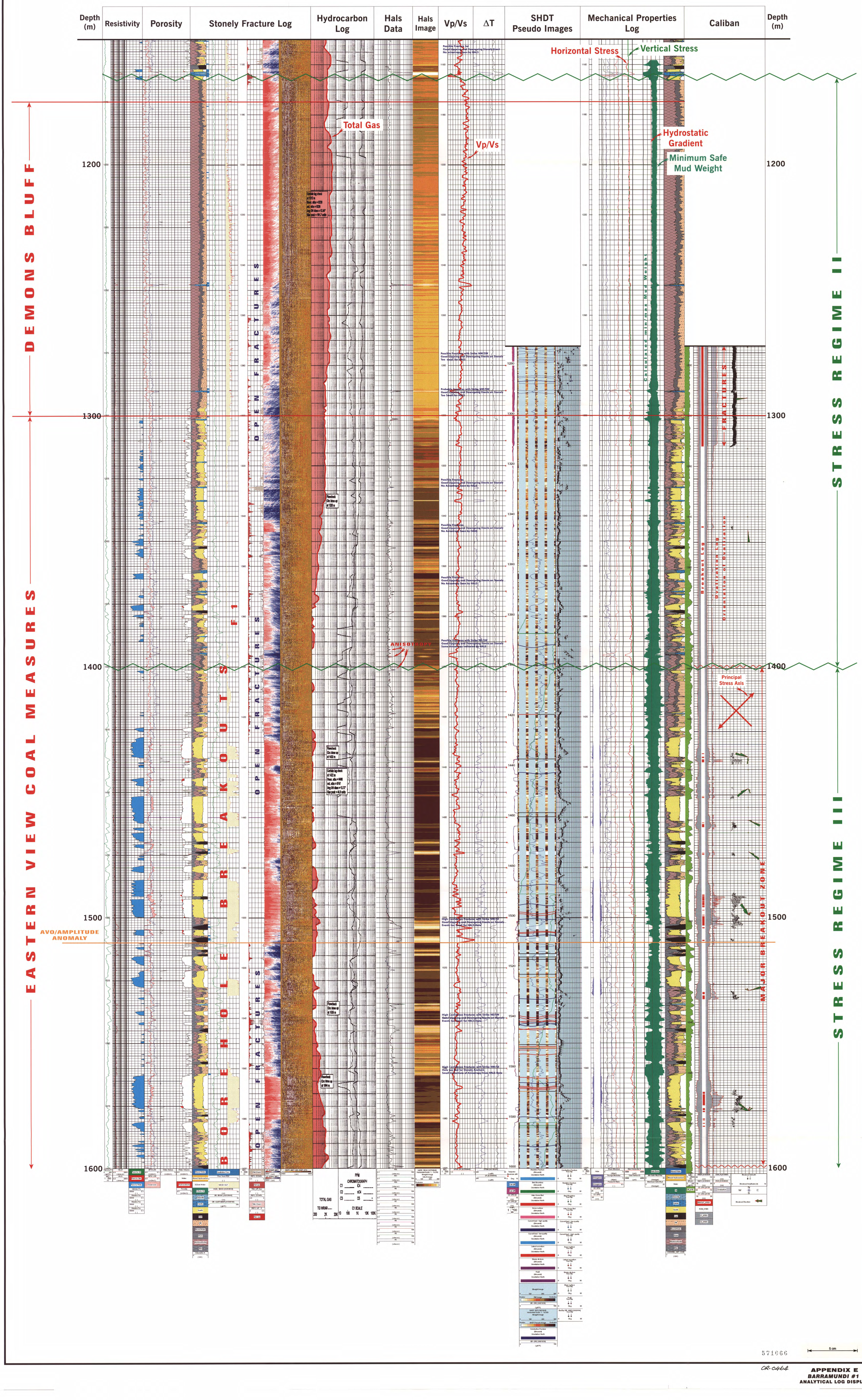

Wave Propagation

Two types of body waves travel in rocks—compressional and shear. Compressional waves, or P-waves, are waves of rock compression and expansion. They are created when a rock is sharply compressed, such as when struck by a hammer (Fig. 1). With compressional waves, small particle vibrations occur in the same direction the wave is traveling. Shear waves, or S-waves, are waves of shearing action as would occur when striking the rock column from the side. In this case, rock particle motion is perpendicular to the direction of wave propagation.

The rock mechanical properties, which can be characterized by the rock density and elastic dynamic constants, control the speeds at which these waves travel. In fluid-saturated rocks, these properties depend on the amount and type of fluid present, the makeup of the rock grains, and the degree of intergrain cementation. Soft, loosely consolidated rocks exhibit smaller elastic stiffness. As a result, sound waves travel slower in soft rock than in hard.

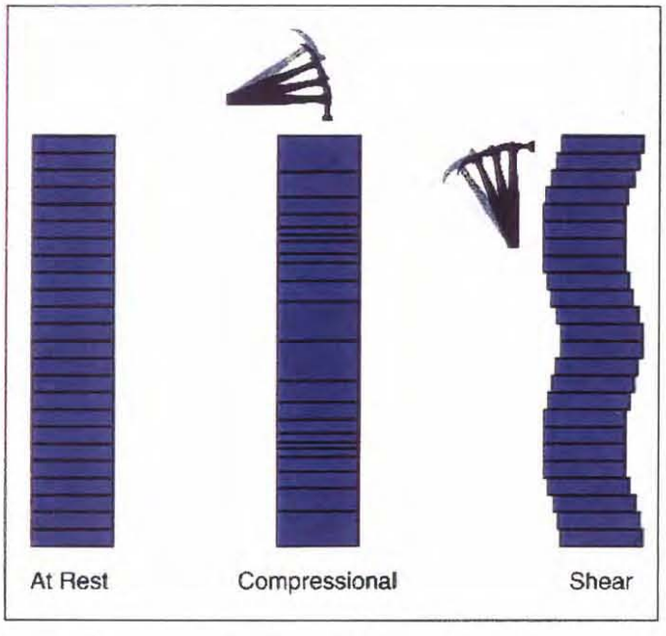

Figure 1. *Compressional and shear wave propagation.*

Conventional (monopole) sonic tools

In monopole sonic tools, an omnidirectional pressure source creates a compressional wave pulse in the borehole fluid, which propagates out into the formation. As this pulse enters the formation, it creates a slight uniform bulge around the borehole wall (Fig. 2 top). This in turn excites both compressional and shear waves in the formation. As the compressional and shear waves propagate in the formation, they create head waves in the borehole fluid. It is these head waves, rather than the direct formation compressional and shear waves, that the receivers detect (Fig. 2 bottom).

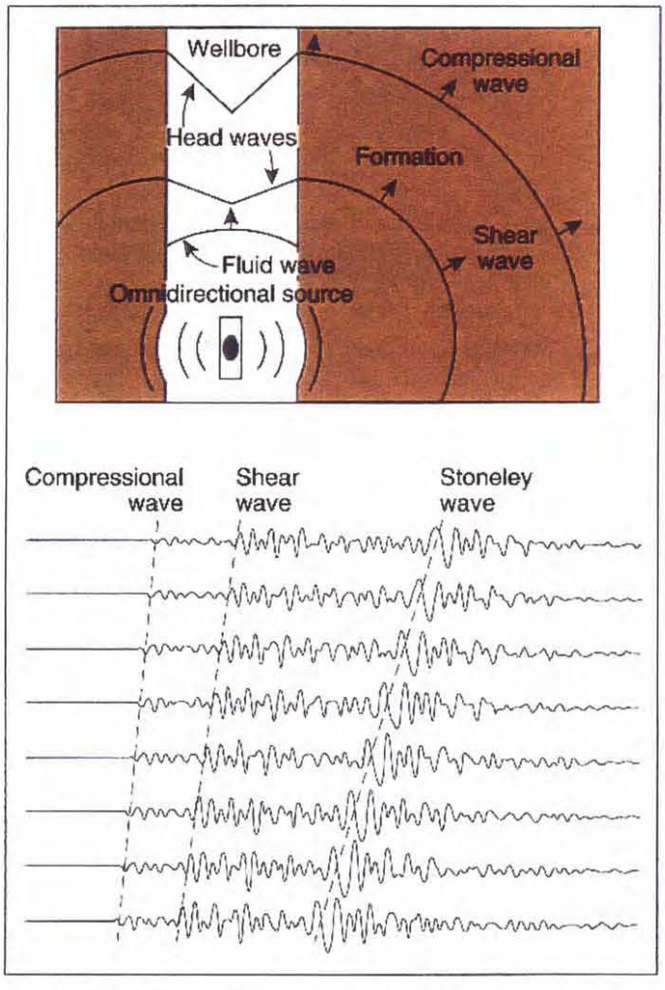

Figure 2. *Body wave propagation in hard formation with monopole source (top); typical sonic waveforms recorded by a monopole tool in hard formations (bottom).*

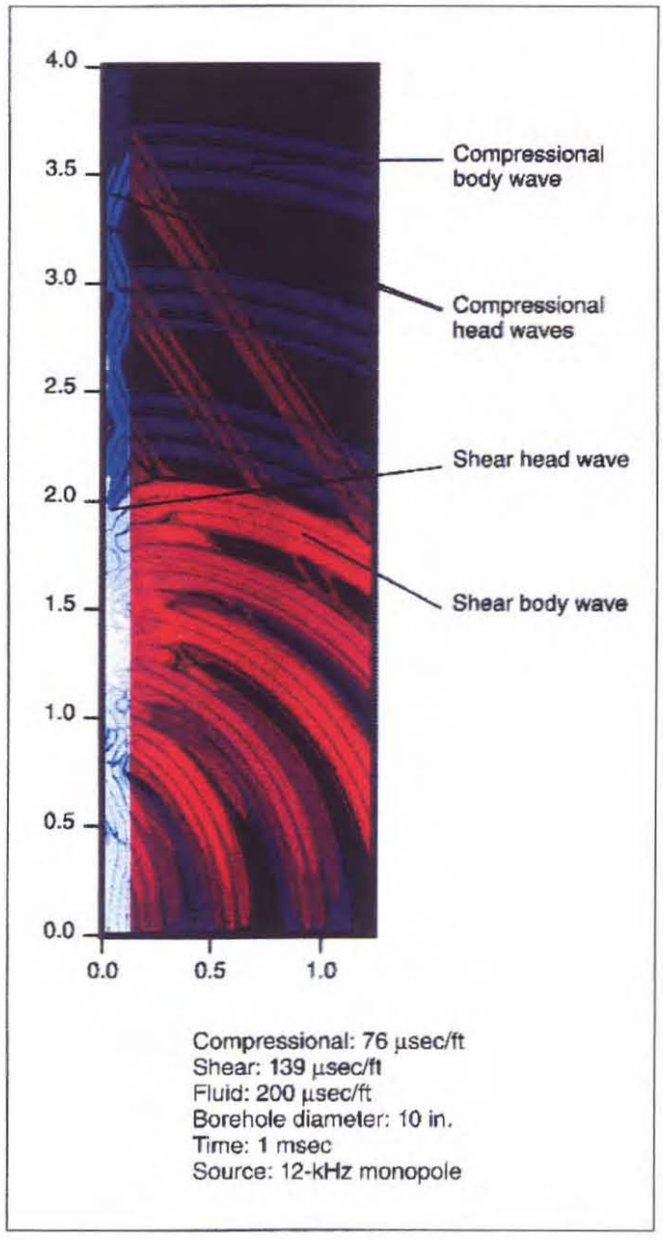

Figure 3. *Snapshot from a finite-difference calculation displaying the elastic fields in a borehole and surrounding fast formations (monopole source).*

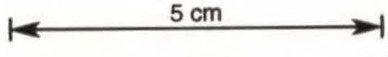

This phenomenon is illustrated in Fig. 3, a snapshot from a finite-difference calculation displaying the elastic fields in a borehole and the surrounding fast formation. The left axis is the borehole axis, and the left and bottom scales are axial and radial distance in meters.

Head waves are created only when the formation waves propagating up the borehole travel faster than the waves created in the fluid. Formation compressional waves are always faster than fluid waves, but that is not the case for shear waves. In slow, poorly consolidated formations, the shear velocity is often less than the fluid velocity—preventing shear measurement from the monopole tool. This is illustrated in the top half of Fig. 4, where the compressional body wave as well as its head wave exists in the borehole. The compressional and fluid modes are the only information carried by the waveform (Fig. 4 bottom).

Trailing the head waves are the more complicated guided borehole waves and the Stoneley wave. The guided borehole waves come from reflections of source waves reverberating in the borehole. The Stoneley wave, a surface-type wave guided by the borehole, travels slower than the fluid waves. Both are dispersive; that is, their velocity is a function of frequency.

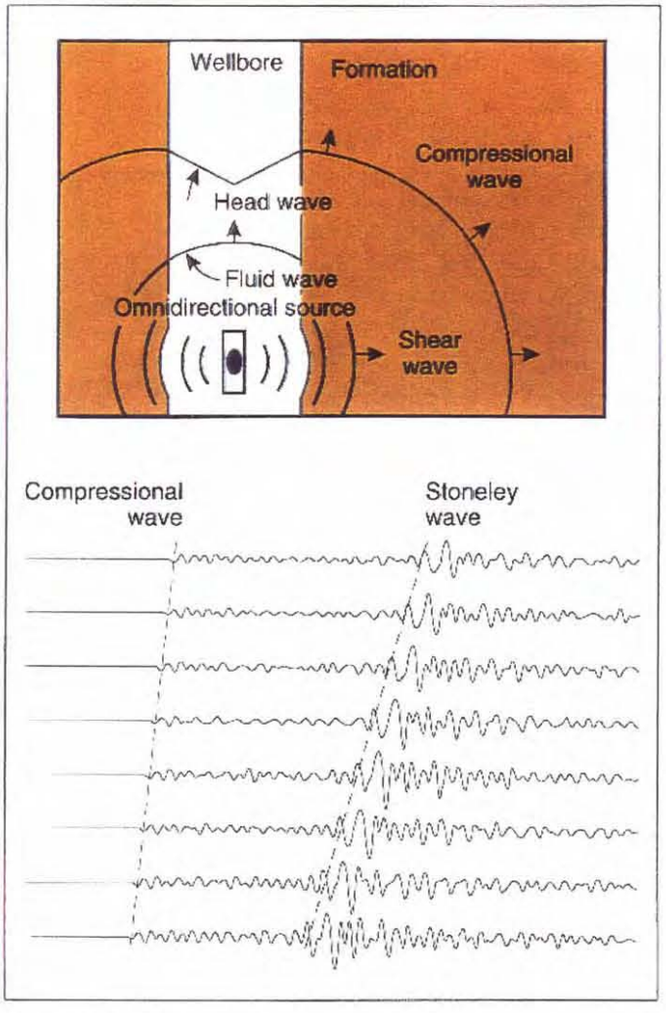

Figure 4. *Sound wave propagation in soft formation with monopole source (top); typical sonic waveforms recorded by a monopole tool in soft formations (bottom).*

Figure 5 is a snapshot from a finite-difference calculation displaying the fields excited by the monopole source in a slow formation. Starting from top to bottom, the illustration shows:

- The formation compressional body wave travels along the borehole, dragging its refracted head wave in liquid, as well as the refracted solid head wave (a shear disturbance).
- Lower in the borehole the fluid modes are present, generating shear disturbances in the formation (the fluid head wave).
- A striking difference between the fast and slow formations occurs in the shear wave field; no shear body or head waves appear. The shear body wave has been directed radially outward away from the borehole.
- The Stoneley mode appears clearly as a surface wave.

Dipole sonic tools

A dipole tool utilizes a directional source and receivers. The dipole source behaves much like a piston, creating a pressure increase on one side of the hole and a decrease on the other. This causes a small flexing of the borehole wall, as illustrated in Fig. 6, which directly excites compressional and shear waves in the formation. Propagation of this flexural wave is coaxial with the borehole, whereas displacement is at right angles to the borehole axis and in line with the transducer. The source operates at low frequencies, usually below 4 kHz, where excitation of these waves is optimum.

A new option provides a low-frequency source operating below 1 kHz. With up to a 20-dB improvement in signal-to-noise ratio, this source gives optimum results in extremely large boreholes and in very slow formations. In addition, the depth of investigation is increased.

The compressional and shear waves radiate straight out into the formation. There is, however, an additional shear/flexural wave propagating up the borehole. It creates a "dipole-type" pressure disturbance in the borehole fluid. It is this pressure disturbance that the directional receivers detect. The shear/flexural wave, initiated by the flexing action of the borehole, is dispersive. At low frequencies it travels at the same speed as the shear wave; at higher frequencies it travels at a slower speed. Unlike monopole-only tools, the dipole tool can record a shear/flexural wave even in slow formations.

In slow formations (Fig. 7), the shear/flexural wave is short in duration and concentrated at lower frequencies. In addition to the shear/flexural wave, there is a higher-frequency compressional arrival in the beginning of the waveform. In this typical slow formation synthetic example, there is a clear flexural wave from which the shear slowness is inferred.

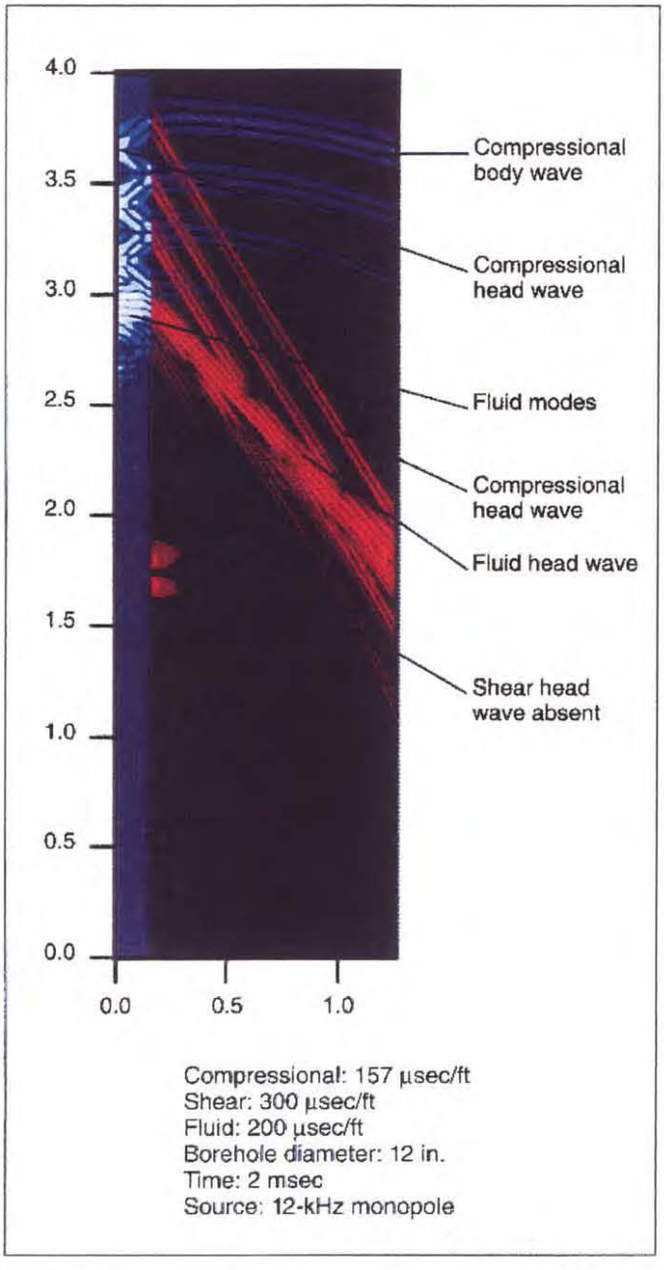

Figure 5. *Snapshot from a finite-difference calculation displaying the elastic fields in a borehole and surrounding slow formations (monopole source).*

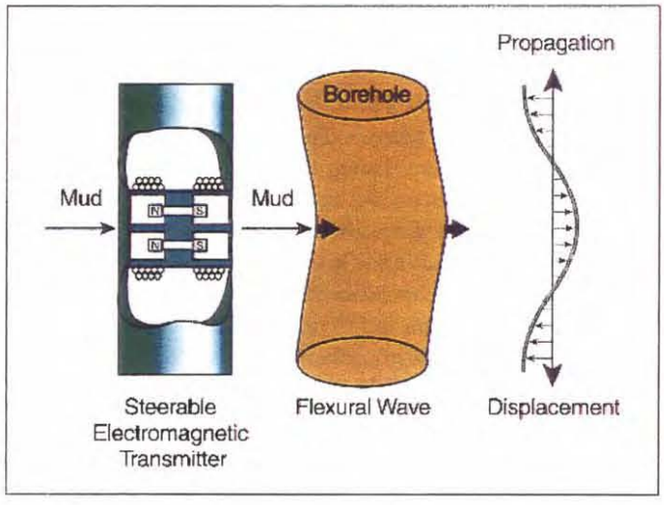

Figure 6. *DSI transducer operation.*

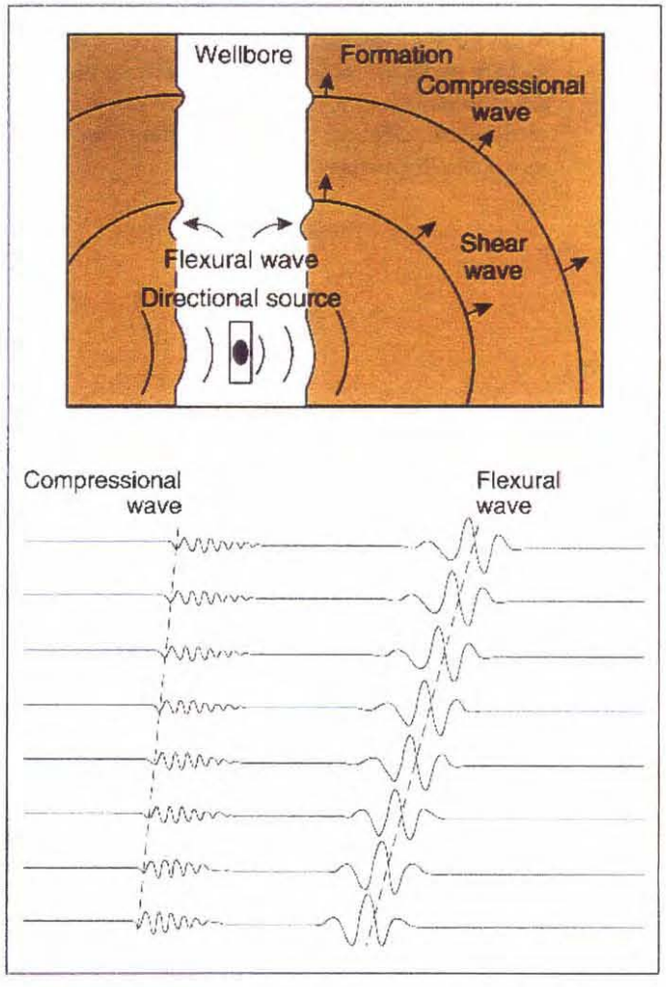

Figure 7. *Sound wave propagation in soft formation with dipole source (top); typical dipole sonic waveforms recorded in soft formations (bottom).*

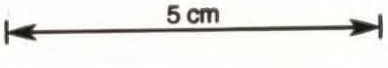

Figure 8 is a snapshot from a finite-difference calculation where a dipole source excites the borehole and surrounding slow formations. The principal features are the compressional body wave, the shear body wave and the borehole flexural mode. The flexural mode is the series of overlapping lobes of compressional and shear disturbance in the formation and of pressure in the borehole fluid, all radially localized near the borehole wall. The leading edge of the flexural mode is coincident with the shear body wave. Its apparent phase velocity in the borehole is that of the formation shear. The trailing edge contains higher-frequency components and travels more slowly, and the mode gradually spreads in axial extent.

Differences have been observed between shear slownesses from monopole and dipole transmitters in the same formation. These are to be expected and are attributed to environmental effects such as different depths of investigation, anisotropy, stress distribution, different vertical resolutions and monopole dispersion.

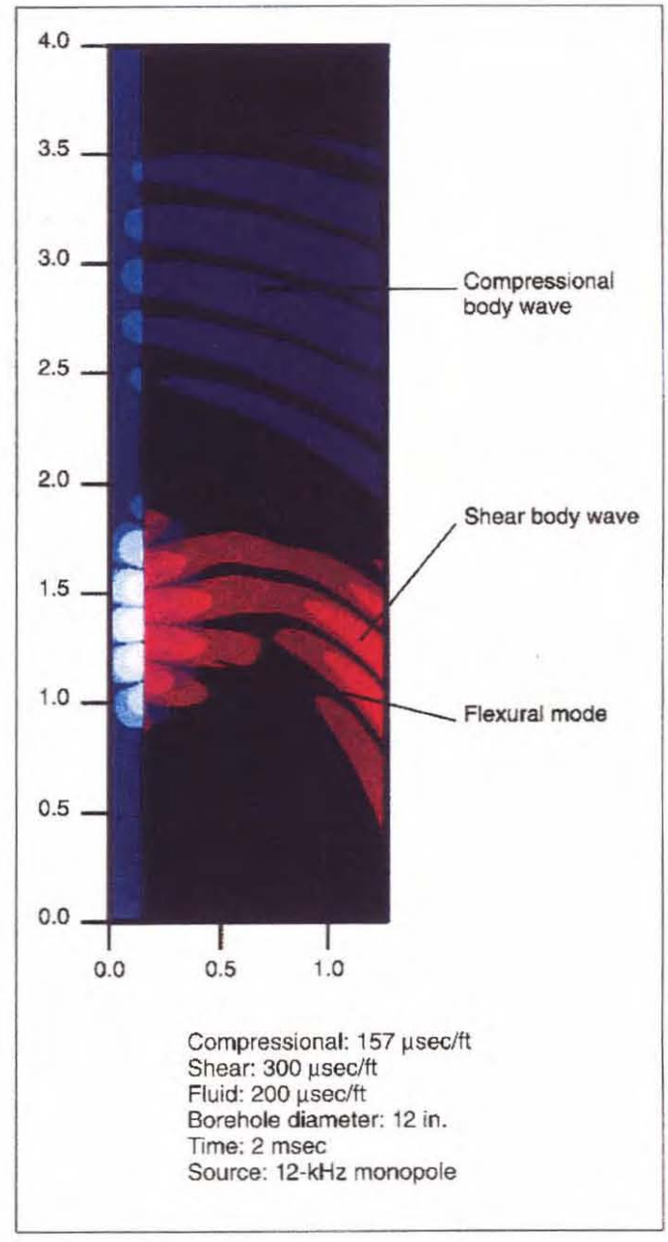

Figure 8. *Snapshot from a finite-difference calculation displaying the elastic fields in a borehole and surrounding slow formation (dipole source).*

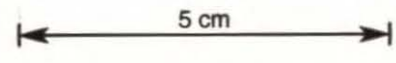

Fracture Evaluation from Inversion of Stoneley Transmission and Reflections

Takeshi Endo[1], Kazuhiko Tezuka[2], Takeshi Fukushima[1], Alain Brie[1], Hitoshi Mikada[1] and Makoto Miyairi[2]

[1]*Schlumberger K.K., Fuchinobe, Kanagawa-ken, Japan*
[2]*JAPEX Research Center., Chiba, Japan*

ABSTRACT

The borehole Stoneley wave has a unique advantage in that it is sensitive to permeable fractures. The main limitation of the Stoneley technique is its sensitivity to borehole irregularities and lithology changes. Recently introduced Stoneley modeling technique proved to be efficient in showing these effects qualitatively. However, a quantitative estimation of fracture parameters has been prevented due to difficulties in correcting these borehole effects.

This study presents a new methodology developed to obtain a quantitative evaluation of the fracture parameters and of the fracture permeability from the borehole Stoneley wave.

The evaluation is made in two steps. The first step consists in the analysis of the Stoneley waveform to extract the transmission and reflections coefficients. This is done with a single integrated process to improve compatibility between transmission and reflection coefficients. This process includes a new parametric wave separation algorithm.

In a second step the fracture aperture distribution is inverted from the transmission and reflection coefficients based on a multi-layers model. The effective fracture width in each layer is inverted by minimizing the difference between the measured reflection and transmission coefficients and the ones from the model. Finally the fracture permeability for each layer is estimated from the effective fracture width.

This new methodology has advantages in that (1) the procedure integrates transmission and reflection analyses; (2) a new wave separation process separates transmitted waves and reflected waves efficiently; (3) the inverse model includes borehole irregularities and lithology effects; and (4) joint inversion with up- and downgoing reflection coefficients and transmission coefficients better determines the fracture aperture.

INTRODUCTION

Fractures are major importance in oil and gas exploration in hard-rock reservoirs. The fracture system dominates the flow of fluids in such reservoirs, and a description of these inter-connecting networks is essential in the reservoir engineering evaluation.

Out of the many measurements that provide information on fractures, the Stoneley wave has a unique advantage in that it is sensitive to the permeability of fractures. The Stoneley wave has a potential not only in detecting fractures but also in evaluating the permeability of fractures. Various methods were attempted to evaluate fractures with Stoneley wave. These methods include Stoneley attenuation analysis(Brie et al.,1988) and Stoneley reflection analysis(Hornby et al.,1989). The main limitation of the Stoneley technique is the sensitivity to borehole irregularities and lithology changes.

Tezuka et al. (1997) proposed a Stoneley modeling technique to evaluate these borehole effects on Stoneley wave propagation. This modeling technique was combined with standard reflection and transmission analyses to differentiate reflections and attenuations due to fractures from those due to borehole irregularities and lithology changes(Tezuka et al., 1995). This combined technique proved to be efficient in showing these effects qualitatively and it was applied successfully to several datasets(Tezuka et al., 1995; Endo et al., 1997). However, a quantitative estimation of fracture parameters was prevented due to difficulties in correcting these borehole effects.

We aim to exploit the full information of measured Stoneley waveform for both attenuation and reflections, and attempt the quantitative fracture aperture inversion including borehole irregularities and lithology changes effects.

In the following section, we will describe a new methodology for Stoneley fracture evaluation. The evaluation will be done in two steps. The first step extracts Stoneley transmission and reflection coefficients and the second step performs fracture aperture inversion. The procedure

integrates transmission and reflection analyses to ensure the compatibility between the up- and down-going reflection coefficients with the transmission coefficients. The inversion process employs a multi-layers model to account for the effects of borehole irregularities and lithology changes.

METHODOLOGY

We use the low-frequency Stoneley waveform acquired by the DSI* Dipole Shear Sonic Imager tool. An overall evaluation procedure is shown in Figure 1. The procedure consists of two parts: (a) Stoneley transmission and reflection analyses and (b) Stoneley fracture aperture inversion. The methodology was implemented in the SonFrac* interpretation software. This software is an interactive module built on the Schlumberger GeoFrame* interpretation system.

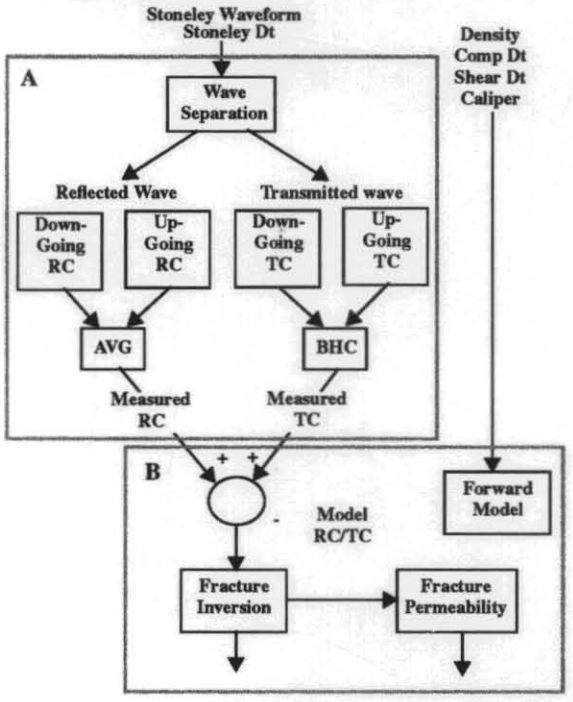

Figure 1: A flow chart of proposed sonic fracture evaluation procedure. The box denoted as **A** contains the Stoneley transmission and reflection analyses part and the one denoted as **B** contains the fracture aperture inversion part.

Stoneley Transmission and Reflection Analysis

This part integrates the transmission analysis by Brie et al. (1988) and reflection analysis by Hornby et al. (1989). The first step performs parametric wave separation taking the advantage that Stoneley slowness is known from STC processing results (Kimball and Marzetta, 1984). The transmitted and the reflected Stoneley waves are separated in frequency domain assuming a moveout derived from input Stoneley slowness. Amplitudes of the down-going and the up-going components are obtained with the least squares method assuming they are constant within three depth levels (1 ft interval). Outputs of this process are transmitted waves, down-going reflected waves and up-going reflected waves. We found that this wave separation process was very important for obtaining high quality reflection coefficients and transmission coefficients.

In the next step, transmitted waves after wave separation are input to transmission coefficients (TC) analysis and transmitted and reflected waves are input to reflection coefficients (RC) analysis. Transmission coefficients are evaluated with the Normalized Differential Energies (NDE) technique (Brie et al, 1988). NDE is converted to transmission coefficients while correcting for the borehole fluid attenuation. A borehole compensation (BHC) is achieved by calculating the average of the receiver and transmitter mode results. The reflection analysis technique, which is based on Hornby et al. (1989), is further enhanced in this study. Waveforms from common-source arrays are used for down-going reflection analysis and those from synthesized common-receiver arrays are used for up-going analysis. The extension of common-source arrays to common-receiver arrays is implied by the reciprocity principle. Combining results of down-going reflection analysis and up-going reflection analysis provides borehole compensation. Here, the borehole compensation is done by averaging the reflection coefficients from the down-going analysis and the up-going analysis.

Stoneley Fracture Aperture Inversion

The measured transmitted and reflection coefficients are compared with those from forward model to invert fracture aperture. Following Tezuka et al.(1997), we employ a multi-layers model where borehole and formation are discretized using a 0.1524 m (6 inch) interval along the borehole axis (Figure 2). Each layer is described with compression slowness (Dtc_i), shear slowness (Dts_i), density (Rho_i) and hole diameter (Hd_i). These parameters are obtained from log measurements. In this study, we extend the formulation by Tezuka et al. (1997) to include fracture parameters for each layer, a number of fracture (n_i) and a width of individual fracture (d_i).

The amplitude coefficients of up- (U_i) and down-going (D_i) waves satisfy the following relation at the boundary:

* denotes a Mark of Schlumberger

$$\begin{bmatrix} U_{i-1} \\ D_{i-1} \end{bmatrix} = M_b M_f \begin{bmatrix} U_i \\ D_i \end{bmatrix} \quad (1)$$

where M_b is the propagator matrix for borehole irregularities and lithology effects and M_f is the one for fracture effects. This equation corresponds to the equation (13) of Tezuka et al.(1997). The propagator matrix is modified to include M_f for fracture effects. The Stoneley wave number is computed with the formula by Chang et al. (1988). We include the borehole irregularities effects, the lithology effects and the fracture effects in the inverse model because we cannot separate these effects because they interact with each other and are not independent (Kostek et al., 1998a). The model reflection coefficients and transmission coefficients at each depth are computed with the five layer model from the ratio of the incoming wave amplitude and the outgoing amplitude by the following formula:

$$\begin{aligned} R &= U_{out}/D_{in} \\ T &= D_{out}/D_{in} \end{aligned} \quad (2)$$

It is assumed that the Stoneley wave responds to an effective fracture width (nd) in the layers because the low-frequency Stoneley wave cannot resolve closely-spaced multiple fractures (Kostek et al., 1998b).

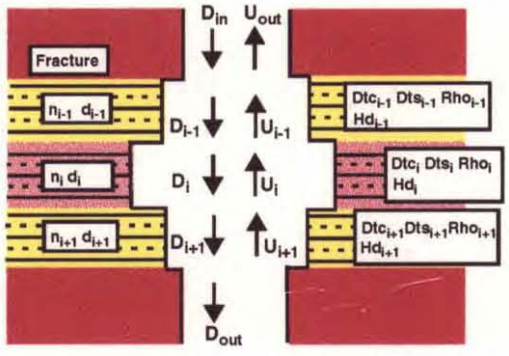

Figure 2: Diagram showing the multi-layered model employed for the fracture inversion. U_i and D_i denote amplitudes of up-going and down-going waves in each layer.

The initial inversion is performed in each layer assuming an horizontal fracture. This initial inversion gives an effective fracture width for a parallel plate of infinite extent and constant aperture. Then dipping effects are corrected using the ratio of a trace of the ellipse and the horizontal circle:

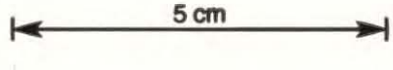

$$d_{dip} = d_{hor}\frac{\pi Hd}{L} \quad (3)$$

where d_{dip}, d_{hor}, L and Hd are an aperture of dipping fracture, an aperture of the equivalent horizontal fracture, a trace of the ellipse in the layer, and a hole diameter, respectively (Figure 3).

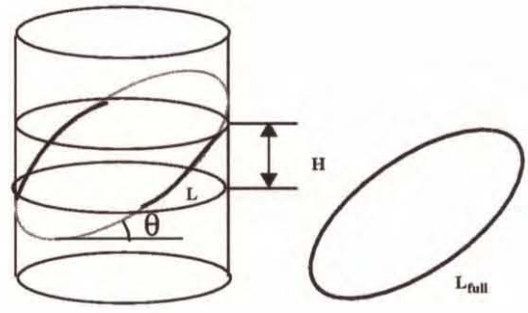

Figure 3: An inclined fracture crossing the borehole at an angle θ.

Fracture Permeability Estimate

Permeability of an isolated horizontal fracture is given by the following formula (Brown, 1989).

$$\kappa = \frac{d^3}{12H} \quad (4)$$

where d is the fracture width of the individual fracture and H is the thickness of the fracture zone. In case of multiple fractures, the formula is extended as:

$$\kappa = \frac{n(d/n)^3}{12H} \quad (5)$$

where n is the number of fractures in the zone and d is the width of an individual fracture. Finally, fracture permeability of dipping fractures are estimated as:

$$\kappa = \frac{n(d_{dip}/n)^3}{12H}\frac{L}{L_{full}} \quad (6)$$

where L_{full} is the perimeter of the ellipse. In these estimations, we can utilize the external information as fracture density and fracture dip measured from micro-resistivity images.

EXAMPLE

The methodology was applied to a fractured reservoir example. The well was drilled through a very hard dolomite formation. Figure 4 shows the results of the wave

separation process. Up- and down-going reflected waves are clearly separated from the transmitted waves though these arrivals are closely overlapped in time. Figure 5 shows the results of the fracture aperture inversion. Both transmission and reflection analyses were performed in the 0 to 2.5 kHz frequency band in this analysis. There are three significant events at X780, X810 and X840 ft. A solid curve in track 2 shows transmission coefficients from measured waveforms and a dashed curve shows reconstructed transmission coefficients computed from the fitted model. Tracks 3 and 4 show the down- and up-going reflection coefficients from the measured waveforms and the reconstructed reflection coefficients from the fitted model. Track 5 shows the inverted fracture aperture. Fracture apertures at X780, X810 and X840 ft take the values of 1 to 2 millimeters. These values are fairly large, however, we should note that these values are an effective aperture integrated in each layer. The low-frequency Stoneley wave cannot resolve closely-spaced multiple fractures. Agreements between reconstructed and measured reflection and transmission coefficients are generally good. These indicate that the inversion model fits the real data. These reconstruct logs are useful quality indicators for inversion.

CONCLUSIONS

We have developed the improved methodology for Stoneley fracture evaluation. In order to obtain high-quality reflection and transmission coefficients for input to the fracture parameter inversion, transmission and reflection analyses are integrated into one process. A new parametric wave separation in frequency domain has been developed to separate transmitted wave and reflected waves. The fracture aperture inversion is performed, based on a multi-layers model at every 6-inch interval. Fracture permeability can be estimated from the effective fracture aperture. The major advantages of the proposed methodology are:

- The procedure integrates transmission and reflection analyses to ensure the compatibility of reflection and transmission coefficients.

- The procedure employs a new parametric wave separation developed to separate transmitted and reflected waves without altering amplitudes.

- The inverse model includes borehole irregularities and lithology effects rather than correcting these effects before the inversion.

- Joint inversion with up- and down-going reflection coefficients and transmission coefficients better determines the fracture aperture than with an independent inversion with either reflection coefficients or transmission coefficients only.

The procedure was applied to a fractured reservoir example in dolomite formation which showed reasonable agreements between the measurements and the inversion model.

REFERENCES

Brie, A., Hsu, K. and Eckersley, C., 1988, Using the Stoneley Normalized Differential Energies for Fractured Reservoir Evaluation: *Transaction the 29th Annual Logging Symposium of the SPWLA*, Paper XX.

Brown, 1989, Transport of Fluid and Electric Current Through a Single Fracture: *J. Geophys. Res.*, B7, 9429-9438.

Chang, S.K., Liu, H.-L. and Johnson, D.L., 1988, Low-frequency tube waves in permeable rocks: *Geophysics*, **53**, 519-527.

Endo, T., Ito, H., Brie, A., Badri, M., and El Sheikh, M., 1997, Fracture and Permeability Evaluation in a Fault Zone from Sonic Waveform Data: *Transactions of the SPWLA 38 th Annual Logging Symposium, Houston, Texas, USA, June 15-18, 1997*, Paper R.

Hornby, B.E., Johnson, D.L., Winkler, K.H. and Plumb, R.A., 1989, Fracture evaluation using reflected Stoneley-wave arrivals: *Geophysics*, **54**, 1274-1288.

Kimball, C.V. and Marzetta, T.L., 1984, Semblance processing of borehole acoustic array data: *Geophysics*, **49**, 274-281.

Kostek, S., Johnson, D.L., and Randall, C.J., 1998a, The interaction of tube waves with borehole fractures, Part I, Numerical models: *Geophysics*, **63**, 800-808.

Kostek, S., Johnson, D.L., Winkler, K.W.,and Hornby, CB., 1998b, The interaction of tube waves with borehole fractures, Part II, Analytical models: *Geophysics*, **63**, 809-815.

Tezuka, K., Endo, T., Miyairi, M. and Brie, A., 1995, Fast Stoneley Modeling and Its Application for Permeable Fracture Evaluation: *Proceedings of the First Annual Well Logging Symposium of Japan, September 21-22*, Paper S.

Tezuka, K., Cheng, C.H., and Tang, X.M., 1997, Modeling of low-frequency Stoneley-wave propagation in an irregular borehole: *Geophysics*, **62**, 1047-1058.

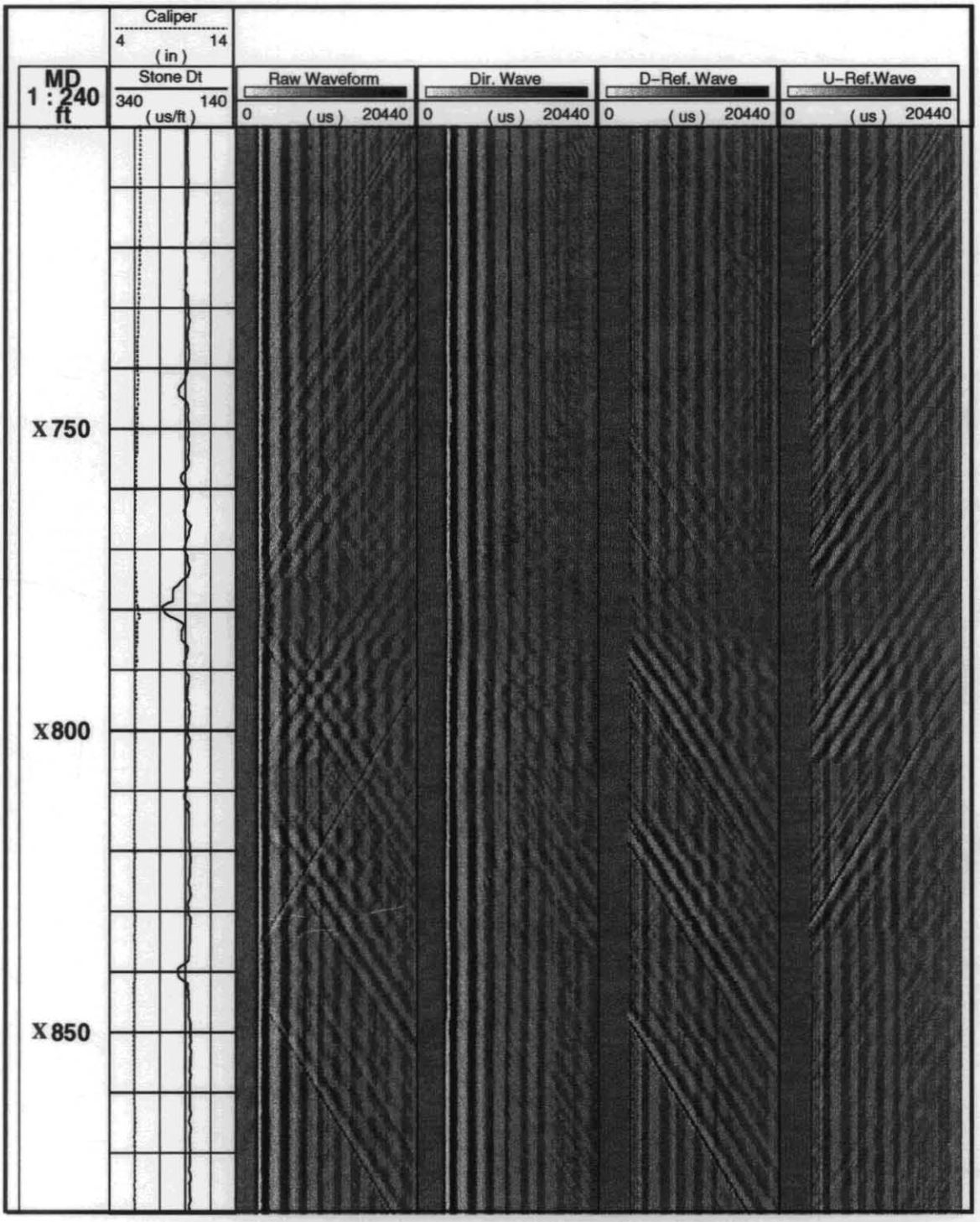

Figure 4: An example of wave separation. Raw waveforms are processed to obtain direct transmitted waves, up-going and down-going reflected waves.

5 cm

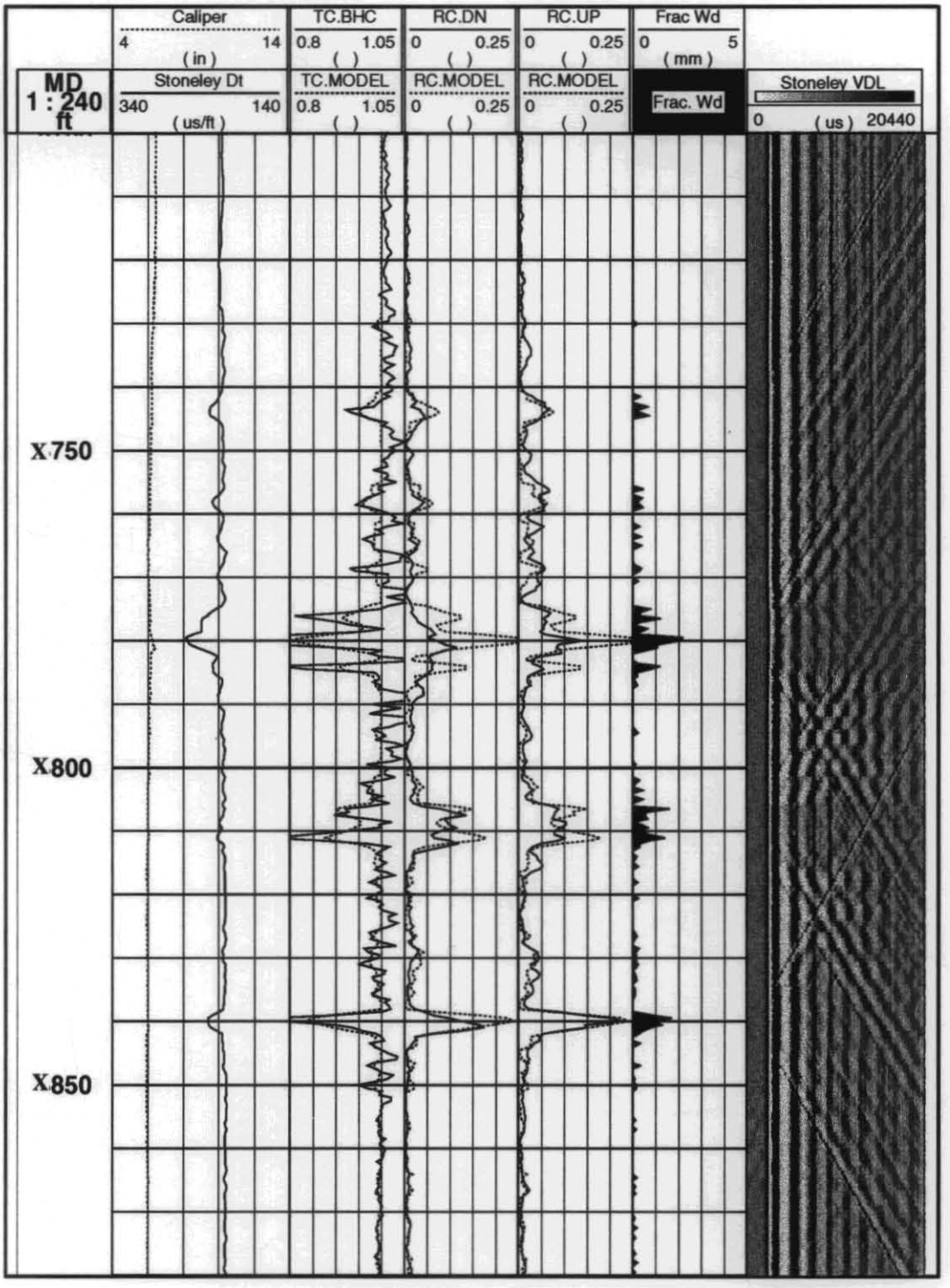

Figure 5: An example of an fracture aperture inversion. The caliper and Stoneley slowness are shown in track 1. Track 2 shows transmission analysis results after BHC computation. Tracks 3 and 4 show the reflection analysis results for down-going and up-going waves. Track 5 shows fracture aperture logs inverted from transmission and reflection coefficients.

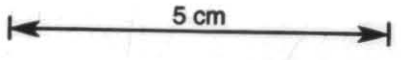

PREPRINT

SUBMITTED FOR PRESENTATION AT THE SPWLA ANNUAL SYMPOSIUM IN JUNE 1997

Fracture and Permeability Evaluation in a Fault Zone from Sonic Waveform Data

Takeshi Endo, Schlumberger K.K., Wireline & Testing, Fuchinobe, Japan,
Hisao Ito, Geological Survey of Japan, Tsukuba, Japan,
Alain Brie, Schlumberger K.K., Wireline & Testing, Fuchinobe, Japan,
Mohammed Badri, Schlumberger Logelco Inc., Wireline & Testing, Cairo, Egypt, and
Mohamed El Sheikh, Agiba Petroleum Company, Cairo, Egypt,

ABSTRACT

Identification and evaluation of fracture systems are important in oil and gas exploration in hard-rock areas and for scientific drilling. In fracture systems, faults are major events that impact not only the fracture distribution but also the rock structure and stresses. Near faults are significant rock deformation, fracturing and variations of the stress field. Faults have, therefore, large effects on the producibility and stability of a reservoir and must be accounted for when completing the well.

We integrated various sonic interpretation techniques to evaluate these effects. Stoneley wave reflections and attenuation analysis are known techniques for fracture evaluation. They have the advantage of showing open permeable fractures but also are sensitive to borehole irregularities. Stoneley modeling, when added to these techniques, estimates the effect of the borehole and improves the reliability of Stoneley fracture evaluation. Stoneley permeability analysis evaluates the slowdown of the Stoneley wave to indicate fluid mobility in the pore space, both from fractures and porosity. The recently introduced dipole shear anisotropy evaluation provides information on aligned cracks and stress directions. The technique evaluates shear wave splitting resulting from acoustic anisotropy. These techniques react in different ways to the presence of fractures in the formation. Combining these indications provides additional information on the reservoir characteristics, especially the location of fault zones.

We applied these techniques in two wells. The first well was drilled for scientific purposes to intercept a known large active fault in a granodiorite formation. In this data set, near the fault the Stoneley wave shows evidence of strong fracturing and deformed zones. Acoustic anisotropy indicates significant perturbations of the stress field. Stoneley permeability analysis detects high fluid mobility. The second well was drilled in a granite formation in an oil field. We observed similar signatures in the Stoneley and anisotropy results that strongly suggest the presence of a fault intercepting the wellbore. In this data set, systematic variations of the fracture's dip and strike, consistent with sonic evaluation results, are also observed on the microresistivity images. High mobility indications from Stoneley analysis are confirmed by the production data.

Integrating anisotropy information with conventional fracture evaluation techniques uncovers new possibilities for reservoir evaluation. Fractures can be identified and better understood with the resulting fracturing and rock alteration to give new insights on reservoir properties and producibility.

INTRODUCTION

In hard-rock reservoirs production is often mostly done through fractures. Therefore, the knowledge of the fracture locations and of their characteristics is of primary importance for well completion design and for field development. Of the many measurements that provide information on fractures, the most important ones are azimuthal resistivity, microresistivity imaging, ultrasonic imaging, and sonic techniques. Sonic techniques include Stoneley wave reflections evaluation(Hornby et al., 1989), and Stoneley attenuation(Brie et al., 1988). The advantage with Stoneley techniques is that they detect major open fractures, the one from which most of the production comes from. The reliability of Stoneley fracture evaluation was improved through the use of Stoneley modeling, which allows separation of the effect of borehole irregularities and lithology changes from permeable fractures (Tezuka et al., 1995). Permeability-added Stoneley slowness is another technique that has proved useful in identifying potentially producing intervals. It is based on the difference between a Stoneley slowness computed from elastic theory, without the effect of permeability and the measured Stoneley slowness (Winkler et al., 1989). The difference is an indicator of permeability in the formation.

Recently, dipole shear anisotropy evaluation from cross dipole measurements was introduced (Esmersoy et al., 1995). This technique also provides information on fractures through the evaluation of acoustic anisotropy and has been used with success in identifying producing intervals. The direction of the fast shear wave also provides information on stress and fracture orientation. The indications provided by this measurement differ some-

what from the Stoneley techniques indications. In particular shear wave anisotropy investigates a volume of formation up to 3-5 borehole diameters away from the borehole (Sinha et al., 1994) and can indicate fractures missed by other techniques.

In this paper we compare the response of these different techniques in two wells. The first well was drilled for scientific purposes to intercept a known, large active fault in a granodiorite formation. The second well was drilled in a granite formation in an oil field. We examine the sensitivity of the techniques to different types of fractures and to the environment, and determine how they can be combined to provide an improved evaluation.

DIPOLE SHEAR ANISOTROPY ANALYSIS

A tectonically fractured formation exhibits azimuthal anisotropy to shear waves. A shear wave that is polarized parallel to the fracture strike will propagate faster than a shear wave polarized perpendicular to it. A shear (or flexural) wave, such as the ones generated by a dipole source, will split as it propagates along the borehole and give a fast shear wave and a slow shear wave polarized along the anisotropy axis.

With the availability of two sets of dipole transmitters and receivers in orthogonal directions, the DSI* Dipole Shear Sonic Imager tool can measure the shear slowness in different directions in a plane perpendicular to the tool axis. The full evaluation requires recording the waveforms on an axis parallel with the transmitter axis, but also in the perpendicular direction or cross direction (Esmersoy et al., 1995). This is done with both transmitters so that four sets of array waveforms are recorded at every level (Both Cross Receivers acquisition mode). The waveforms are rotated and the fast shear azimuth obtained when the cross energy is minimal (see Appendix A).

Anisotropy indications are evaluated from wave energies, fast and slow shear slownesses, and arrival time differences.

STONELEY PERMEABILITY ANALYSIS

As the Stoneley wave propagates in a permeable formation, it is attenuated and slowed down. The effects of permeability on the slowness and attenuation of the borehole Stoneley wave have been studied extensively. The full Biot theoretical model was established by Chang et al. (1988) and confirmed experimentally (Winkler et al., 1989). But because of the large number of parameters necessary in this model to describe the formation, the borehole and the mudcake, the implementation of the quantitative inversion from Stoneley slowness to fluid mobility is not straightforward. A convenient, simpler, technique is to use the low frequency $S\text{-}S_e$ approximation. $(S\text{-}S_e)$ is the difference between the elastic slowness evaluated from the shear and mud slownesses for a formation without permeability, and the measured slowness. The difference increases with permeability and can be used as an indicator. The principle of this technique is developed in Appendix B.

STONELEY FRACTURE ANALYSIS

As the Stoneley wave propagates past an open fracture, some of the energy is reflected, some is dissipated in the permeable fracture and the remaining part is transmitted. Stoneley attenuation and reflection coefficients provide information on open fractures. Stoneley attenuation was evaluated with the Normalized Differential Energies (NDE) technique (Brie et. al, 1988). The computation was made in the 0 to 1.5 kHz frequency band. A borehole compensation was achieved by calculating the average of the receiver and transmitter mode results.

The evaluation of Stoneley reflections was described by Hornby et al.(1989). The method was further developed to evaluate the up- and down-going reflections after they have been separated from the total waveform with a velocity filter. Both down- and up-going Stoneley reflections were evaluated in the 0.25 to 4.25 kHz frequency band, for the real and model waveforms. In the Stoneley evaluation results presented in the following sections, the down-going reflections are shown on the left side and for the up-going reflection on the right side.

Following the method proposed by Tezuka et al., 1995, model waveforms are generated from log data: compressional slowness, shear slowness, density and hole diameter. These waveforms are processed in the same manner as the real ones to obtain the reflection coefficients and the Stoneley energy losses caused by the borehole irregularities and the bed boundaries. On the final plots these effects are shown in white, and the additional reflection coefficient and energy losses resulting from fractures and permeability are shown in black.

CASE STUDIES

Well A

Well A is a scientific well drilled in Japan. Its purpose was to intercept the Nojima fault, which was active during the Kobe earthquake in January 1995. The displacement across this fault, measured at surface is 1.8 m. The formations in this well are mostly granodiorite. The well

* Mark of Schlumberger

was extensively logged and cored. In addition to conventional logs, monopole and dipole sonic waveforms were acquired with a DSI tool. Both Cross Dipole waveforms were measured to evaluate acoustic anisotropy.

In the upper part of the well (not presented in this paper), the fast shear azimuth from the anisotropy evaluation is stable in a WNW, -60° , orientation. This is confirmed by the FMI* Fullbore Formation Micro Imager fracture orientation results, and the tectonic stress orientation in this area.

Figure 1 shows the Stoneley evaluation results. On the VDL shown on the right of the figure we observe that the Stoneley is highly attenuated and almost completely disappears at 620 m. This is where the well crosses the fault. The Stoneley arrival is also delayed in the 10 m interval below the fault and in another interval at 670 m. There are strong reflections, attenuation and permeability indications in front of the fault. In effect, the slowness values in the vicinity of the faults are large, and the model waveforms could not be calculated in the interval at 610-640 m. Therefore only total reflections and attenuation are presented with gray shading in this zone. Porosity is significant from 625 m to 675m as shown by the sonic porosity curve. Granodiorite rocks are normally not porous. In this case, the porosity is caused by rock deformation associated with the movement of the fault. Fracturing and breaking of the rock into fragments are responsible for the porosity and high permeability in this zone.

We can clearly observe up-going reflections from the upper boundary (623 m) of the fault zone but there are almost no down-going reflections from this boundary because they are severely attenuated across the porous zone. Below the fault we observe a succession of reflections and attenuation events that are larger than the model calculated values, indicating open permeable fractures. Above the fault, however,few events are detected, and little porosity. This shows that most of the deformation took place below the fault.

The shear wave was very attenuated in this well, especially below the fault zone, probably because of the presence of many fractures. This made anisotropy evaluation difficult in the lower section. On the anisotropy evaluation results (Fig. 2), we observe strong anisotropy above the fault, between 604 and 623 m. The fast shear azimuth is in the NS direction. Below the fault, the sonic anisotropy is small. The fast shear azimuth rotates to NW 60° at 650 m. There is no correlation between the sonic anisotropy indications and the presence of fractures. The strike of fractures detected by a borehole televiewer log at 600-650 m is almost in the NE direction (Ito et al.,1996a; Ito et al., 1996b). Therefore, in this case, anisotropy does not appear to be related to fractures, and is likely to be stress induced, or caused by cracks which are too small to be detected by other fracture indicators. The rotation of the fast shear azimuth is more pronounced near the fault. This shows the strong influence of the fault on the stress field.

The features we observed on the sonic in well A are

1. The well crosses a major fault at 620 m.
2. The fast shear azimuth moves gradually away from the regional trend above the fault. It then rotates rapidly across the fault, and finally goes gradually back to the regional trend below.
3. Sonic anisotropy is significant above the fault, absent across it, and small below.
4. No major fractures are observed in the interval above the faults, but many fractures are detected below.
5. Porosity and permeability are small above the fault, high at the fault, and significant below, with a succession of porous, highly permeable, intervals probably consisting of broken rock.
6. The fracture orientation observed on the FMI images is different from the fast shear azimuth in the vicinity of the fault.

Well B

Well B was drilled in a fractured granite basement in Egypt. The DSI log in this well includes the monopole P&S, monopole Stoneley and Both Cross Dipole modes. Conventional openhole logs and the FMI data were also recorded, and a detailed fracture orientation evaluation made from FMI data.

In the upper part of the well (not presented in this paper), both the FMI fracture orientation results, and the fast shear azimuth from the anisotropy evaluation coincide, giving a NW, -40°, orientation. This suggests that the direction of major tectonic stress in this area is about -40°.

Upper Zone (X280-X380 ft):

Figure 3 shows the Stoneley evaluation results. In the upper part of the section few fractures are detected. The attenuation shows a few minor events from X350 to X370 ft, and above X300 ft. On the reflection analysis there is a minor up-going reflection at X360 ft and a small down-going reflection at X280 ft. These events are not correlated between the various Stoneley results, giving little confidence in the fracture indications. The Stoneley permeability indicator, (S - Se), shows some increase between X345 and X370 ft, and above x300 ft. These indications coincide with zones where Stoneley attenuation is observed and seem related to porosity per-

meability. There is also good correlation between (S - Se) and porosity. From field experience this zone is not a potential producer. On the anisotropy evaluation results (Fig. 4), the fast shear azimuth moves gradually from the general trend at -40° to -20° below X325 ft. There is substantial anisotropy at X300 ft as indicated on the energy, slowness and time differences. However at this location there is no indication of major fractures from the Stoneley indicators. The FMI analysis shows fractures of various dip angles, but few are opened. The fracture strike is well defined on the polar plot at about -45° (Fig. 5, top right), and therefore in good agreement with the anisotropy indications.

Lower Zone (X380-X520 ft):

In this section major events are detected by the fracture indicators between X380 and X460 ft. These events cause significant Stoneley reflections both in the down- and up-going directions, and Stoneley attenuation. The borehole effect evaluated with Stoneley modeling is usually small giving good confidence in the fracture indications. The porosity is almost 15% from X380 to X460 ft. Permeability indications from (S - Se) are also large down to X490 ft. There are good permeability indications in front of events detected by the Stoneley fracture techniques. On the anisotropy results we observe a rotation of the fast shear azimuth that goes from -45° above X400 ft to +20° below and then to 0° for the lower part of the interval. There is no significant acoustic anisotropy detected where these changes take place. However there is strong anisotropy detected between X455 ft and X490 ft.

These indications suggest that the well crosses a fault at about X400 ft. The event detected as fractures may actually be the fault itself or fractures caused by the presence of the fault. Faults are common in granite, but we do not have additional confirmation of the presence of this fault. Although various faults have been identified in the vertical seismic profile results in higher sections of the well, there is no such data available in the interval of interest.

Again in this well the peaks of sonic anisotropy do not correspond to fractures events on the Stoneley, with the exception of the indication at X460 ft. This is because the sonic wavelength is short in comparison with the size of these fractures. It would certainly be different at seismic frequencies, and we expect that the observed fractures would cause significant anisotropy on seismic measurements. Sonic anisotropy is caused mostly by small cracks in the rock. These cracks are open only when oriented parallel to the major stress direction. Therefore sonic anisotropy is a good indication of the present stress direction.

The FMI analysis in this zone shows two sets of open fractures with low dips (30 to 50°), increasing to 70° above X425 ft. Three trends are observed on the fracture polar plot. The main trend, composed of fractures with a strike azimuth of about of -70°, possibly extensional fractures, have low dip. This is quite different from the fast shear azimuth which in this zone ranges from 0 to 10°. The two smaller trends at -30 and +40° may represent shear conjugate fractures. They are mostly from in the lower part of the interval. Sonic anisotropy is indicative of the present state of stress, and the different fracture orientation from the fast shear azimuth in the vicinity of the fault suggests that most of these fractures were created at a time when stresses were different. It is most likely that the state of stress changes every time a fault is active.

This well is a good oil producer. Most of the production comes from the zone next to the fault. Other wells in the same field that did not intercept this fault did not reach commercial production levels.

The features we observed on the sonic in well B are

1. There are indications that the well crosses a fault at about X400 ft.
2. The fast shear azimuth changes slightly 70 ft above the fault, then changes by nearly 65° across the fault and goes back to an intermediate value for 100 ft below the fault until it finally returns to the regional trend. These changes of dominant anisotropy azimuth according to depths are clearly observed in anisotropy azimuthal plot(Fig. 6).
3. Sonic anisotropy is absent close to the fault, but is significant at some distance above and below the fault.
4. No major fractures are observed in the interval above the fault, but large fractures are detected at and below the fault.
5. Porosity and permeability are small above the fault, but significant below.
6. The fracture orientation observed on the FMI images is different from the fast shear azimuth in the vicinity of the fault.
7. The fault zones have a high permeability and have a high potential for production.

INTERPRETATION IN A FAULT ZONE

Last and McLean (1996) studied the effect of a major fault on earth stresses in the Cusiana field in Columbia. They used a computer model and predicted that the major stress orientation changes gradually as one get close to the fault, then rotates by 90°, and then goes gradually back to the background stress direction. Barton and Zoback (1994) studied stress orientation from borehole

breakout logs in the vicinity of faults, and reported a similar pattern. They also discussed stress magnitudes, and concluded that stress anisotropy disappears at the fault. Auzias (1995) confirmed computer modeling results with model Plexiglas experiments, and showed that the major stress direction commonly rotates to become parallel to the fault on one side, and then perpendicular to it on the other side, thus rotating by 90° . This combined with Barton and Zoback's remark that stresses equalize at the fault suggests that stresses become equal and exchange roles when crossing a fault. Auzias also studied the influence of multiple faults and showed the importance of the fault friction coefficient and of the presence of contact points on the stress distribution.

We observed these various phenomena in the two examples we described. In particular the rapid stress rotation at the fault is clearly seen on the fast shear azimuth log. We also noticed the absence of anisotropy immediately next to the fault.

The formation layers close to the fault are deformed when the fault moves. Deformation causes bending and breaking of the rock, with the creation of fractures and even porosity. Both extension and compression shear fractures can be created. Deformation may not been symmetrical on both side of the fault. In the examples we studied, we noticed that the lower side of the fault is usually more fractured, and more porous, hence more deformed, than the upper side. But we do not know if this is a general feature. Certainly the fractures and porous rock associated with a fault in hard rock are very permeable. Because the fault has a large extent, it can drain and carry fluid a long way, which is very important for production.

CONCLUSIONS

We evaluated two wells crossing a fault with sonic techniques. The Stoneley wave was used to evaluate fractures and permeability, and cross-dipole shear measurements were used to evaluate sonic anisotropy. The results were compared with other measurements sensitive to fractures, such as FMI images or BHTV. We concluded the following:

- Stoneley attenuation and reflections are indicative of open fractures and fault zones.
- Permeability-added Stoneley slowness is a good indicator of permeable zones in hard rocks. It is sensitive to both fractures and rock permeability.
- Stoneley attenuation is sensitive to large open fractures and also to a lesser extent to rock permeability.
- Stoneley modeling is effective in showing what fraction of Stoneley reflections and attenuation is caused by borehole effect or bed boundaries.
- In a stable tectonic environment, the fast shear azimuth indicates the direction of maximum stress and is parallel to the fracture strike.
- Sonic anisotropy is not sensitive to the large fractures seen with the Stoneley techniques. It is sensitive mostly to a high density of small cracks in the rock which also causes good permeability. Small cracks are aligned with the current state of stress in the rock, so that the fast shear azimuth reflects the maximum stress direction.
- Because of their much larger wavelength seismic waves would behave differently from sonic ones. In particular large fractures are known to cause anisotropy on the seismic shear.
- Abrupt changes in fast shear azimuth can be indicative of the presence of a fault, and therefore of zones with high potential for production.
- In the vicinity of a fault major disruptions to the stress and fracture orientation occur. Fast shear azimuth and fracture strike, are no longer parallel.
- Sonic Stoneley information, shear anisotropy and FMI images complement each other to provide a more complete understanding of the fractured reservoir, and provide essential information for field development.

REFERENCES

Auzias, V., 1995, "Contribution a la caracterization tectonique des reservoirs fractures," Ph.D. Thesis, Universite Montpellier II.

Barton, C.A. and Zoback, M.D., 1994, Stress perturbations associated with active faults penetrated by boreholes: Possible evidence for near-complete stress drop and a new technique for stress magnitude measurement: Journal of Geophysical Research, **99**, 9373-9390

Brie, A., Hsu, K. and Eckersley, C., 1988, Using the Stoneley Normalized Differential Energies for Fractured Reservoir Evaluation: the 29th Annual Logging Symposium of the SPWLA, Paper XX.

Chang, S.K., Liu, H.-L. and Johnson, D.L., 1988, Low-frequency tube waves in permeable rocks: Geophysics, **53**, 519-527.

Esmersoy, C., Boyd, A., Kane, M. and Denoo, S., 1995, Fracture and Stress Evaluation Using Dipole-Shear Ani-

sotropy Logs: the 36th Annual Logging Symposium of the SPWLA, Paper J.

Hornby, B.E., Johnson, D.L., Winkler, K.H. and Plumb, R.A., 1989, Fracture evaluation using reflected Stoneley-wave arrivals: Geophysics, **54**, 1274-1288.

Ito, H., Brie, A. and Yamamoto, H., 1996a, Subsurface Structure of the Nojima Fault from Dipole Shear Velocity / Anisotropy and Borehole Stoneley Waves, Proceed. 95th SEGJ Conference, 136-140.

Ito, H., Kuwahara, Y., Miyazaki, T., Nishizawa, O., Kiguchi, T., Fujimoto, K., Ohtani, T., Tanaka, H., Higuchi, T., Agar, S., Brie, A. and Yamamoto, H., 1996b, Structure and Physical Properties of the Nojima Fault by the Active Fault Drilling:, BUTSURI-TANSA, **49**, 522-535.

Kimball, C.V. and Marzetta, T.L., 1984, Semblance processing of borehole acoustic array data: Geophysics, **49**, 274-281.

Last, N.C., and McLean, M.R., 1996, Assessing the Impact of Trajectory on Wells Drilled in an Overthrust Region, Journal of Petroleum Technology, **48**, 620-626.

Sinha, B., Norris, A., and Chang, S.K., 1994, Borehole flexural modes in anisotropic formations: Geophysics, **59**, 1037-1052.

Tezuka, K., Endo, T., Miyairi, M. and Brie, A., 1995, Fast Stoneley Modeling and Its Application for Permeable Fracture Evaluation: Proceedings of the First Annual Well Logging Symposium of Japan, September 21-22, Paper S.

Winkler, K.W., Liu, H.-L. and Johnson, D.L., 1989, Permeability and borehole Stoneley waves: comparison between experiment and theory: Geophysics, **54**, 66-75.

ABOUT THE AUTHORS

Takeshi Endo is the manager of the Sonic Interpretation Group at Schlumberger K.K. in Japan. He joined Schlumberger in 1985 after graduating the University of Tokyo with a Dr.Sc. degree in geophysics. He is a member of SPWLA, SEG, and EAGE.

Hisao Ito is a research geophysicist for Geological Survey of Japan since 1975. He graduated from Tokyo University in 1971 and received a Dr. Sc. degree in geophysics from University of Tokyo in 1979. His recent activities are on characterization on subsurface fracture system through logging and borehole experiments. He is a member of AGU, SPWLA, SSA, SEGJ and SSJ.

Alain Brie is the manager of the Interpretation Product Line for Schlumberger K.K. in Japan. He graduated from Ecole Nationale Superieure de Mecanique et Aerothechnique in Poitiers, France, in 1971, and joined Schlumberger in 1973 as a field engineer. He subsequently occupied various positions as log analyst, research scientist, interpretation training manager, and interpretation development expert. He is a member of SPWLA, SEG and SPE.

Mohammed Badri is a division geophysicist for the East Mediterranean Region covering Turkey, Syria, Jordan, Egypt and Sudan. He graduated from the University of Minnesota, USA, in 1985 with a Ph.D. degree in geophysics. He is responsible for borehole seismic and sonic data acquisition, processing, and interpretation and development. His main interests are reservoir anisotropy and permeability using various measurements, shear waves and borehole imaging. He is a member of SEG and EAGE.

Mohamed El Sheikh is the department head of petrophysics in Agiba Petrroleum Company, Egypt. He graduated from Alexandria University in 1979 from Faculty Of Science with B.Sc. degree in geology. From 1982 to 1988 he was employed by the same company as wellsite geologist. In 1989 he held the position of petrophysics section head until 1994. His main areas of experience are formation evaluation and reservoir geology.

APPENDIX A, Rotation and evaluation of BCR waveforms for anisotropy

The 4-components data can be rotated to obtain the waveform vector along any azimuth using a rotation matrix;

$$\begin{bmatrix} Vxx & Vxy \\ Vyx & Vyy \end{bmatrix} = R \begin{bmatrix} Uxx & Uxy \\ Uyx & Uyy \end{bmatrix} R^T \qquad \text{(A-1)}$$

$$R = \begin{bmatrix} \cos\theta & \sin\theta \\ -\sin\theta & \cos\theta \end{bmatrix} \qquad \text{(A-2)}$$

where

θ : angle of rotation

Uxx : pre-rotation upper dipole in-line waveform

Uxy : pre-rotation upper dipole cross-line waveform

Uyy : pre-rotation lower dipole in-line waveform

Uyx : pre-rotation lower dipole cross-line waveform

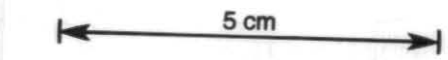

Vxx : rotated upper dipole in-line waveform

Vxy : rotated upper dipole cross-line waveform

Vyy : rotated lower dipole in-line waveform

Vyx : rotated lower dipole cross-line waveform

The waveforms are rotated to find the azimuth for which the energy of the shear wave at the cross receiver is minimum. The shear wave at this azimuth is compared with the one in the perpendicular direction, if it arrives earlier, then this is the fast shear azimuth. Otherwise the fast shear azimuth is the perpendicular direction since the fast and slow shear directions are perpendicular. The tool orientation measured by a general inclinometry device is then used to obtain the fast shear azimuth with respect to true north. Fast and slow shear velocities can then be evaluated using the Slowness-time-coherence processing on the rotated waveforms (Kimball and Marzetta,1984).

APPENDIX B, Stoneley Permeability from the S-Se principle

At a frequency that is much lower than the Biot critical frequency and where the wavelength is much larger than the borehole diameter, omitting the complication of mudcake, the Stoneley slowness, *S*, in a borehole of radius r_b through a permeable formation of frame shear modulus *G* can be expressed as:

$$S^2 = \rho_m\left(\frac{1}{K_m} + \frac{1}{G} - \frac{2}{i\omega r_b Z_0}\right) \qquad \text{(B-1)}$$

where

ρ_m : mud density

K_m : mud bulk modulus

$\omega = 2\pi f$: angular frequency

Z_0 : wall impedance of the permeable formation including the elastic effect of the solid frame.

In equation (B-1), the successive terms are the contribution of the fluid expansion, the borehole expansion, and the fluid flow in the pore space. The impedance Z_0 can be expressed in term of Biot slow wave number k_{c2} and mobility $\frac{\kappa}{\eta}$ (permeability/viscosity) as:

$$\frac{1}{Z_0} = k_{c2}(\kappa/\eta)\frac{H_1^{(1)}(k_{c2}r_b)}{H_0^{(1)}(k_{c2}r_b)} \qquad \text{(B-2)}$$

where $H_0^{(1)}$ and $H_1^{(1)}$ are the Hankel function of the first kind order 0 and 1 respectively. k_{c2} is a complicated function of ω, ϕ - porosity, G - frame shear modulus, K_s - sold grain modulus, K_b - frame bulk modulus, K_f - pore fluid bulk modulus and also κ/η.

We can express the measured Stoneley slowness, S in two terms; $S^2 = S_e^2 + S_p^2$ where S_e is the zero frequency elastic slowness and S_p is the permeability-added slowness. S_e^2 is the first terms of (B-1),

$$S_e^2 = \rho_m\left(\frac{1}{K_m} + \frac{1}{G}\right) \qquad \text{(B-3)}$$

In the DSI tool, the Stoneley frequency is below 1 kHz, therefore $S_e >> S_p$. Therefore, using (B-1),(B-2) and (B-3), we can write;

$$2S_e(S - S_e) = S_p^2 = (Cp)^2\sqrt{\frac{\kappa}{\eta}} \qquad \text{(B-4)}$$

where the coefficients $(Cp)^2$ is a function of ω, ρ_m, κ/η, ϕ, *G*, K_s, K_b, K_f, *S, and* K_m.

The expression of *Cp* is complex and also depends on (κ/η). Strictly speaking, $S_e(S\text{-}S_e)$ is not proportional to $\sqrt{\kappa/\eta}$. However, C_p is a slowly varying function and can be considered a constant in the first approximation as indicated in Fig. B-1 which shows the relation between mobility and *(S-Se)* computed from the model. Therefore *(S-S_e)* can be used as a qualitative indicator of pore fluid mobility.

For clarity (B-4) was shown with the low frequency approximation for the elastic slowness S_e. However, in the processing the full elastic Stoneley slowness algorithm was used (Chang et al., 1988), and the calculated *S-Se* indicator uses the frequency dependent elastic Stoneley slowness.

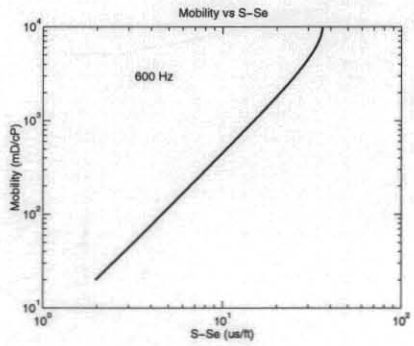

Figure B1 Relation between mobility versus S-Se computed from model. Used parameters are:
Compressional slowness: 77.0 us/ft, Shear slowness: 132.0 us/ft, Formation density: 2.42 g/cc, Porosity: 0.2, Solid grain bulk moduls: 35 GPa, Pore fluid bulk modulus: 2.25 GPa, Pore fluid density: 1.0 g/cc, Hole diameter: 8.0 inch, Viscosity: 1 cP

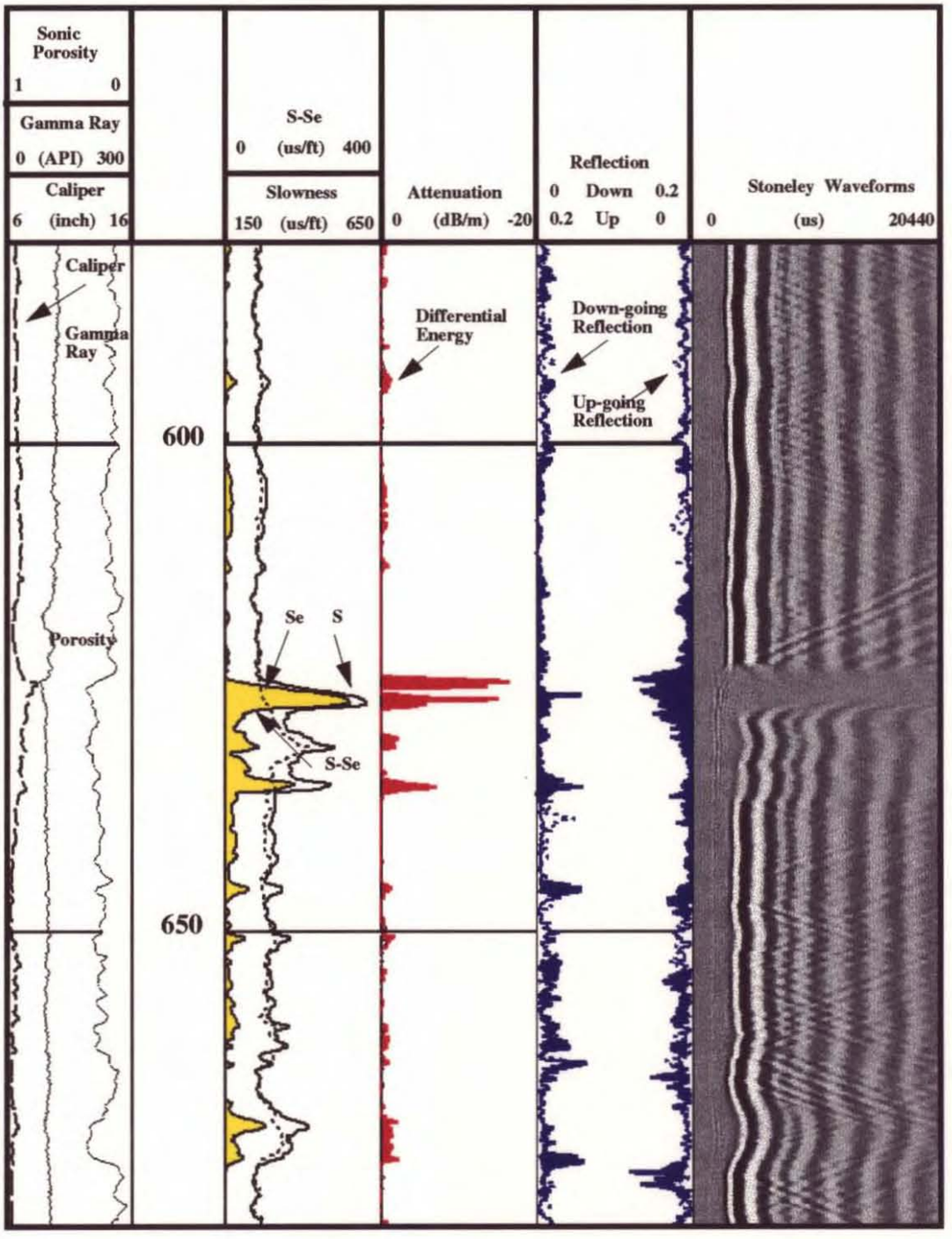

Figure 1 Stoneley evaluation results for Well A

5 cm

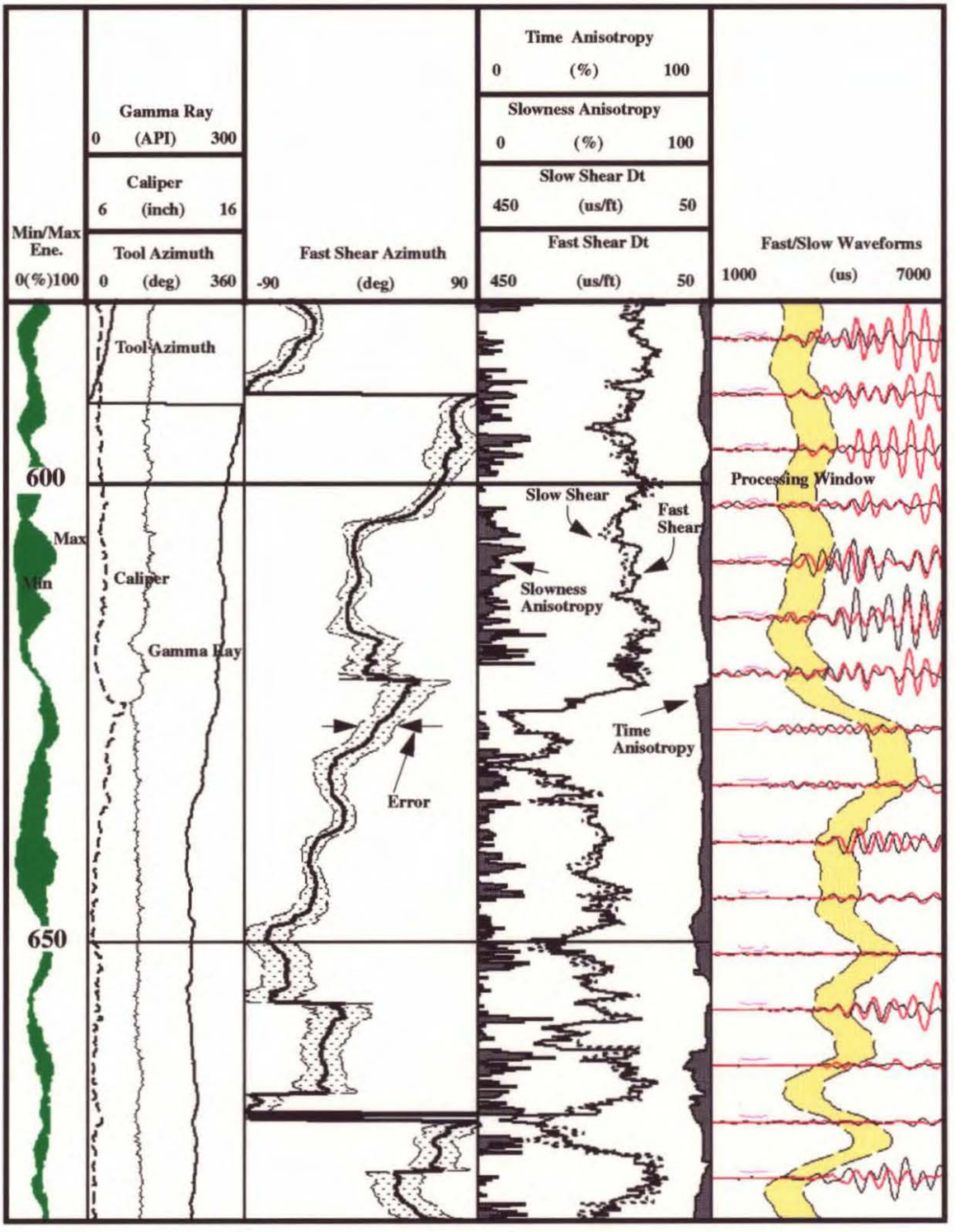

Figure 2 Anisotropy evaluation results for Well A

5 cm

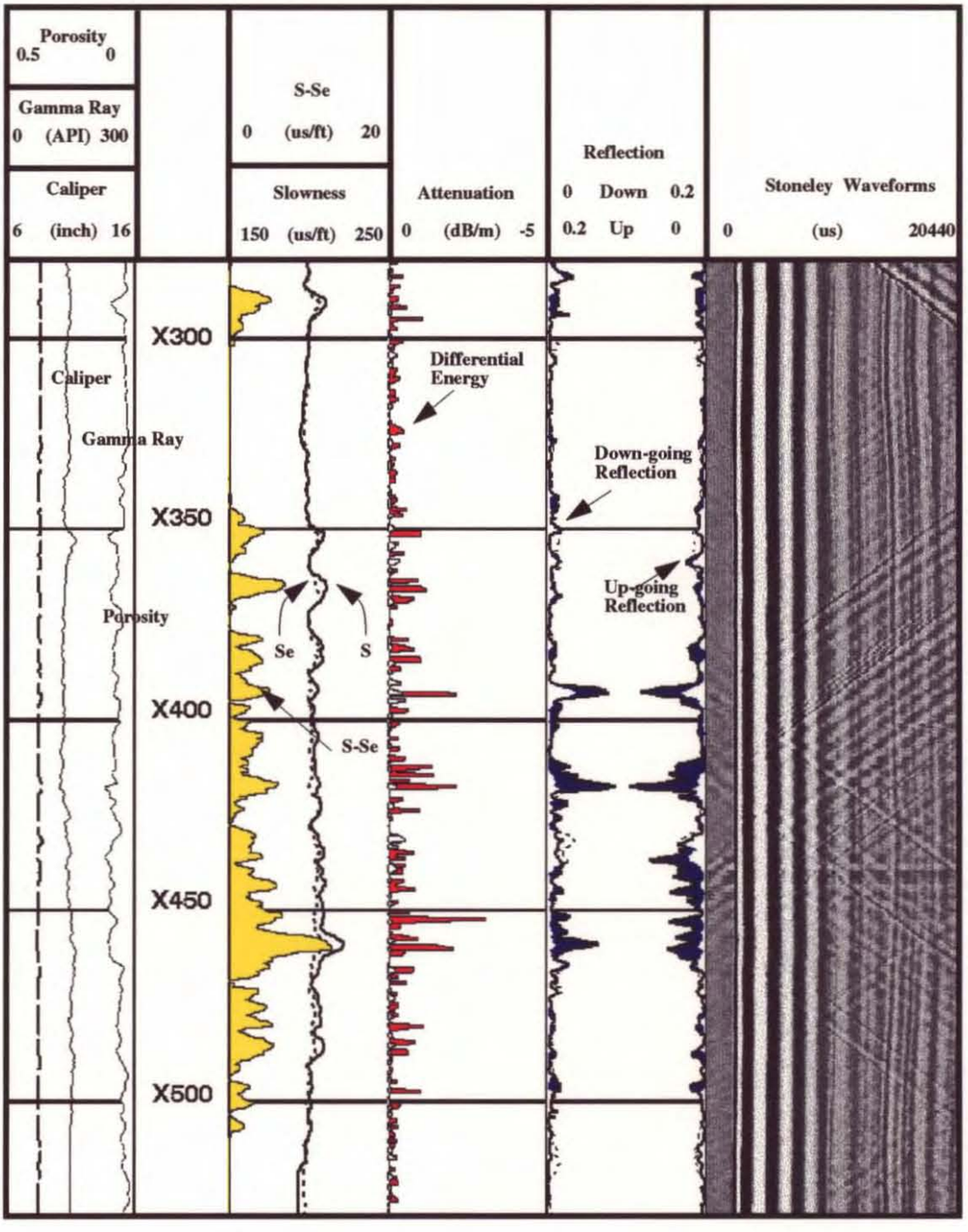

Figure 3 Stoneley evaluation results for Well B

5 cm

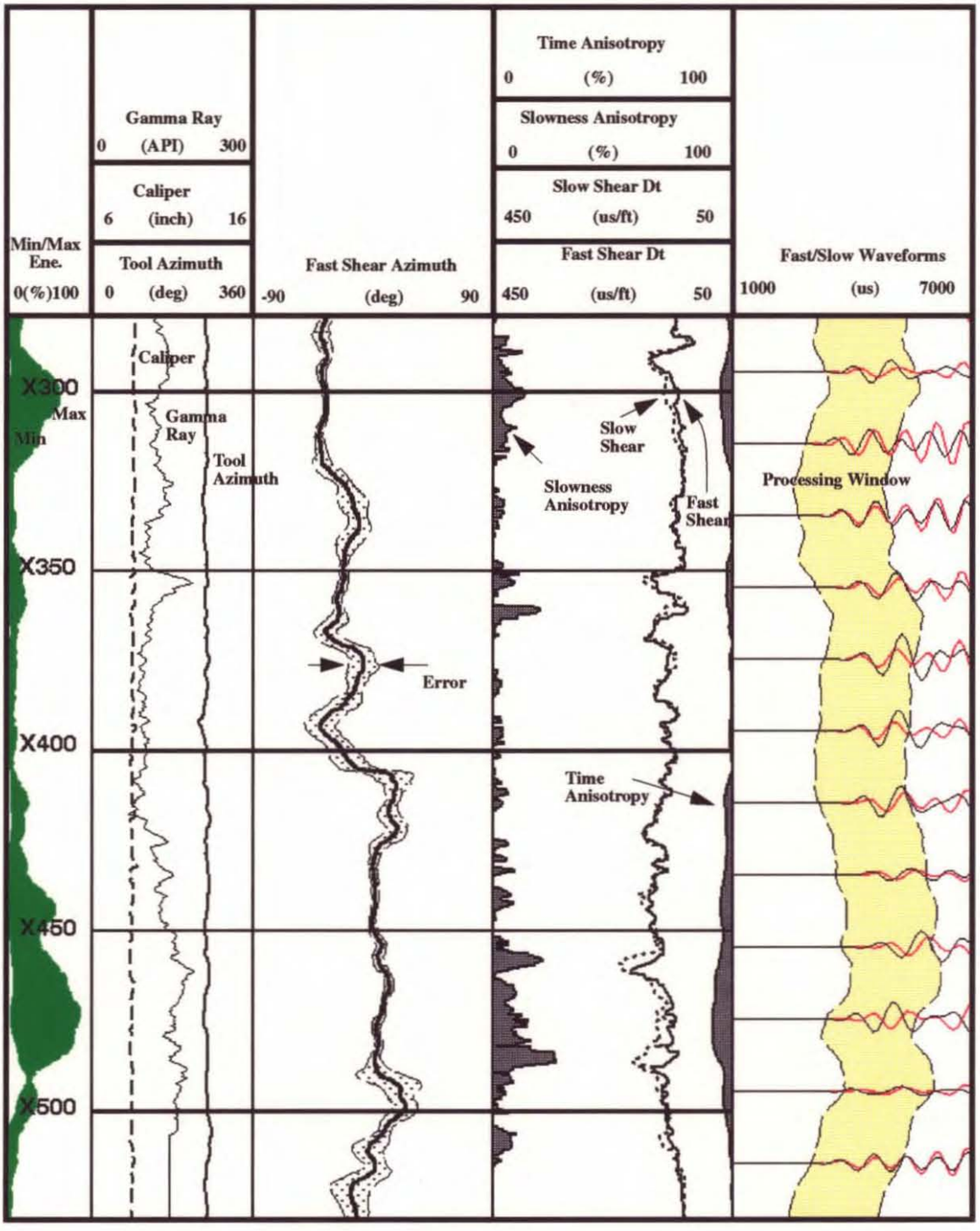

Figure 4 Anisotropy evaluation results for Well B

5 cm

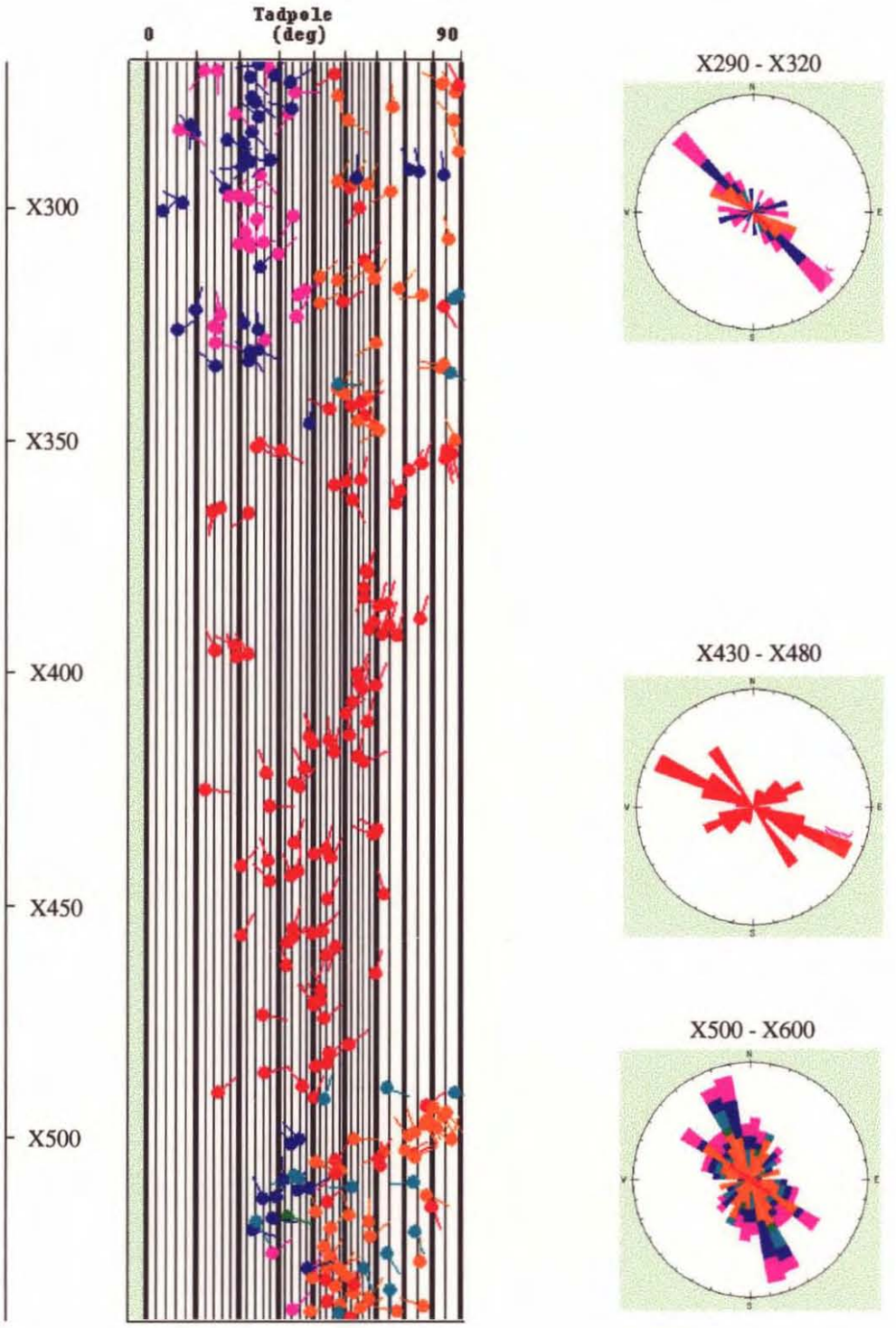

Figure 5 Dip and orientation of fractures from borehole resistivity image data of Well B

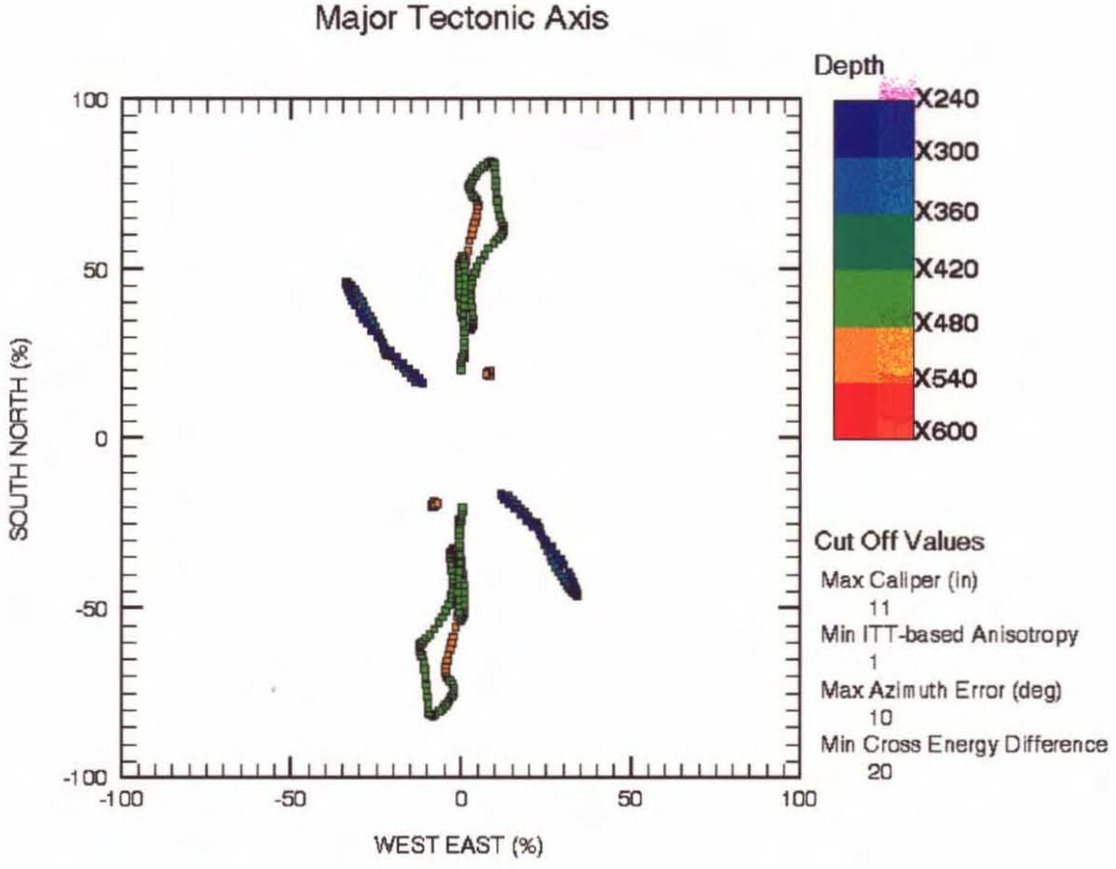

Figure 6: Anisotropy azimuthal plot. for Well B An azimuth of a point is the fast shear azimuth and a distance from the origin corresponds to a difference between maximum and minimum cross energies. Different color corresponds to a depth of frame.

Fracture Evaluation from Dipole Shear Anisotropy and Borehole Stoneley Waves

Takeshi Endo*, Alain Brie* and Mohammed Badri**

*Schlumberger K.K., Fuchinobe, Kanagawa-ken, Japan
**Schlumberger Logelco Inc., Cairo, Egypt

ABSTRACT

Identification and evaluation of fracture systems is of primary importance to the development of hard rock reservoirs. Sonic measurements are sensitive to fractures and can contribute in many ways to their evaluation. Stoneley wave reflections and attenuation analysis are commonly used techniques. They have the advantage of showing open permeable fractures. Last year Tezuka et al improved the reliability of Stoneley fracture evaluation using Stoneley modeling, a technique which evaluates the effect of borehole irregularities and lithology changes, and permits differentiation of permeable fractures. Permeability added Stoneley slowness is another useful technique. It compares the measured Stoneley slowness to the elastic slowness obtained from a model without permeability. The difference, the permeability added slowness, is an indication of the mobility of the pore fluid in the formation.

The recently introduced dipole shear anisotropy evaluation also provides information on fractures. This technique evaluates shear wave splitting resulting from acoustic anisotropy. Fractures and anisotropic stresses being the main causes of acoustic anisotropy in a transversely isotropic horizontal (TIH) formation, the direction of the fast shear wave provides information on fractures and stress orientation. The indications provided by this measurement differ somewhat from the Stoneley techniques indications; in particular shear wave anisotropy investigates a volume of formation up to 3-5 borehole diameters away from the borehole and can indicate fractures missed by other techniques. In this study we evaluated a data-set with these different acoustic techniques: dipole shear anisotropy, permeability added Stoneley slowness, Stoneley attenuation and Stoneley reflections, including modeling of the effects of borehole irregularities. We compared the results from the different techniques to determine their sensitivity to different types of fractures and to the environment, and discussed how they can be combined to provide an improved evaluation of fractured reservoirs.

INTRODUCTION

In hard rock reservoirs production is often mostly done through fractures. Therefore the knowledge of the fracture locations and of their characteristics is of primary importance for well completion design and for field development. Many measurements provide information on fractures, the most important ones are azimuthal resistivity, micro-resistivity imaging, ultra-sonic imaging, and sonic techniques. Sonic techniques include Stoneley wave reflections evaluation (Hornby et al, 1989), and Stoneley attenuation (Brie et al, 1988). The advantage with Stoneley techniques is that they detect major open fractures, the one from which most of the production comes from. Last year the reliability of Stoneley fracture evaluation was improved through the use of Stoneley modeling which allows separation of the effect of borehole irregularities and lithology changes from permeable fractures (Tezuka et al, 1995). Permeability added Stoneley slowness is another technique which has proven useful in identifying potentially producing intervals. It is based on the difference between a Stoneley slowness computed from elastic theory, without the effect of permeability and the measured Stoneley slowness (Winkler et al, 1989). The difference is an indicator of permeability in the formation.

Recently, dipole shear anisotropy evaluation from cross dipole measurements was introduced (Esmersoy et al, 1995). This technique also provides information on fractures through the evaluation of acoustic anisotropy and has been used with success in identifying producing intervals. The direction of the fast shear wave also provides information on stress and fracture orientation. The indications provided by this measurement differ somewhat from the Stoneley techniques indications. In particular shear wave anisotropy investigates a volume of formation up to 3-5 borehole diameters away from the borehole (Sinha et al., 1994) and can indicate fractures missed by other techniques.

In this paper we compare the response of these different techniques in a fractured reservoir. We will examine their sensitivity to different types of fractures and to the environment, and see how they can be combined to provide

an improved evaluation.

DIPOLE SHEAR ANISOTROPY ANALYSIS

A tectonically fractured formation exhibits azimuthal anisotropy to shear waves. A shear wave that is polarized parallel to the fracture strike will propagate faster than a shear wave polarized perpendicular to it. A shear (or flexural) wave, such as the ones generated by a dipole source, will split as it propagates along the borehole and give a fast shear wave and a slow shear wave polarized along the anisotropy axis (Fig. 1).

With the availability of two sets of dipole transmitters and receivers in orthogonal directions, the DSI* Dipole Shear Sonic Imager Tool can measure the shear slowness in different directions in a plane perpendicular to the tool axis. The full evaluation requires recording the waveforms on an axis parallel with the transmitter axis, but also in the perpendicular direction or cross direction. This is done with both transmitters so that four sets of array waveforms are recorded at every level (Both Cross Receivers acquisition mode). The 4-components data can be rotated to obtain the waveform vector along any azimuth using a rotation matrix;

$$\begin{bmatrix} RWxx & RWxy \\ RWyx & RWyy \end{bmatrix} = R \begin{bmatrix} PWxx & PWxy \\ PWyx & PWyy \end{bmatrix} R^T$$

$$R = \begin{bmatrix} \cos\theta & \sin\theta \\ -\sin\theta & \cos\theta \end{bmatrix}$$

where

θ : Angle of rotation

$PWxx$: Pre-rotation upper dipole in-line waveform

$PWxy$: Pre-rotation upper dipole cross-line waveform

$PWyy$: Pre-rotation lower dipole in-line waveform

$PWyx$: Pre-rotation lower dipole cross-line waveform

$RWxx$: Rotated upper dipole in-line waveform

$RWxy$: Rotated upper dipole cross-line waveform

$RWyy$: Rotated lower dipole in-line waveform

$RWyx$: Rotated lower dipole cross-line waveform

The waveforms are rotated to find the azimuth for which the energy of the shear wave at the cross receiver is minimum. The shear wave at this azimuth is compared with the one in the perpendicular direction, if it arrives earlier, then this is the fast shear azimuth. Otherwise the fast shear azimuth is the perpendicular direction since the fast and slow shear directions are perpendicular. The tool orientation measured by a general inclinometry device is then used to obtain the fast shear azimuth with respect to true North. Fast and slow shear velocities can then be evaluated using the STC processing on the rotated waveforms (Kimball and Marzetta, 1984).

STONELEY PERMEABILITY ANALYSIS

As Stoneley wave propagates in permeable formation, it is attenuated and slowed down as depicted in Figure 2. The effects of permeability on the slowness and attenuation of the borehole Stoneley wave have been studied extensively both theoretically (Chang et al., 1988) and experimentally (Winkler et al., 1989). Due to a large number of formation, borehole and mud cake parameters involved, the implementation of the quantitative inversion from Stoneley slowness to fluid mobility is not straightforward. Therefore in practice we use the low frequency S-Se approximation which is simpler to implement. The basis of this method is as follows.

At a frequency which is much lower than the Biot critical frequency and where the wavelength is much larger than the borehole diameter, omitting the complication of mud cake, the Stoneley slowness, S, in a borehole of radius r_b through a permeable formation of frame shear modulus G can be expressed as:

$$S^2 = \rho_m \left(\frac{1}{K_m} + \frac{1}{G} - \frac{2}{i\omega r_b Z_0} \right) \qquad \text{(Eq. 1)}$$

where

ρ_m : Mud density

K_m : Mud bulk modulus

$\omega = 2\pi f$: Angular frequency

Z_0 : Wall impedance of the permeable formation including the elastic effect of the solid frame.

In equation (Eq 1), the successive terms are the contribution of the fluid expansion, the borehole

expansion, and the fluid flow in the pore space. The impedance Z_0 can be expressed in term of Biot slow wave number k_{c2} and mobility $\frac{\kappa}{\eta}$ (permeability/viscosity) as:

$$\frac{1}{Z_0} = k_{c2}(\kappa/\eta)\frac{H_1^{(1)}\left(k_{c2}r_b\right)}{H_0^{(1)}\left(k_{c2}r_b\right)} \qquad \text{(Eq. 2)}$$

where $H_0^{(1)}$ and $H_1^{(1)}$ are the Hankel function of the first kind order 0 and 1 respectively. k_{c2} is a complicated function of ω, ϕ - porosity, G - frame shear modulus, K_s - sold grain modulus, K_b - frame bulk modulus, K_f - pore fluid bulk modulus and also κ/η.

We can express the measured Stoneley slowness, S in two terms; $S^2 = S_e^2 + S_p^2$ where S_e is the zero frequency elastic slowness and S_p is the permeability added slowness. S_e^2 is the first terms of (Eq. 1),

$$S_e^2 = \rho_m\left(\frac{1}{K_m} + \frac{1}{G}\right) \qquad \text{(Eq. 3)}$$

In the DSI tool, the Stoneley frequency is below 1 kHz, therefore $S_e >> S_p$. Therefore, using (Eq. 1),(Eq. 2) and (Eq. 3), we can write;

$$2S_e\left(S - S_e\right) = S_p^2 = (Cp)^2\sqrt{\frac{\kappa}{\eta}} \qquad \text{(Eq. 4)}$$

where the coefficients $(Cp)^2$ is a function of ω, ρ_m, κ/η, ϕ, G, K_s, K_b, K_f, S, and K_m.

The expression of Cp is complex and also depends on (κ/η). Strictly speaking, $S_e(S\text{-}S_e)$ is not proportional to $\sqrt{\kappa/\eta}$. However, C_p is a slowly varying function and can be considered a constant in the first approximation. Therefore $(S\text{-}S_e)$ can be used as a qualitative indicator of pore fluid mobility.

For clarity (Eq. 4) was shown with the low frequency approximation for the elastic slowness Se. However in the processing the full elastic Stoneley slowness algorithm was used (Chang et al, 1988), and the calculated S-Se indicator uses the frequency dependent elastic Stoneley slowness.

STONELEY FRACTURE ANALYSIS

As the Stoneley wave propagates past an open fracture, part of the energy is reflected and a part of the energy is transmitted as depicted in Figure 3.

Stoneley attenuation and reflection coefficients provides information on opened fractures. Stoneley attenuation was evaluated with the Normalized Differential Energies (NDE) technique (Brie et. al, 1988). The computation was made in the 0 to 1.5 kHz frequency band. A borehole compensation was achieved by calculating the average of the receiver and transmitter mode results.

Following the method proposed by Tezuka et al, 1995, model waveforms were generated from log data: compressional slowness, shear slowness, density and hole diameter. These waveforms were processed in the same fashion as the real ones to estimate borehole, and bed boundaries effects. On the final plots the attenuation due to borehole variations and lithology is shown in white. The additional attenuation due to fractures and permeability is shown in black.

To evaluate Stoneley reflections, up and down going reflected fields were first separated from the total waveform with a velocity filter. Both down and up going Stoneley reflections were evaluated in the 0.25 to 4.25 kHz frequency band, for the real and model waveforms. The resulting reflection coefficients are presented on Figures 4 and 6. The results for the down going reflections are shown on the left side, and for the up going reflection on the right side. The model waveforms were also evaluated to estimate the borehole and bed boundary effects. The model reflection coefficient is coded white, while the added reflection coefficient caused by fractures are shown in black.

CASE STUDY

The data of this case study is from a well drilled in the fractured granite basement. The DSI log in this well includes the monopole P&S, monopole Stoneley and dipole BCR modes. Conventional open hole logs and the FMI * Formation Micro Imager data were also recorded, and a detailed fracture evaluation from the FMI data was performed (Fig. 9).

The sonic results are presented in two sections, the upper one from x260 to x380 ft (Fig. 4 and 5), and the continuation in the lower zone from x380 to x510 ft (Fig. 6 and 7). In each section the results are presented in two parallel plots. One with Stoneley fracture evaluation results, Stoneley permeability indicator, and porosity, and another one with acoustic anisotropy results.

In the upper section there are very few fractures detected by the Stoneley techniques. The attenuation shows a few minor events from x345 to x370 ft, and above x300 ft. On the reflection analysis there is a minor up going reflection at x360 ft and a small down going reflection at x280 ft. These events are not correlated between the various Stoneley techniques so that the results have a low confidence level. The Stoneley permeability indicator, S - Se, shows some increase between x345 and x370 ft, and

above x300 ft. These indications coincide with zones where Stoneley attenuation indications were observed. There is also good correlation between S - Se and porosity. This suggests that Stoneley permeability and attenuation are seeing porosity from small fractures and cracks, and that there are no fracture with large enough flow potential to generate Stoneley reflections. This confirm the field experience which says that this zone is not a potential producer. The anisotropy evaluation results (Fig. 5) show that the fast shear azimuth is stable at about -40 degrees. There is substantial anisotropy at x300 ft seen on the energy, slowness and time differences. However at this location there is no indication of major fractures from the Stoneley indicators. The FMI analysis shows fractures at varying dipping angles, but very few are opened. The fracture strike is well defined on the polar plot at around -45 degrees (Fig. 9 top left), and therefore in good agreement with the anisotropy indications. This suggests that the direction of major tectonic stress in this area is about -40 degrees.

In the lower section major events are detected on all Stoneley techniques at x394, x420, and x460 ft. These events cause significant Stoneley reflections both in the down and up going directions, and Stoneley attenuation. The borehole effect evaluated with Stoneley modeling is small except for the event at x394 ft for which half of the reflection seems to come from the borehole. Some smaller events are detected between x430 and x460 ft. The S - Se Stoneley permeability indicator shows more mobility here than in the previous section. It also shows peaks of permeability in front of the events detected by the other Stoneley techniques. Porosity also is overall higher in this interval. On the anisotropy results we observe large variations of the fast shear azimuth which is 70 degrees at the top, then goes down to 20 degrees between x408 ft and x425 ft, then reads 0 to 10 degrees below x425 ft. There is no significant acoustic anisotropy detected where these changes take place. However there is strong anisotropy detected between x455 ft and x490 ft. Although the strong anisotropy indication at x408 ft corresponds with a fracture detected with the Stoneley technique, the other anisotropy peak at x485 ft does not correspond to any event on the Stoneley. The FMI analysis in this zone shows two sets of fractures with low dips (30 to 50 degrees), increasing to 70 degrees above x425 ft, in a way similar to the fast shear azimuth. Two trends are observed on the fracture polar plot: one main trend at an azimuth of -70 degrees, and two smaller ones at -30 and +40 degrees. These last ones being mostly from the lower part of the interval.

The fast shear azimuth and the fractures strike are both at -40 degrees in the upper section. This suggest that this is the regional tectonic state of stress. But how can we interpret the various phenomenon we observe in the lower section: the change in fast shear azimuth, the low fracture dips, and the difference between the fast shear azimuth and the fracture strike.

Two hypotheses can be proposed:

1 - Thermal stresses: granite is an igneous rock which came from large depths and high temperatures as a plastic rock in the form of a diapir. When reaching shallow depths the rock mass cooled down rapidly which produced shrinkage and fracturing, especially close to the diapir borders. The orientation of these fractures is a function of the thermal stresses and are not related to the regional state of stress. But with this hypothesis it is difficult to explain all the features we observed.

2 - Presence of a fault: a fault perturbs the stress field around it. Faults are common in granite, and various faults were mapped with VSP images acquired over the reservoir. Identification of a fault in a basement reservoir with fractures is not straight forward, however, a fault can be present when a zone with relatively no, or little, fractures is observed next to a zone with extensive fractures. This is what we have in this interval. If we look at the Stoneley reflections we see the number of large open fractures is much higher starting at x410 ft compared to the upper zone x250 to x400 ft.

A fault causes a drag zone in which rock deformation is large. Bending of the beds next to the fault causes extensional stresses, and extensional fractures on one side of the bed and compressional stresses, with conjugate shear fractures, on the other. We expect the stress direction to change rapidly when the well crosses the fault. Looking at the log we observe that the stress direction changes rapidly between x410 and x425 ft, and that the Stoneley indicators show a very strong event at x420 ft. This is probably a fault intercepting the well. This fault is open and seen on the logs as a large fracture. Below the fault is a deformed zone with a sequence of extensional fractures, and compression shear conjugate fractures. We notice that the porosity is good in this zone because of the substantial rock deformation. The FMI analysis in this zone shows these extension fractures have low dip, and a strike azimuth of about -75 degrees. Shear conjugate fractures have strike azimuths at -35 and -115 degrees, which is consistent with a maximum stress direction as -75 degrees. However, the fast shear azimuth in this zone is very different between 0 to 10 degrees. It suggests that the fractures could have been created at the early stage of faulting, before the present state of stress was established. On the other hand, the fast shear azimuth (0 - 10 degrees) indicates the present maximum stress direction.

Option 2, the fault hypothesis seems to be the most likely, although we do not have additional confirmation of the presence of a fault in this interval. It is believed that

most of the production in this well which is a good oil producer comes from the fault zone. Other well in the same field which did not intercept this fault did not produce any oil.

CONCLUSION

We have evaluated fractures from Stoneley reflections and attenuation, permeability from Stoneley slowness, and acoustic shear anisotropy. These results were compared with the information provided by FMI images. In this well drilled in a granite formation we concluded the following:

- Stoneley attenuation and reflection see large open fractures and fault zones.

- Permeability added Stoneley slowness is a good indicator of permeable zone in hard rocks. It is sensitive to both fractures and rock permeability.

- Stoneley attenuation is sensitive to large open fractures and also to a lesser extent to rock permeability.

- Stoneley modeling is effective in showing what fraction of Stoneley reflections and attenuation is caused by borehole effect or bed boundaries.

- In a stable tectonic environment the fast shear azimuth indicates the direction of maximum stress and is parallel to the fracture strike.

- Acoustic anisotropy indications are often not directly correlated with large fractures. However they can be indicative of cracks or small fracture systems, and are usually good producibility indicators.

- Abrupt changes in fast shear azimuth can be indicative of the presence of a fault, and therefore of high potential zones for production.

- In the vicinity of a fault major disruptions to the stress and fracture orientation occur. Fast shear azimuth and fracture strike are no longer parallel.

- Sonic Stoneley information, shear anisotropy, and FMI images complement each other to provide a more complete understanding of the fractured reservoir, and provide essential information for field development.

ACKNOWLEDGEMENT

We thank Agiba Petroleum Company for their permission to publish the data-set used in this study.

REFERENCES

Brie, A., Hsu, K. and Eckersley, C., 1988, Using the Stoneley Normalized Differential Energies for Fractured Reservoir Evaluation: the 29th Annual Logging Symposium of the SPWLA, Paper XX.

Chang, S.K., Liu, H.-L. and Johnson, D.L., 1988, Low-frequency tube waves in permeable rocks: Geophysics, **53**, 519-527.

Esmersoy, C., Boyd, A., Kane, M. and Denoo, S., 1995, Fracture and Stress Evaluation Using Dipole-Shear Anisotropy Logs: the 36th Annual Logging Symposium of the SPWLA, Paper J.

Hornby, B.E., Johnson, D.L., Winkler, K.H. and Plumb, R.A., 1989, Fracture evaluation using reflected Stoneley-wave arrivals: Geophysics, **54**, 1274-1288.

Kimball, C.V. and Marzetta, T.L., , 1984, Semblance processing of borehole acoustic array data: Geophysics, **49**, 274-281.

Sinha, B., Norris, A., and Chang, S.K., 1994, Borehole flexural modes in anisotropic formations: Geophysics, **59**, 1037-1052.

Tezuka, K., Endo, T., Miyairi, M. and Brie, A., 1995, Fast Stoneley Modeling and Its Application for Permeable Fracture Evaluation: Proceedings of the First Annual Well Logging Symposium of Japan, September 21-22, Paper S.

Winkler, K.W., Liu, H.-L. and Johnson, D.L., 1989, Permeability and borehole Stoneley waves: comparison between experiment and theory: Geophysics, **54**, 66-75.

ABOUT THE AUTHORS

Takeshi Endo is the Manager of the Sonic Interpretation Group at Schlumberger K.K. in Japan. He joined Schlumberger in 1985 after graduating the University of Tokyo with a Dr.Sc. degree in geophysics. He is a member of SPWLA and SEG.

Alain Brie is the Manager of the Interpretation Product Line for Schlumberger K.K. in Japan. He graduated from Ecole Nationale Superieure de Mecanique et Aerothechnique in Poitiers, France, in 1971, and joined Schlumberger in 1973 as a field engineer. He subsequently occupied various positions as log analyst, research scientist, interpretation training manager, and interpretation

development expert. He is a member of SPWLA and SPE.

Mohammed Badri is a Division Geophysicist for the East Mediterranean Region covering Turkey, Syria, Jordan, Egypt and Sudan. He graduated from the University of Minnesota, USA, in 1985 with a Ph.D. degree in Geophysics. He is responssible for borehole seismic and sonic data acquistion, processing, and interpretation and development. His main interests are reservoir anisotropy and permeability using various measurements, shear waves and borehole imaging. He is a member of SEG and EAGE.

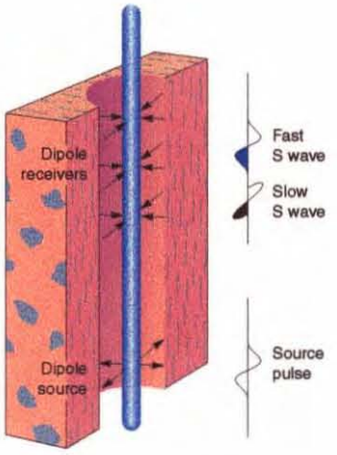

Figure 1: Shear-wave splitting in dipole logging. Fast-shear waves are polarized in the fracture strike and/or maximum stress direction, and slow-shear waves are polarized perpendicular to that.

Figure 2: Permeability effects on Stoneley wave. As Stoneley wave propagates in permeable formation, it is attenuated and slowed down.

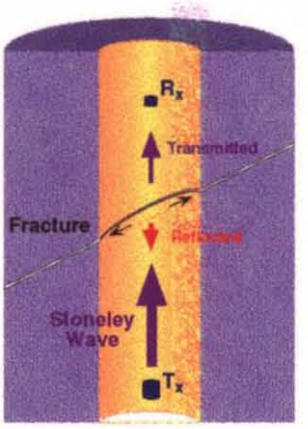

Figure. 3: Fracture effects on Stoneley wave. As Stoneley wave propagates past an open fracture, a part of the energy is reflected and a part of the energy is transmitted.

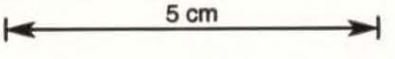

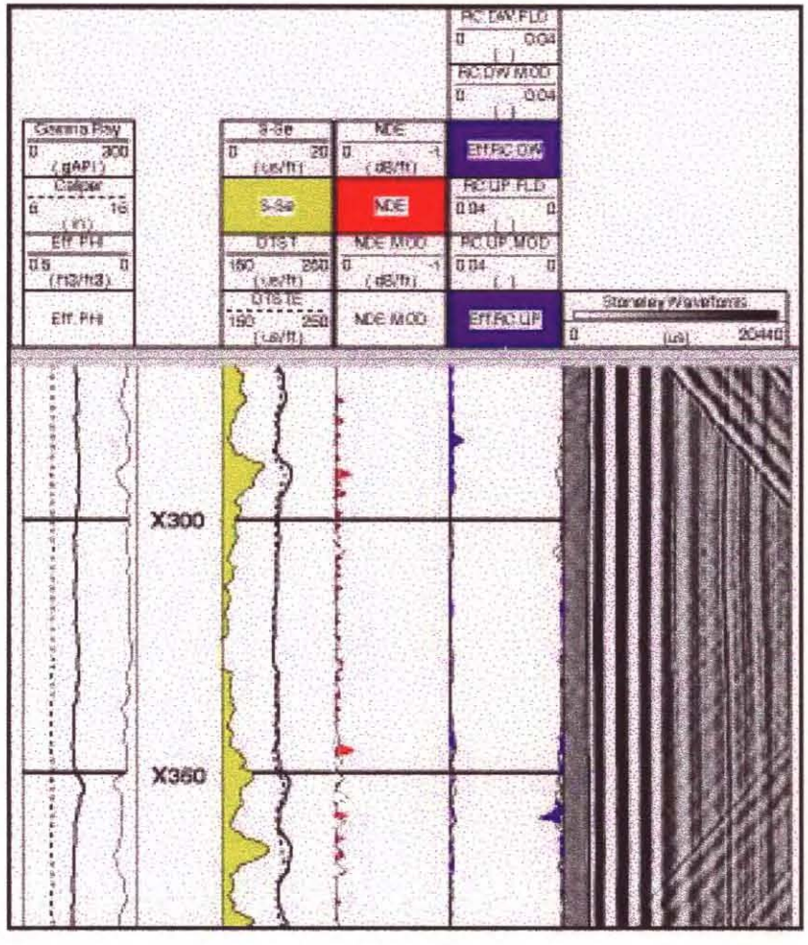

Figure 4: Stoneley fracture permeability analysis result for the upper section

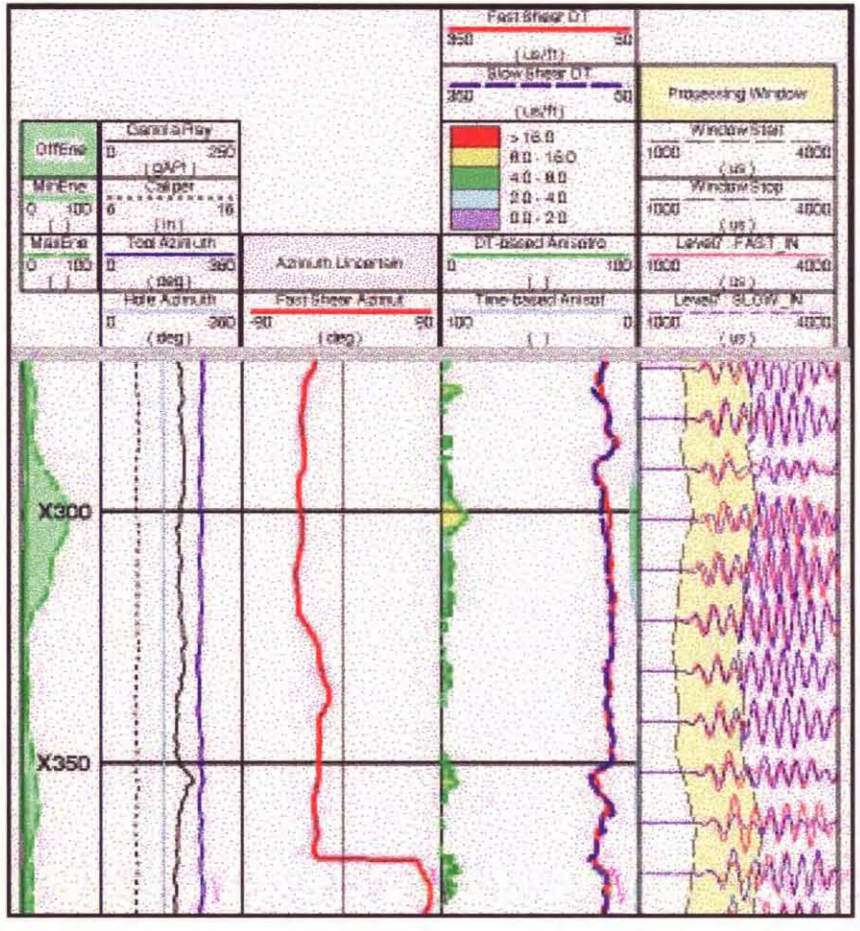

Figure 5 Shear anisotropy analysis result for the upper section

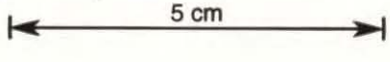

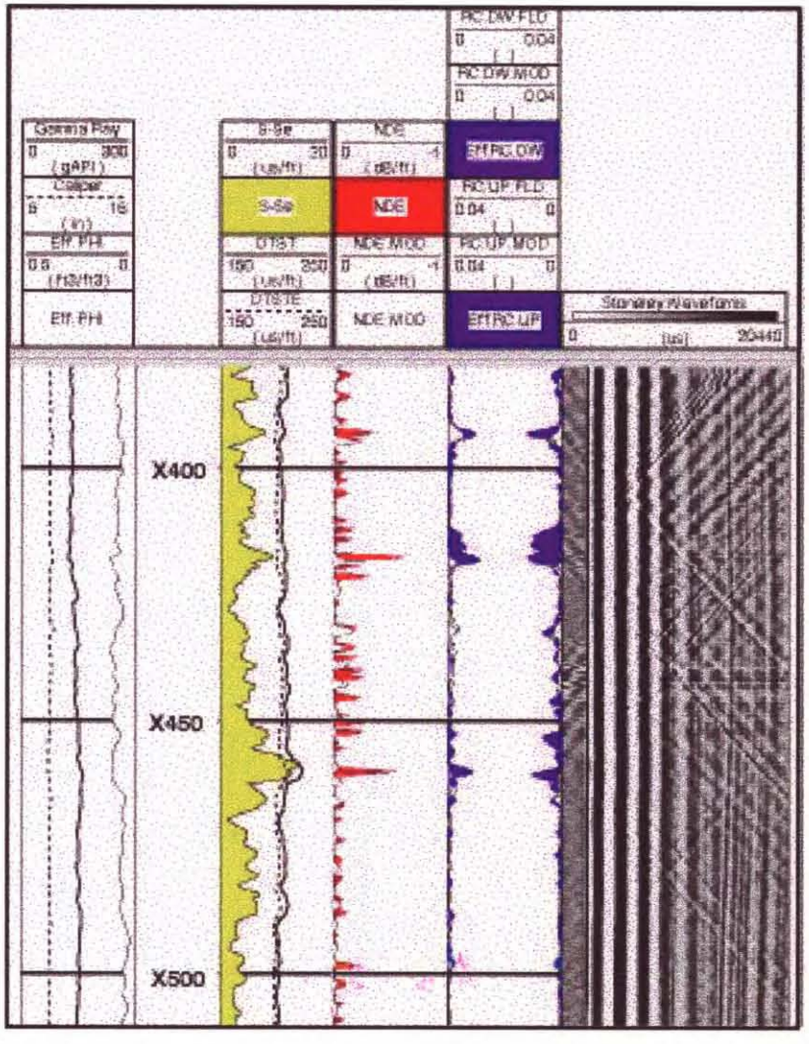

Figure 6: Stoneley fracture permeability analysis result for the lower section

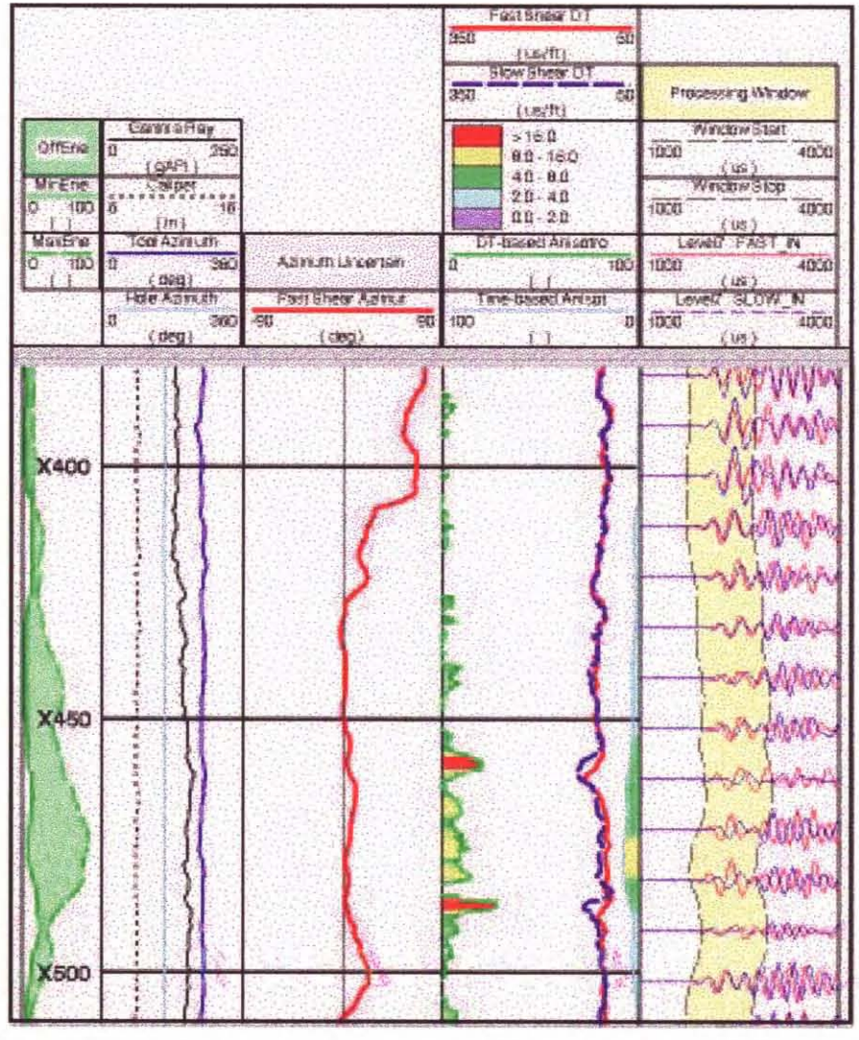

Figure 7 Shear anisotropy analysis result for the lower section

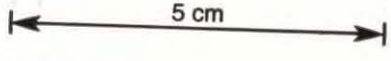

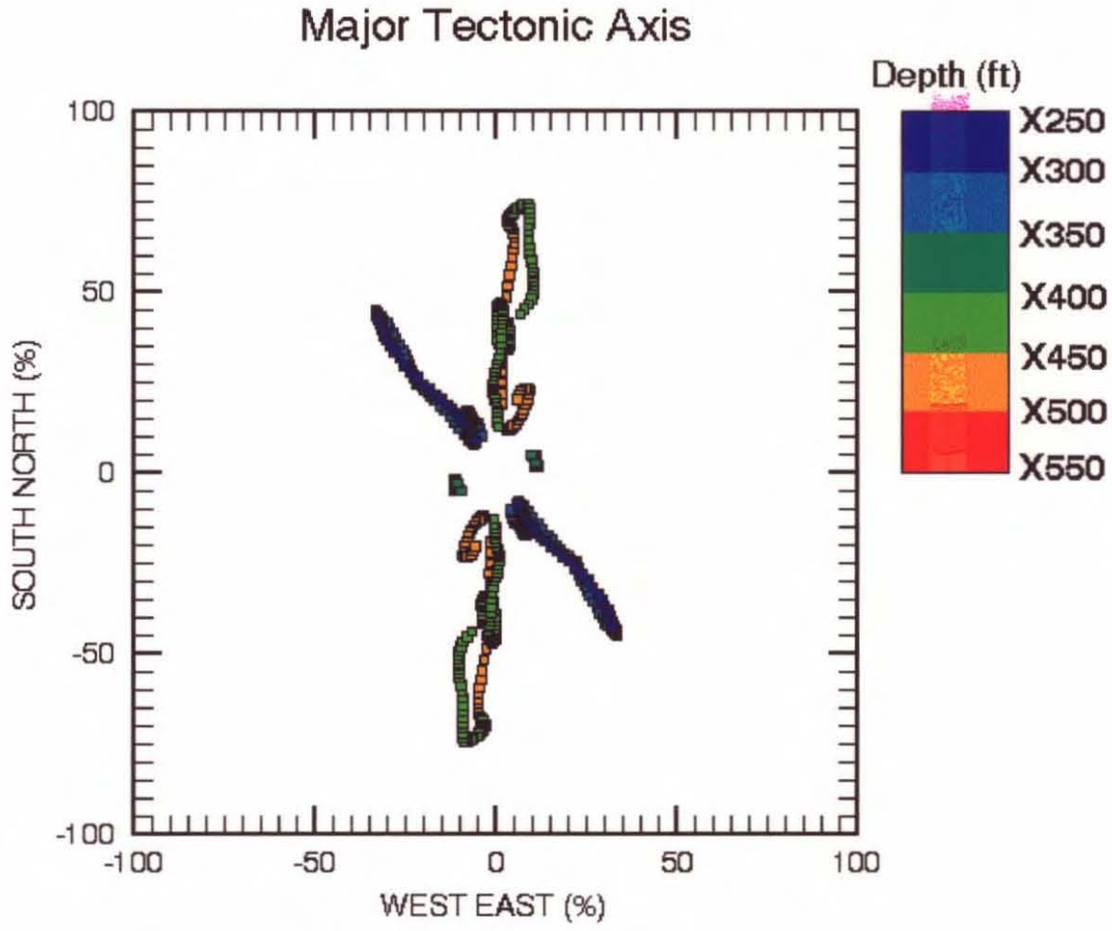

Figure 8: Anisotropy azimuthal plot. An azimuth of a point is the fast shear azimuth and a distance from the origin corresponds to a difference between maximum and minimum cross energies. Different color corresponds to a depth of the point.

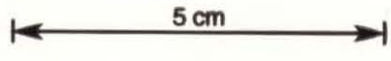

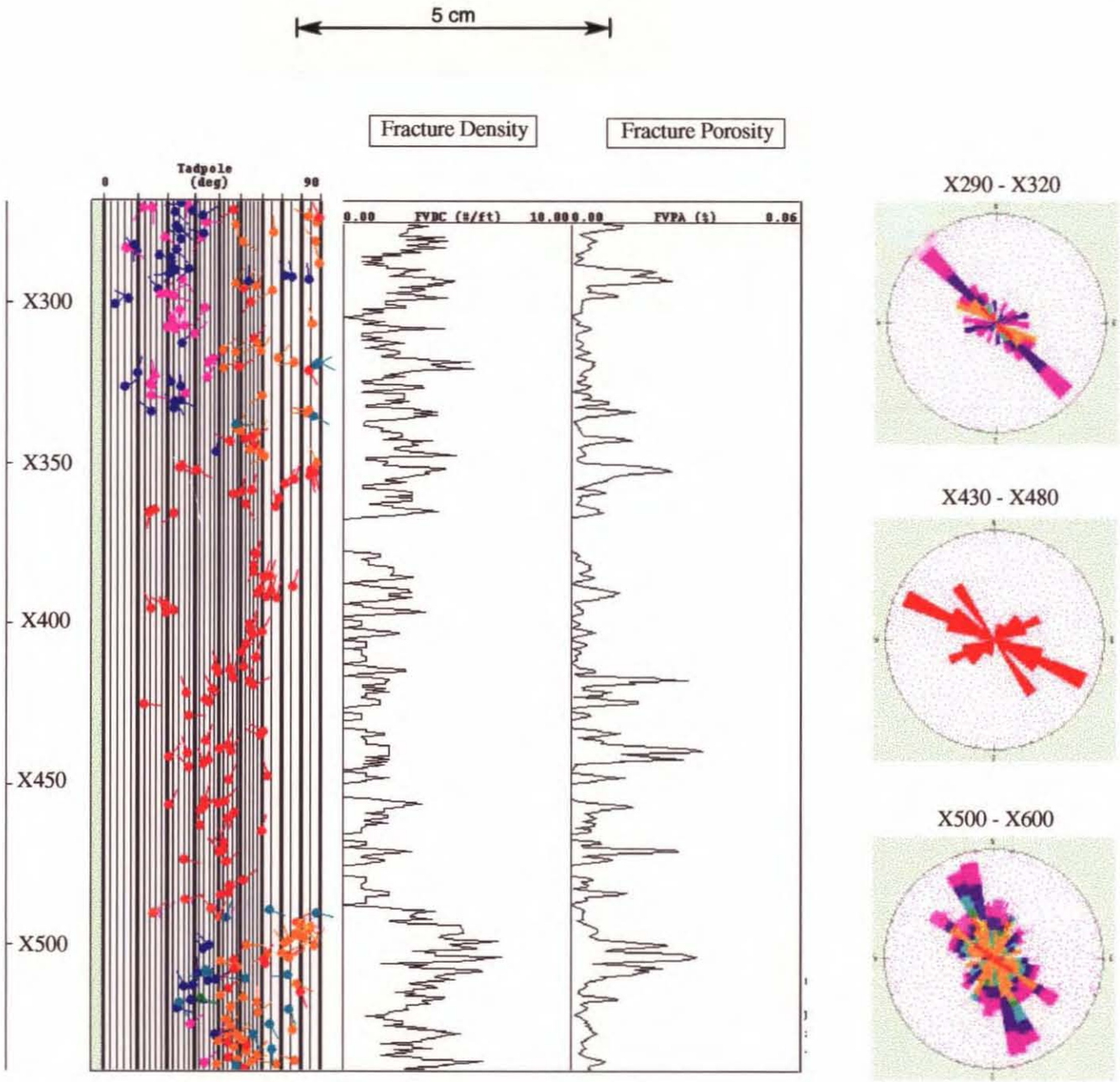

Figure 9. Dip and orientation of fractures from borehole resistivity image data

GLOBEX Far East — BARRAMUNDI #1 SEISMIC DISPLAY

YOUNG'S MODULUS: E

$$E = \rho V_s^2 \left(\frac{3V_p^2 - 2V_s^2}{V_p^2 - \frac{1}{3}V_s^2} \right) \sim \frac{\text{Stress}}{\text{Strain}}$$

ρ = Density
V_p = P Wave Velocity
V_s = P Wave Velocity

POISSON'S RATIO: υ

$$\upsilon = \frac{V_p^2 - 2V_s^2}{2(V_p^2 - V_s^2)} \sim \frac{\text{Shear Strain}}{\text{Axial Strain}}$$

V_p = P Wave Velocity
V_s = P Wave Velocity

THEORETICAL FRACTURE GRADIENT

$$\sigma_{min} = \frac{\upsilon}{1-\upsilon}\left(\sigma_v - P_\rho\right) + P_\rho + \sigma_\tau$$

υ = Poisson's Ratio
σ_v = Overburden Stress
P_ρ = Pore Pressure
σ_τ = Far Field (Tectonic) Stress

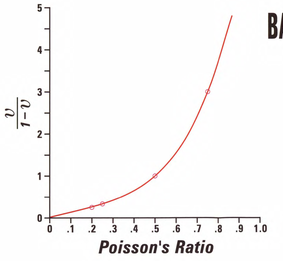

BARRAMUNDI FRACTURE GRADIENT

$$\sigma_{min} = \frac{\upsilon}{1-\upsilon}\sigma_v + \sigma_\tau$$

Since P_ρ = Hydrostatic